

SEISMIC WIDE-ANGLE STUDIES OF EARLY ARCHEAN AND PROTEROZOIC
CRUST IN GREENLAND, MINNESOTA, AND WYOMING

by
Karsten Gohl

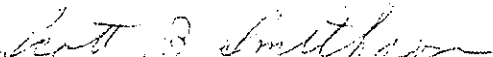
A dissertation
submitted to the Department of
Geology and Geophysics and The Graduate School of
The University of Wyoming in Partial Fulfillment of
Requirements for the Degree of

DOCTOR OF PHILOSOPHY
in
GEOPHYSICS

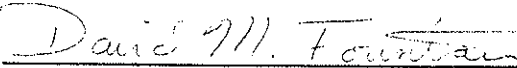
Laramie, Wyoming
August, 1991

TO THE OFFICE OF THE GRADUATE SCHOOL:

The members of the Committee approve the dissertation of
Karsten Gohl presented on June 20, 1991.



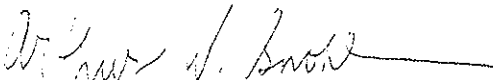
Scott B. Smithson, Chairman



David M. Fountain



Charles L. Angevine

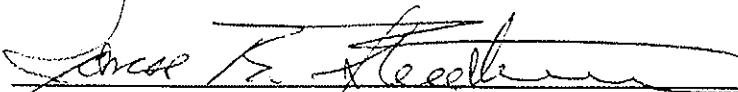


Arthur W. Snoke

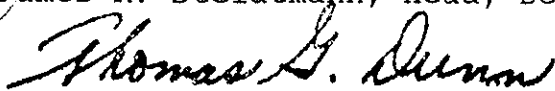


William P. Iverson

APPROVED:



James R. Steidtmann, Head, Dept. of Geology and Geophysics



Thomas G. Dunn, Dean of the Graduate School

Gohl, Karsten, Seismic Wide-Angle Studies of Early Archean and Proterozoic Crust in Greenland, Minnesota, and Wyoming, Ph.D., Department of Geology and Geophysics, August, 1991.

The composition and structure of the Precambrian crust, especially the Archean crust, are poorly known by geoscientists. In order to place constraints on the seismic velocity distribution of these crusts, large-offset, densely spaced wide-angle data were acquired from the Archean crust in southwest Greenland and southern Minnesota, and the Early Proterozoic crust in southeastern Wyoming. The data, generated by air-gun, vibroseis, quarry blasts, and dynamite shots, were inverse and forward modeled using techniques such as tau-p and travel-time inversion, ray theory, and the reflectivity method. Results from southwest Greenland show that the Archean crust is strongly affected by the Cretaceous and Tertiary rifting event of the Labrador Sea and Davis Strait. Observations of a 25 to 30° dipping Moho and a 5-8 km thick high-velocity zone at the bottom of the transitional crust suggest asymmetrical rifting of the original Archean block. A comparison of data from southwest Greenland and southern Minnesota indicates differences in the seismic character of continental Archean crust-mantle boundaries. The Moho in SW Greenland may consist of a wide gradient zone, possibly a

transitional phase change. A laminated Moho transition zone with small impedance contrasts of high-velocity mafic to ultramafic rocks might be responsible for strong pre-critical reflections in southern Minnesota. Data from southeastern Wyoming show features of a Proterozoic volcanogenic crust that accreted to the Archean Wyoming Province. A band of reflective interfaces from the middle into the lower crust is an indication for intermediate/mafic interlayering. Models of these data from different Precambrian regions evaluate the range of possible crustal composition and structure.

DEDICATION

To my parents

ACKNOWLEDGEMENTS

Special thanks to Scott Smithson, who guided me through the projects of this dissertation and who encouraged me to investigate Precambrian crust with seismic wide-angle data. His emphasis in linking seismic data with petrological information had a great influence. Gratefully appreciated is the cooperation with Robert Hawman who spent a lot of time discussing the results from inversion and forward modeling. He also reviewed the dissertation thoroughly. David Fountain, Arthur Snoke, Bill Iverson, and Charles Angevine provided critical comments and helped improve the manuscript. Thanks to Bill Clement, Steve Larkin and Nick Boyd who looked carefully over the manuscript and commented on it. I am grateful to the members of the University of Wyoming seismic crew and the crew of the R.V. "Haakon Mosby", without whom these data would not have been acquired. Responsible for the wonderful time I have had in Laramie during my studies as well as in social and cultural activities was the fantastic group of graduate students in the seismic lab and the department.

TABLE OF CONTENTS

CHAPTER	PAGE
<p>I. STRUCTURE OF ARCHEAN CRUST AND PASSIVE MARGIN OF SOUTHWEST GREENLAND FROM SEISMIC WIDE-ANGLE DATA</p>	<p>1</p>
Introduction	1
Geology and Tectonic Framework	4
Previous Geophysical Studies	8
Data Acquisition	10
Data Processing	11
Description of Seismic Phases	14
Tau-P Processing and 1-D Inversion	39
2-D Inversion and Forward Modeling	56
Interpretation and Discussion of Modeling Results	91
Implications for Evolution of Labrador Sea	100
Conclusions	104
<p>II. SEISMIC CHARACTER OF EARLY ARCHEAN CRUST IN SOUTHWEST GREENLAND AND SOUTHERN MINNESOTA</p>	<p>107</p>
Introduction	107
Archean Terranes	108
Acquisition of Wide-Angle Data	116
Processing and Data Description	117
Inversion	127
Reflectivity Modeling	137
Conclusions	143
<p>III. SEISMIC WIDE-ANGLE STUDY OF ACCRETED PROTEROZOIC CRUST IN SOUTHEASTERN WYOMING</p>	<p>146</p>
Introduction	146
Geology and Previous Geophysics	147
Seismic Experiment	151
Processing	152
Inverse and Forward Modeling	164
Discussion	173
Conclusions	175
<p>REFERENCES</p>	<p>178</p>

LIST OF FIGURES

	Page
Figure 1.1. General map of the northeastern Atlantic region	2
Figure 1.2. Map of the general geology of study area in SW Greenland including seismic source and receiver locations	5
Figure 1.3. Seismic section before and after deconvolution (a), autocorrelation of P_mP phase (b), power versus time for single trace (c)	14
Figure 1.4. Elimination of near-offset S-wave noise, a) without coherency filter, b) with coherency filter, c) with tau-p filter, d) with tau-p filter, threshold for semblance filter: 0.98, e) with tau-p filter, threshold for semblance filter: 0.95	18
Figure 1.5. Receiver gathers of WA profile, vertical component, deconvolution applied, no coherency filter applied, a) UM-North, b) UM-South, c) KA, d) IK, e) GR	22
Figure 1.6. Receiver gather of station IK (WA profile), vertical component, deconvolution applied, reduction velocity 8 km/s, window for P_1P and P_mP phases	28
Figure 1.7. Receiver gathers of AM profile, vertical component, AGC 3 sec., no coherency filter applied, reduction velocity 8 km/s, a) KA, b) IK, c) AM1, d) AM7	31
Figure 1.8. Receiver gather of station IK (AM profile), vertical component, AGC 3 sec., reduction velocity 8 km/s, window for P_1P and P_mP phases	36

Figure 1.9.	Horizontal components of station KA from shot profile WA, S_n phase, a) transverse, b) radial	39
Figure 1.10.	Amplitude versus offset for P_1P and P_mP phase of recordings KA (a+c) and IK (b+d)	41
Figure 1.11.	Slant stack (a) of offset window (92 - 115 km) of recording KA, b) semblance, c) coherency-filtered slant stack (envelope) with semblance threshold 0.98, and d) 0.90	45
Figure 1.12.	Coherency-filtered, vertically stacked tau-p gathers (envelope), a) UM-North, b) UM-South, c) IK, d) KA, e) GR	48
Figure 1.13.	Results of extremal inversion; curves illustrate minimum and maximum depth bounds for each layer of constant slowness with slowness displayed as velocity	54
Figure 1.14.	2-D travel-time inversion for AM profile, rays shot through final model and calculated and observed travel-times for stations a) KA, b) IK, c) AM1, d) AM2, e) AM4, f) AM5, g) AM6, and h) AM7	62
Figure 1.15.	2-D travel-time inversion for WA profile, rays shot through final model and calculated and observed travel-times for stations a) UM, b) KA, and c) GR	70
Figure 1.16.	Final 2-D P-wave velocity models for profiles AM (a) and WA (b)	73
Figure 1.17.	Fence diagram of perpendicular P-wave velocity models	77
Figure 1.18.	Ray-synthetic seismograms of stations UM (a) and KA (b) of shot profile WA	80
Figure 1.19.	True amplitude plots of averaged five adjacent traces of station KA (profile WA) at 76 and 104 km offset	82

Figure 1.20. Reflectivity seismogram (a) and relative amplitudes at 76 and 104 km distance (b) to model 1st-order discontinuity velocity contrasts for P_2P , P_3P , P_1P , and P_mP phases	84
Figure 1.21. Reflectivity seismogram (a) and relative amplitudes at 76 and 104 km distance (b) to model narrow gradients for P_2P , P_3P , and P_mP phases and a 1st-order discontinuity the P_1P phase	87
Figure 1.22. Free-air and Bouguer gravity anomaly and water-depth profiles of line AM (a) and WA (b)	92
Figure 1.23. Schematic cross-section of Labrador Sea conjugate margins	101
Figure 2.1. Map of the general geology of study area in SW Greenland including seismic source and receiver locations	109
Figure 2.2. Schematic map of southern-central Minnesota that includes the main geologic units and the seismic source and receiver locations	114
Figure 2.3. Record sections of Greenland fjord shots, stations IK (a) and AM7 (b), profile AM, AGC 3 sec	119
Figure 2.4. MN vibroseis record from profile PCN, max. offset 79.4 km	122
Figure 2.5. MN quarry blast record from profile PCN, max. offset 107.2 km, section containing a) P_mP , b) S_mS phases	124
Figure 2.6. Coherency-filtered slant stacks (t-p) of MN quarry blast record (max. offset 107.2 km), a) P_mP and P_mS , b) S_mS arrivals	128
Figure 2.7. Coherency-filtered slant stacks (tau-p) of all MN quarry blast and vibroseis records, used to pick arrivals for extremal inversion	130
Figure 2.8. Final P-wave velocity model from the Greenland profile AM	133

Figure 2.9.	Results of extremal inversion of Minnesota wide-angle data; curves illustrate minimum and maximum depth bounds for each layer of constant slowness with slowness displayed as velocity	135
Figure 2.10.	Reflectivity seismograms with corresponding velocity-depth models for Archean Moho in Minnesota and Greenland, a) gradient zone, b) laminated zone	138
Figure 3.1.	Schematic map of geologic units in SE Wyoming including seismic wide-angle shot and receiver locations	148
Figure 3.2.	Vibroseis records from receiver profiles SY87 (a) and BR87 (b); sources are on reversed profiles	153
Figure 3.3.	Coherency-filtered slant stacks (t-p) of vibroseis records from profiles SY87 (a) and BR87 (b)	155
Figure 3.4.	Dynamite shot records (BR89), vertical component, sources location TS (a), WL (b), horizontal component, source location WL (c)	158
Figure 3.5.	Coherency-filtered slant stack (t-p) of transverse component of dynamite record BR89 (source location WL)	162
Figure 3.6.	Summed slant stacks of vibroseis records SY87 (a) and BR87 (b), and dynamite records BR89 from source locations TS and WL (c)	165
Figure 3.7.	Results from 1-D extremal inversion, curves represent upper and lower depth bounds	167
Figure 3.8.	Synthetic seismograms with corresponding velocity-depth models by using the reflectivity method (a-d)	170

CHAPTER I

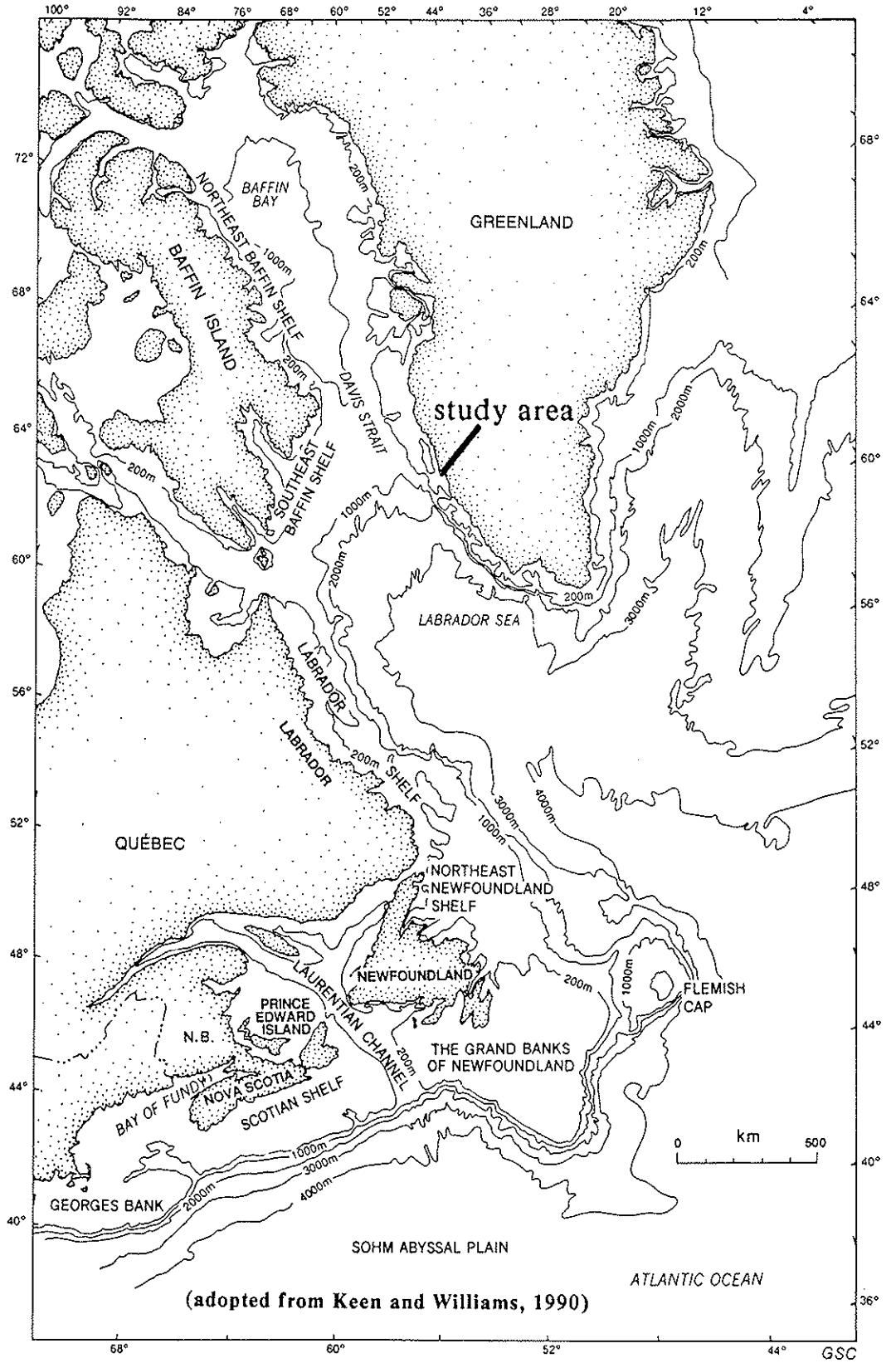
STRUCTURE OF ARCHEAN CRUST AND PASSIVE MARGIN OFF SOUTHWEST GREENLAND FROM SEISMIC WIDE-ANGLE DATA

INTRODUCTION

New densely-spaced seismic wide-angle data reveal detailed information about the structure and composition of the passive margin next to the oldest Archean block of southwest Greenland. The Labrador Sea and Davis Strait basins divide the conjugate margins of oldest Archean crust in Greenland and Labrador, Canada [Fig. 1.1]. To study the effect that Cretaceous and early Tertiary rifting had on an early Archean terrane, a large offset wide-angle and normal-incidence seismic experiment was conducted parallel to the southwest Greenland coast and along two fjords. The goal of the experiment was to obtain velocity information along a transect from continental crust into the transitional oceanic-continental crust of the basin. This paper analyzes the wide-angle seismic data obtained mainly on the transitional crust to determine the structure of the continental margin and its implications for the development of the asymmetric Labrador Sea basin.

The experimental design allowed the integration of

Figure 1.1. General map of the northeastern Atlantic region. Greenland rifted from the North American continent between Late Cretaceous and Oligocene creating a relatively thick oceanic crust of the Davis Strait and northern Labrador Sea. The narrow width of the SW Greenland shelf as opposed to the wider shelf off Labrador indicates the asymmetry of the Labrador Sea margins. Map was adopted from Keen and Williams (1990).

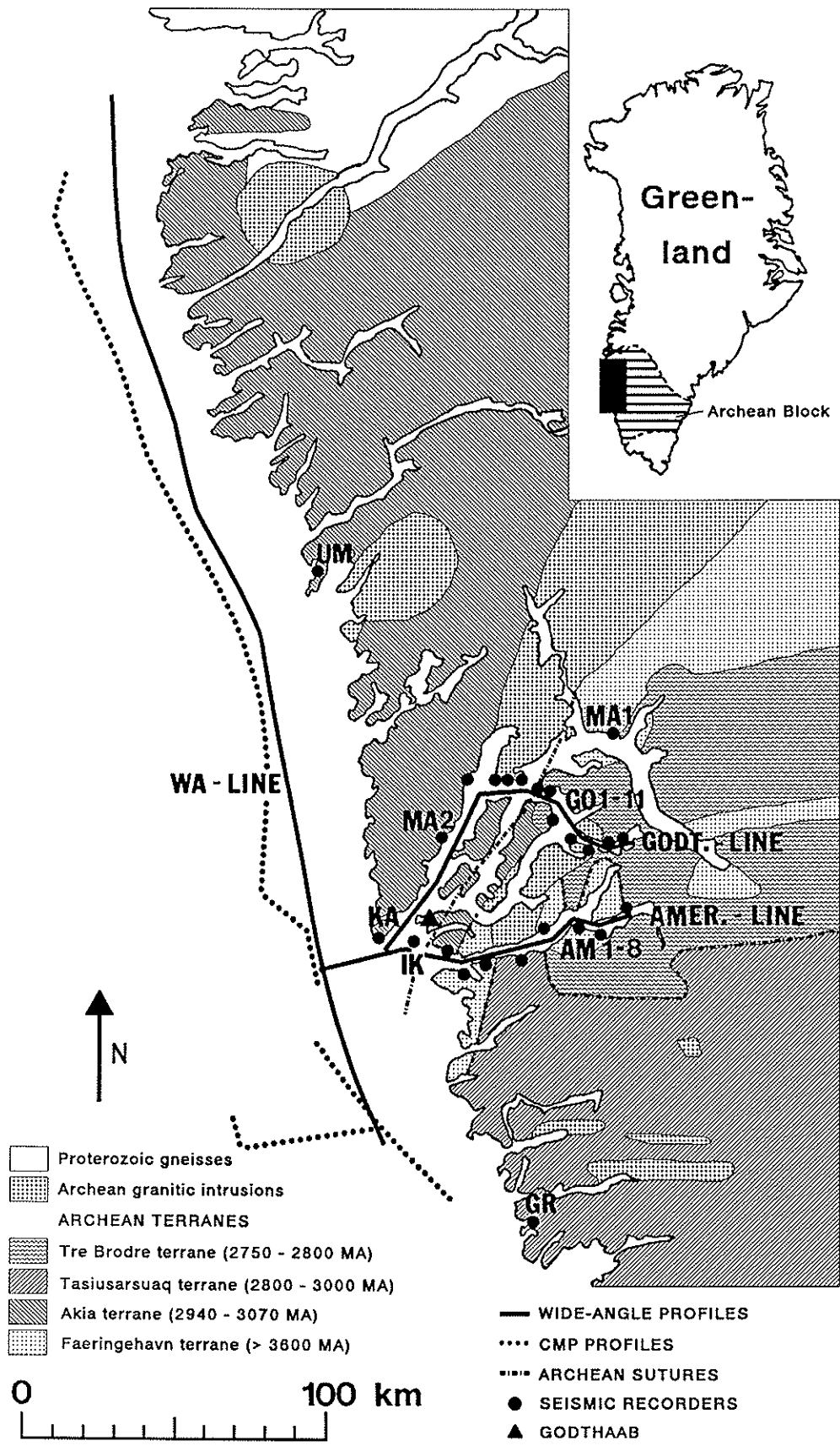


processing techniques from reflection seismology, such as deconvolution and coherency filtering, inverse and forward modeling, and amplitude analyses. To approximate an initial model for a two-dimensional inversion, localized one-dimensional models were derived using a tau-p inversion. A 2-D travel-time inversion was performed and supplemented by the forward modeling of amplitudes. The modeling results provide new implications for the composition of the passive margin, in particular the lowermost crust, the asymmetry of the Labrador Sea basin, and the break-up of an early Archean crust. They combine models of extended basins such as those by Wernicke (1985), Lister et al. (1986), and Bonatti and Seyler (1987).

GEOLOGY AND TECTONIC FRAMEWORK

The Archean block of SW Greenland [Fig. 1.2] consists of several gneissic, granitic, and supracrustal complexes with ages between 2750 and 3800 Ma (McGregor, 1973, 1979; Bridgwater et al., 1976; Brown et al., 1981; McGregor et al., 1986). Nutman and others (1989) suggest a juxtaposition of four Archean sub-terrane at about 2750 Ma, each terrane having evolved separately prior to juxtaposition. They base their conclusion on observations of thin mylonitic zones along terrane boundaries. These sutures have been highly deformed and tilted by subsequent tectonic events (Nutman et al., 1989).

Figure 1.2. Map of the general geology of study area in SW Greenland including seismic source and receiver locations. Compilation of published maps from Geological Survey of Greenland (1982), Nutman et al. (1989), and Friend and Nutman (1991). Three-component seismic instruments located along the coast (UM, KA, IK, GR) and two fjords, Godthaabfjord and Ameralik (GO 1 to 11, AM 1 to 8, MA 1 and 2) recorded densely-spaced air-gun shots from profiles WA, GO, and AM.



Rifting started in the southern Labrador Sea during the Late Cretaceous, expanded into the northern Labrador Sea in the Early Paleocene and ended in the Davis Strait and Baffin Bay during the Early Oligocene (Laughton, 1971,1972; Le Pichon et al., 1971; Hyndman; 1973,1975; van der Linden, 1975; Srivastava, 1978,1983; Hinz et al., 1979; Srivastava et al., 1980; Johnson et al., 1982; Srivastava and Tapscott,1986). The rifting event separated the Archean block of Greenland from its counterpart in Canada, the Nain Province (Taylor, 1972). The evolution of the Labrador Sea area has been derived mainly from studies of oceanic magnetic anomalies and the delineation of fracture zones.

The Labrador Basin is characterized by asymmetric continental margins [Fig. 1.1]. The SW Greenland shelf is particularly narrow, less than 70 km in the south, and gradually widens northward to about 230 km width. In contrast the Labrador shelf has a width of 110 km to 220 km (Srivastava et al., 1980), widening northward. Srivastava (1978) and Hinz et al. (1979) observe a steep dip of the continental slope of SW Greenland between 60 and 62° North latitude and attribute it to normal faulting.

The continental margins of the Labrador Sea are considered to be "non-volcanic", due to the lack of exposed extensive volcanism associated with the rifting (White and McKenzie, 1989). Approximately 500 to 600 km farther north on Disko Island and surrounding areas, however, a large area of

basaltic volcanic rocks (Clark and Pederson, 1976) with thicknesses of up to 8 km (Denham, 1974) are observed. Identical basalts are found on the conjugate margin on Baffin Island (Clarke, 1970; Clarke and Upton, 1971). The basalts on either side were emplaced about 61 - 58 Ma (Clarke and Upton, 1971; Soper et al., 1982) during the time of spreading of the Davis Strait and Baffin Bay. Hyndman (1975) developed a model for the region, in which an active hot spot under the Davis Strait produced volcanism and thickened the crust after sea floor was created. White and McKenzie (1989) argue that the extensive rift-margin volcanism and associated crustal thickening in the Davis Strait was generated by an intersection of the rift with the asthenospheric plume that caused the rifting in the North Atlantic and migrated underneath Greenland, or was caused by a separate hot spot that had been initiated under the Davis Strait.

PREVIOUS GEOPHYSICAL STUDIES

GRAVITY AND MAGNETICS. Gravity and magnetic profiles across the Labrador Sea show evidence for the asymmetry of the margins (Hinz et al., 1979; Thorning, 1984, 1986; Geological Survey of Canada, 1988a,b; Woodside and Verhoef, 1989). Both continental margins exhibit strong positive free-air anomalies of 30 to 50 mgal on the landward side of the shelves with a negative free-air anomaly representing the base of the

continental slope. Generally, narrower features with steeper gradients and higher amplitudes of the positive and negative anomalies are observed on the Greenland margin, except where the margin broadens to the north (Hinz et al., 1979; Woodside and Verhoef, 1989). These features are associated with an abrupt break-up of the continental crust, a steeply dipping basement, and a thin or, in places, non-existent sequence of shelf sediments (Hinz et al., 1979; Woodside and Verhoef, 1989). Also, large magnetic anomalies on the Greenland margin indicate a lack of thick shelf sediments.

A detailed gravity study of the Godthaabsfjord and Ameralik region by Speece (unpublished data) and the gravity map of Forsberg (unpublished data) reveal a positive seaward gradient of the long-wavelength Bouguer anomaly of 30 mgal/km, indicating a steep slope of the crust-mantle boundary along the transitional crust. A northeast-southwest trending gradient of the low-frequency gravity wave field north of 64.5° N indicates increasing crustal thickness northward along the continental edge as well.

SEISMIC STUDIES. An extensive seismic reflection and refraction study by Hinz et al. (1979) revealed the asymmetry of the continental margins. While the data across the Labrador shelf show a thick sedimentary wedge of several seismic reflectors, there are thin or non-existent sedimentary rocks on the Greenland shelf above a strongly faulted acoustic

basement. The sedimentary cover thickens northward toward the Davis Strait (Manderscheid, 1980). The basement does not show any major continuous reflections, but contains diffractions, possibly caused by steeply dipping normal faults. Hinz et al. (1979) related the flat acoustic basement on the Labrador shelf and sub-basement reflectors to possible younger basalt flows that overlay pyroclastic or sedimentary sequences on top of a slightly older oceanic crust. Their refraction study revealed a high-velocity zone (7.28 km/s) at the base of the crust off the coast of Labrador. Stergiopoulos (1984) observed a high-velocity layer (7.22 - 7.64 km/s) at the bottom of the oceanic crust, adjacent to the Greenland margin. Densely spaced wide-angle data from the shelf crossing the boundary of the southern Archean block and the Ketilidian belt of Greenland do not contain evidence for a high-velocity zone at the base of the transitional crust (Chian and Loudon, submitted paper).

DATA ACQUISITION

The seismic wide-angle experiment was designed to obtain a velocity distribution from a profile along the NNW-SSE striking shelf [profile WA on Fig. 1.2] and to acquire information on the E-W striking structure of the transitional crust. In order to sample the interior of the continent and to cross Archean sutures, profiles were shot along two major

fjords with the Archean block, Godthaabfjord (profile GO) and Ameralik (profile AM).

The use of an air-gun array permitted the recording of densely spaced, mostly unaliased seismic data that allows accurate correlation of phases and detailed inverse and forward modeling. A source array of five air-guns (19.7 l or 1200 cu.in. each) with a peak pressure of 140 bar was fired at 15 m depth at a spacing of 100 to 150 m. Fifteen REF TEK PASSCAL 72A digital seismic recording instruments situated at 35 locations along the coast and two fjords recorded approximately 10,000 shots, from offsets between 2.5 and 400 km. All instruments recorded three components. The horizontal geophones were oriented in N-S and E-W direction. To avoid the danger of losing data due to possible failure in their first deployment in a large-scale controlled source experiment, two recorders were placed at several key locations. Unfortunately, the instruments on the site of the Isua gneiss complex and at the northern end of shot profile WA failed to record. With these exceptions, the overall performance was very satisfactory.

DATA PROCESSING

Unfiltered, amplitude-normalized receiver gathers and a frequency analysis show strong low-frequency noise below 4 Hz, originating from water waves striking the nearby shore. The

dominant signal frequency lies between 7 and 9 Hz. Harmonics of the source signal generated another frequency peak range from 14 to 18 Hz with lower amplitudes. Major high-frequency noise appears only on a few individual traces of some stations. A band-pass filter from 7 to 30 Hz with a taper of one octave on either side was applied to all receiver sections.

Large variations in alignment of the first break are due to datum static problems. Variations in first break velocities do not always follow water-depth changes, indicating velocity variations within the uppermost crust. Several troughs, relics of glacier movements, and over-deepened river valleys cut the shelf to depths reaching 600 m west of the Godthaab region. Water-depths for the Ameralik profile range between 50 and 700 m. A correct assumption would take into account knowledge of the accurate travel path through the correction layer for every seismic phase. Especially in fjord recordings, this information cannot be obtained, because too many three-dimensional effects play a role. In this study, emphasis lies on seismic reflections from the mid- and lower crust. These reflections arrive with steeper angles of incidence than upper crustal events. I applied elevation static corrections to all receiver gathers (shot static) by replacing the water column with a 5.5 km/s velocity layer. This correction velocity corresponds to a velocity of the near-offset first breaks. Also, static corrections to compensate for the air-gun depth

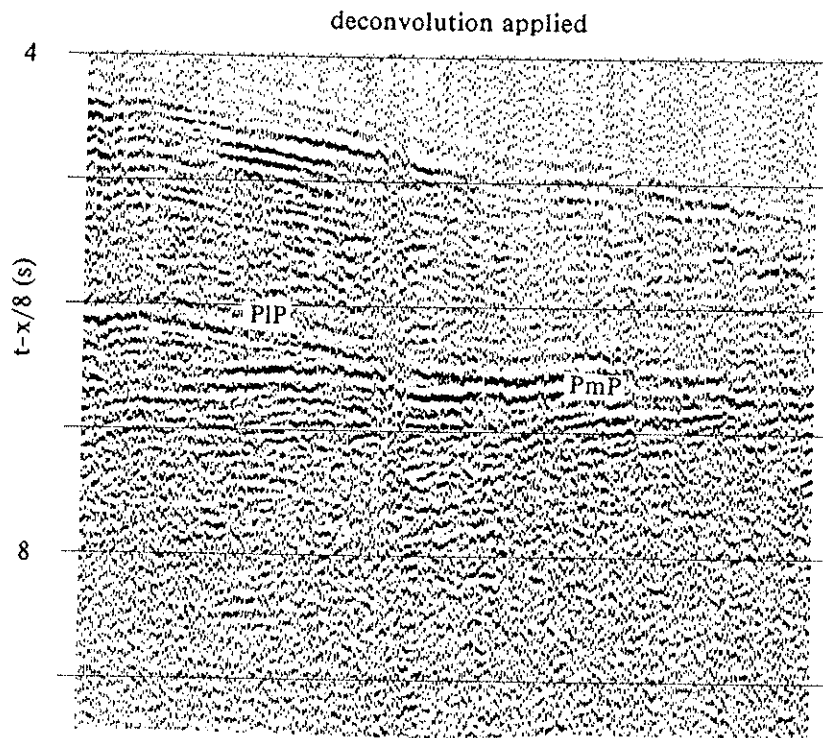
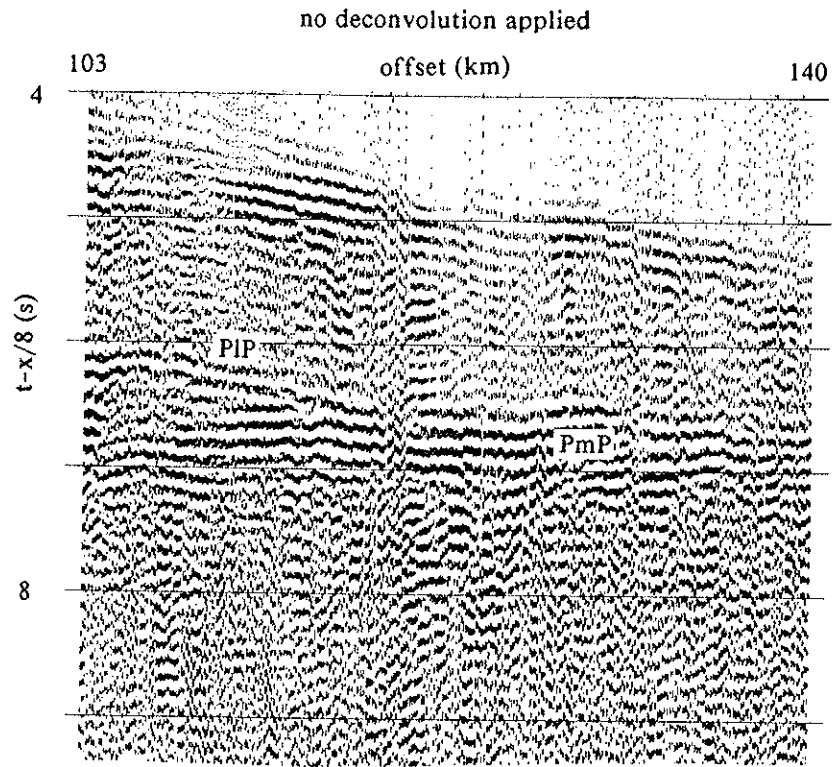
(correction velocity: 1.5 km/s) and for the instrument elevation (elevations between 8 and 20 m; correction velocity: 5.5 km/s) were applied. The results improved the correlation of major phases, although some static shifts remained, especially in the fjord data.

To eliminate reverberations from the bubble of the air-gun array and sea-bottom multiples, predictive deconvolution was applied. An operator of 500 ms length with a gap of 125 ms, which corresponds to the second zero-crossing of an 8 Hz wavelet, provided the best result to compress the wavelet [Fig. 1.3 a-b]. A five second design gate was chosen beginning at the first arrival. The operator was then applied to the entire trace. Plots showing the amplitude power versus time before and after deconvolution illustrate that, in most cases, the reverberations consist of higher amplitudes than the directly reflected arrival [Fig. 1.3 c]. In cases of low signal-to-noise ratios, such as in most pre-critical recordings in Ameralik, I did not deconvolve the data, because the elimination of high-amplitude reverberations made phase correlation more difficult.

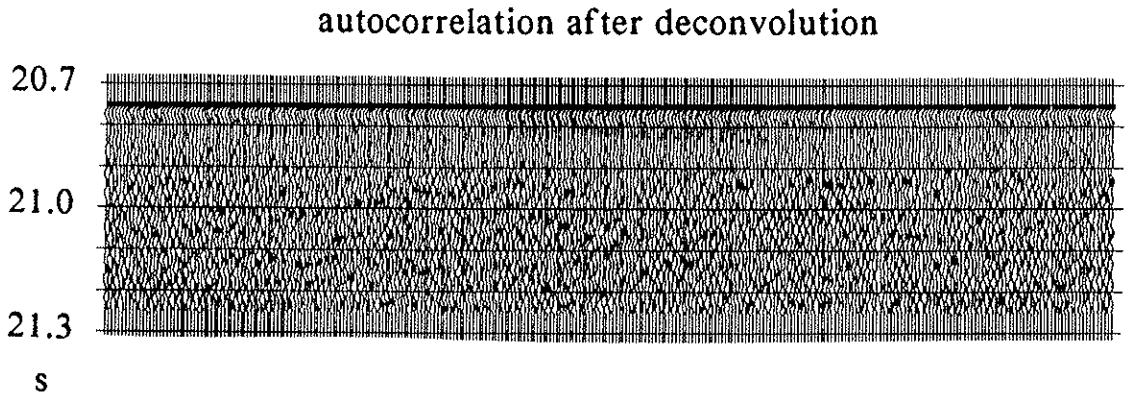
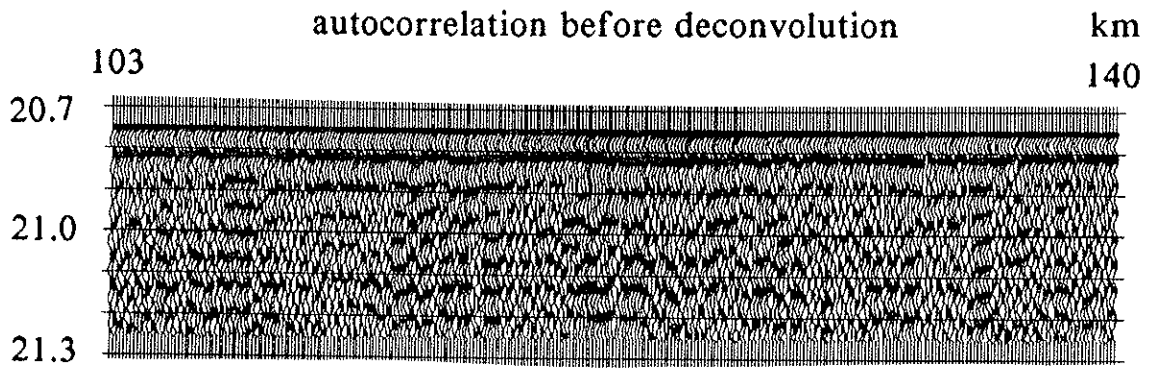
Near offset traces were filtered in the frequency-wavenumber (FK) domain to remove the direct S- and water waves that interfered with several P-wave arrivals. The same FK-filter was used to reject coherent noise reflected as side-echoes from fjord walls travelling with the acoustic velocity of water. I applied a rejection range of 1400-1600 m/s for the

Figure 1.3. Seismic section before and after deconvolution (a). Deconvolution eliminates most of the reverberations and is, therefore, a valuable aid for identifying phases. Note the cross-over of P_1P and P_mP phases. The autocorrelation of P_mP phase (b) illustrates the successful elimination of reverberations. Amplitudes of the principal signal decreases by a small amount, but the power versus time plot of a single trace (c) shows how effectively the high amplitudes of the reverberations have been eliminated. A few long-period multiples following the P_mP remain after deconvolution.

station IK shot profile WA

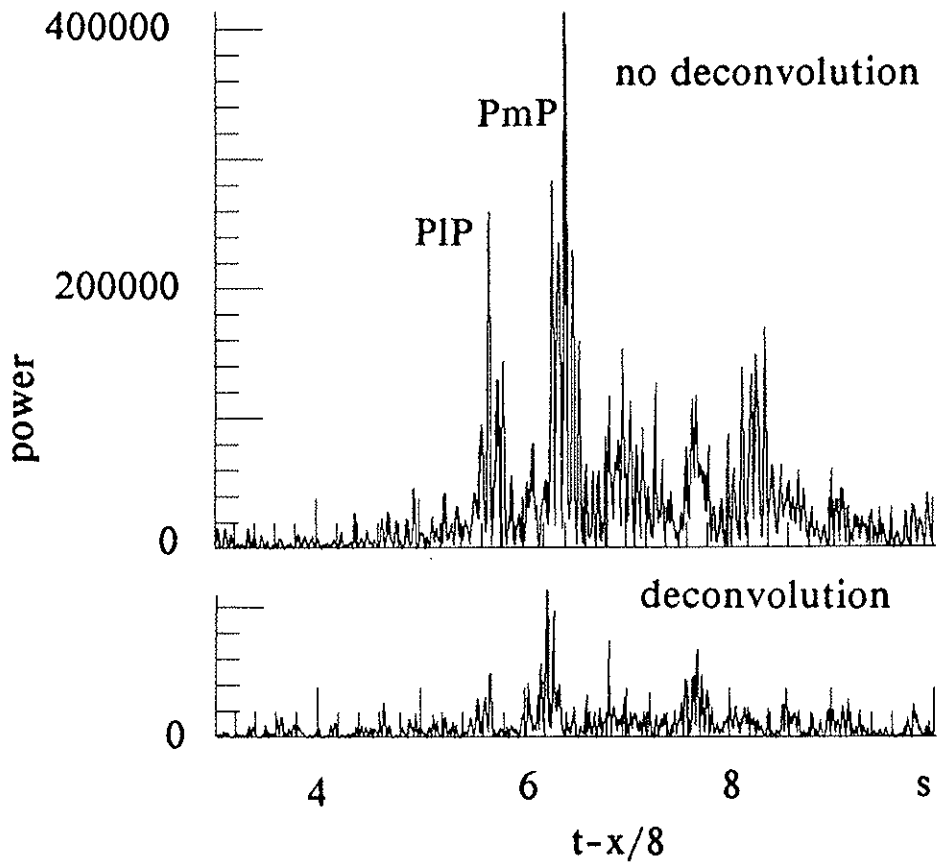


a.



b.

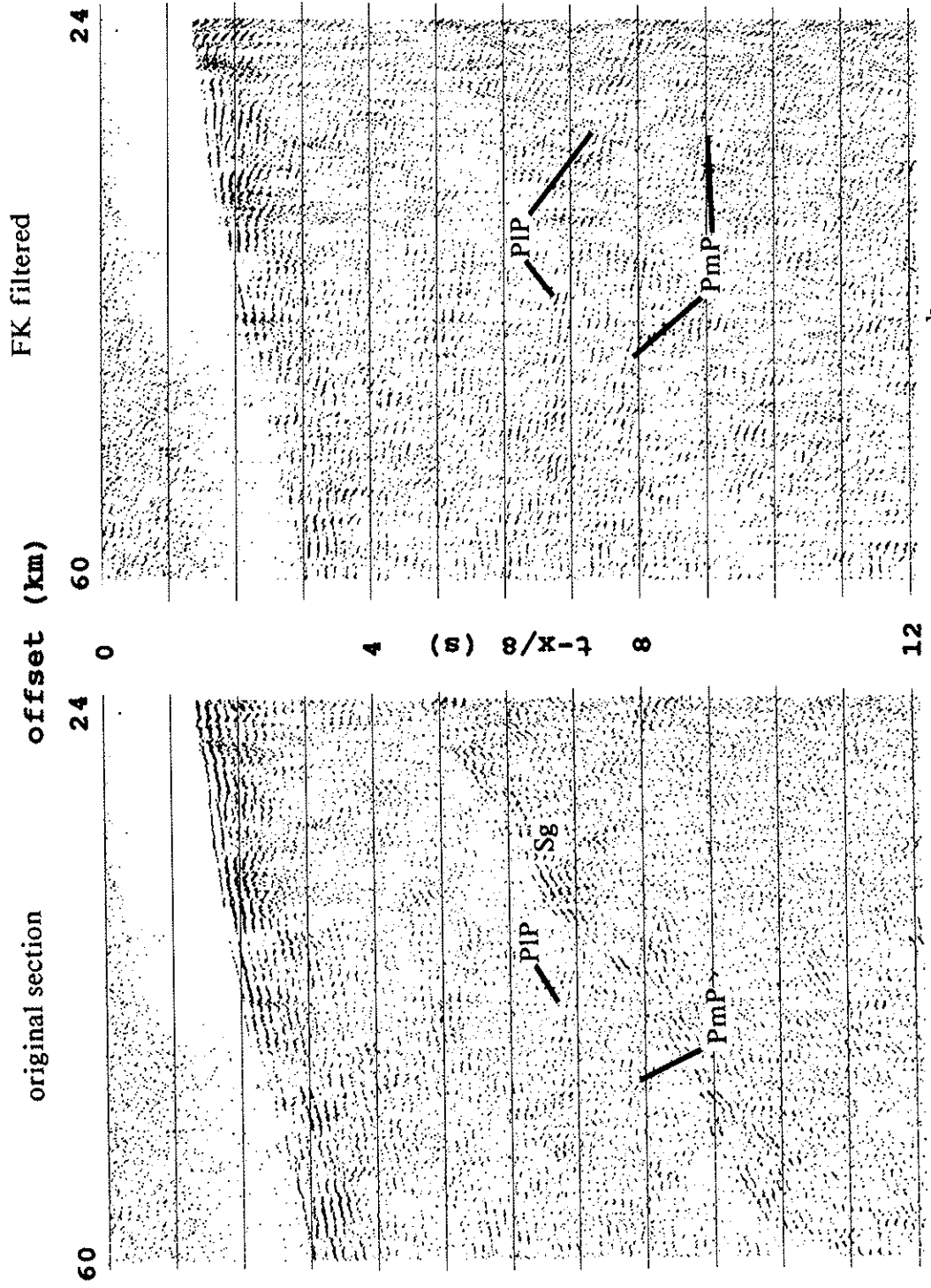
station KA shot profile WA
offset: 104 km



c.

Figure 1.4. Elimination of near-offset S-wave noise, a) without coherency filter, b) with coherency (FK) filter. P_1P and P_mP phases appear at smaller offsets after elimination of most direct S-wave arrivals. By transforming the offset data into the tau-p domain, muting and coherency-filtering in the tau-p domain, and transforming back into the time-offset domain, arrivals are enhanced (c). A coherency filter in the tau-p domain uses the semblance calculation (Stoffa et al., 1981) with different thresholds for noise rejection (d). The lower the threshold the more noise, and eventually signal, is rejected (e). Isolated events of high-amplitude noise in the tau-p domain may transform back as linear events that should not be confused with seismic arrivals.

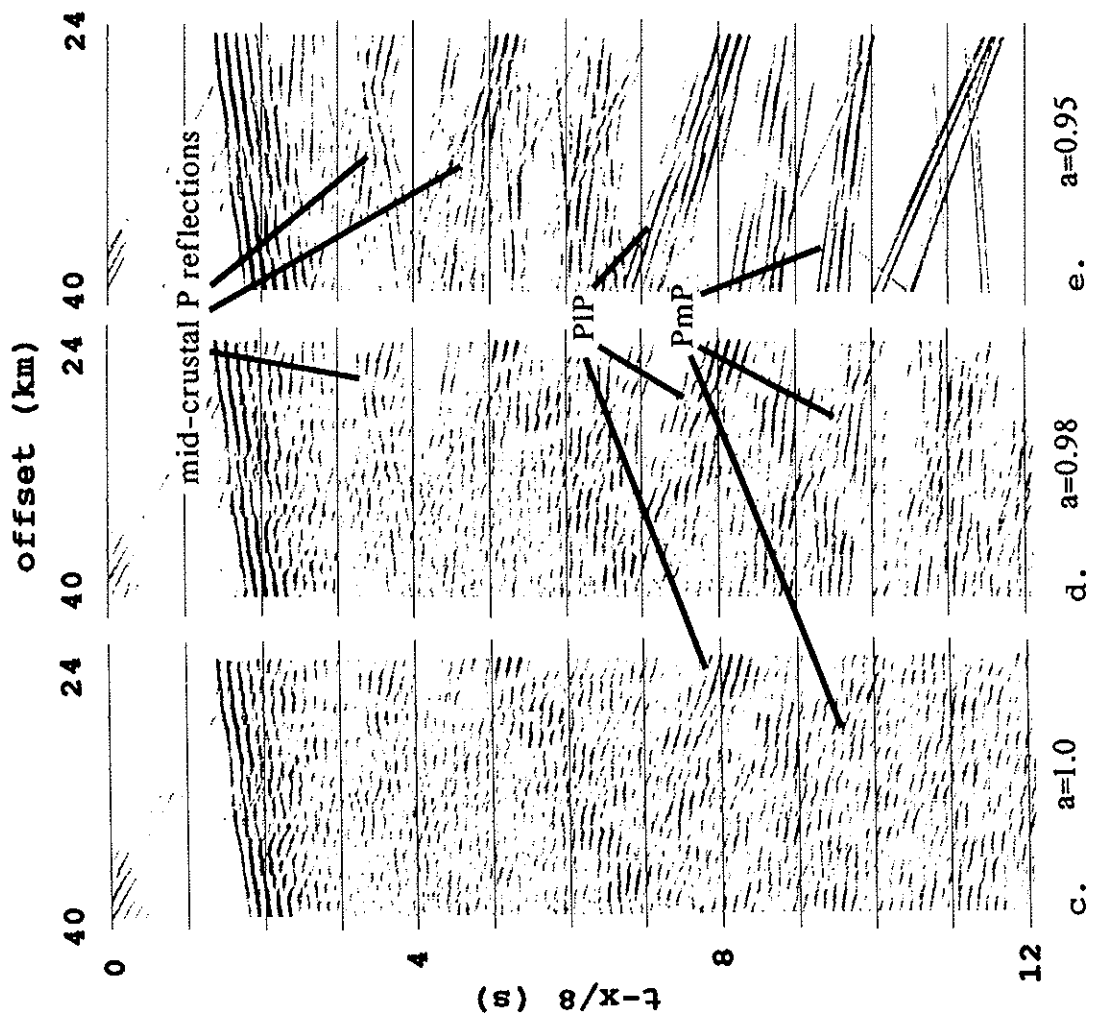
station UM-N shot profile WA



a.

b.

station UM-N shot profile WA tau-p filtered



water wave noise and 3600-3800 m/s for the direct S-waves. A previously applied automatic gain control (AGC) of 3 s improved the filtered results because of an improved signal-to-noise ratio [Fig. 1.4 a-b].

Rejection of direct S-wave and water-wave noise in the tau-p domain also improves the signal-to-noise ratio. A comparison with FK filtering shows that more coherent seismic arrivals from the original x-t domain were extracted by tau-p filtering [Fig 1.4 c-e]. Coherency-filtering in the tau-p domain (Stoffa et al., 1981) improves the signal to noise ratio, but also generates artifacts. I identified seismic phases by comparing both the FK-filtered as well as the tau-p filtered sections based on non-linear moveout and continuation beyond the direct S-wave field.

DESCRIPTION OF SEISMIC PHASES

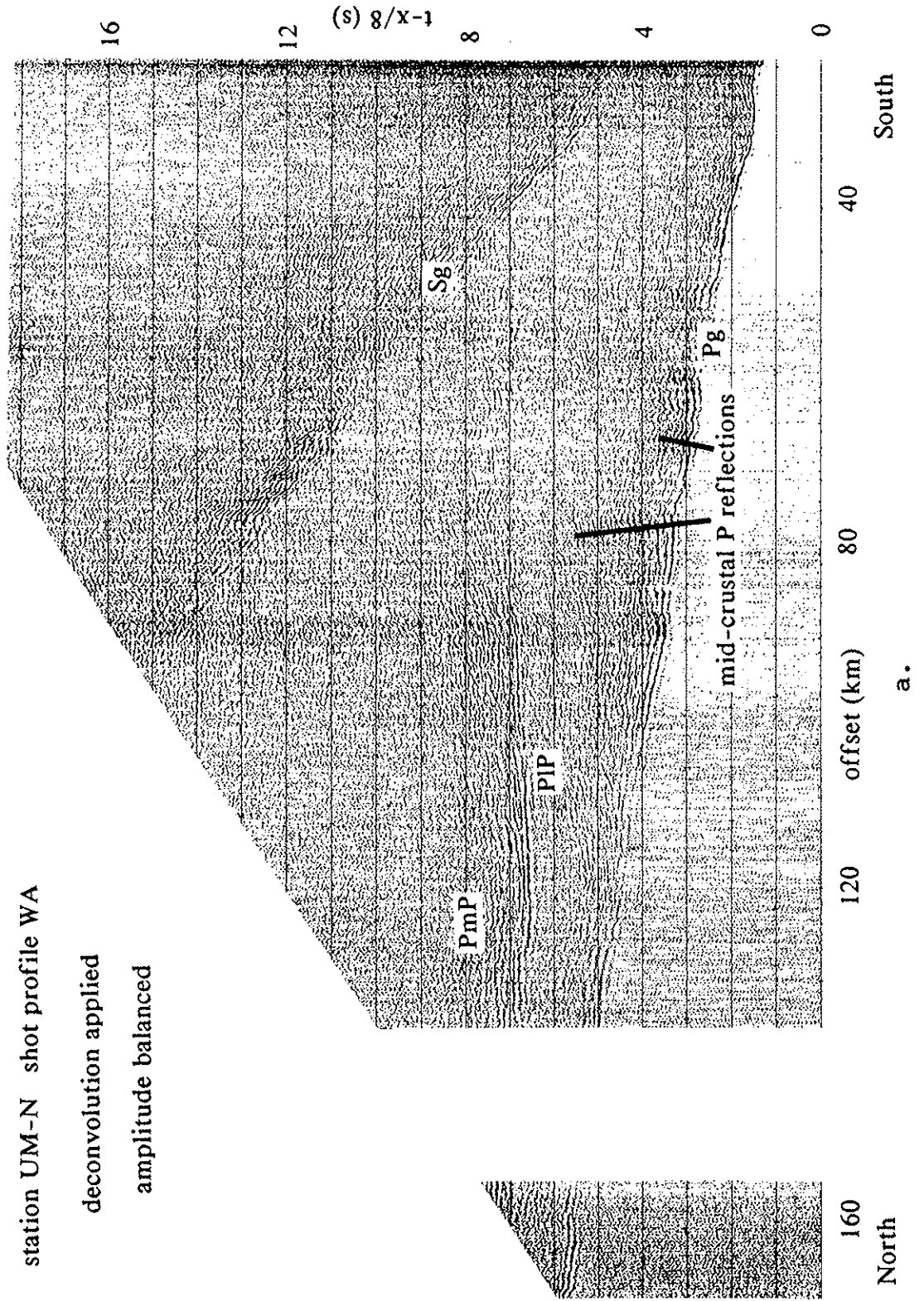
P-WAVES. The P-wave phases from the vertical components of the coast stations, recording the WA profile, are comprised of several middle and lower crustal reflected and refracted events [Fig. 1.5 a-e]. The first arrival (Pg) shows highly varying apparent velocities between 5.4 and 7.1 km/s in all receiver gathers, partly due to remaining static problems and lateral velocity variations as well as dip effects within the uppermost crust. The variations of the Pg phase are even more prominent in the fjord recordings as a result of rough fjord

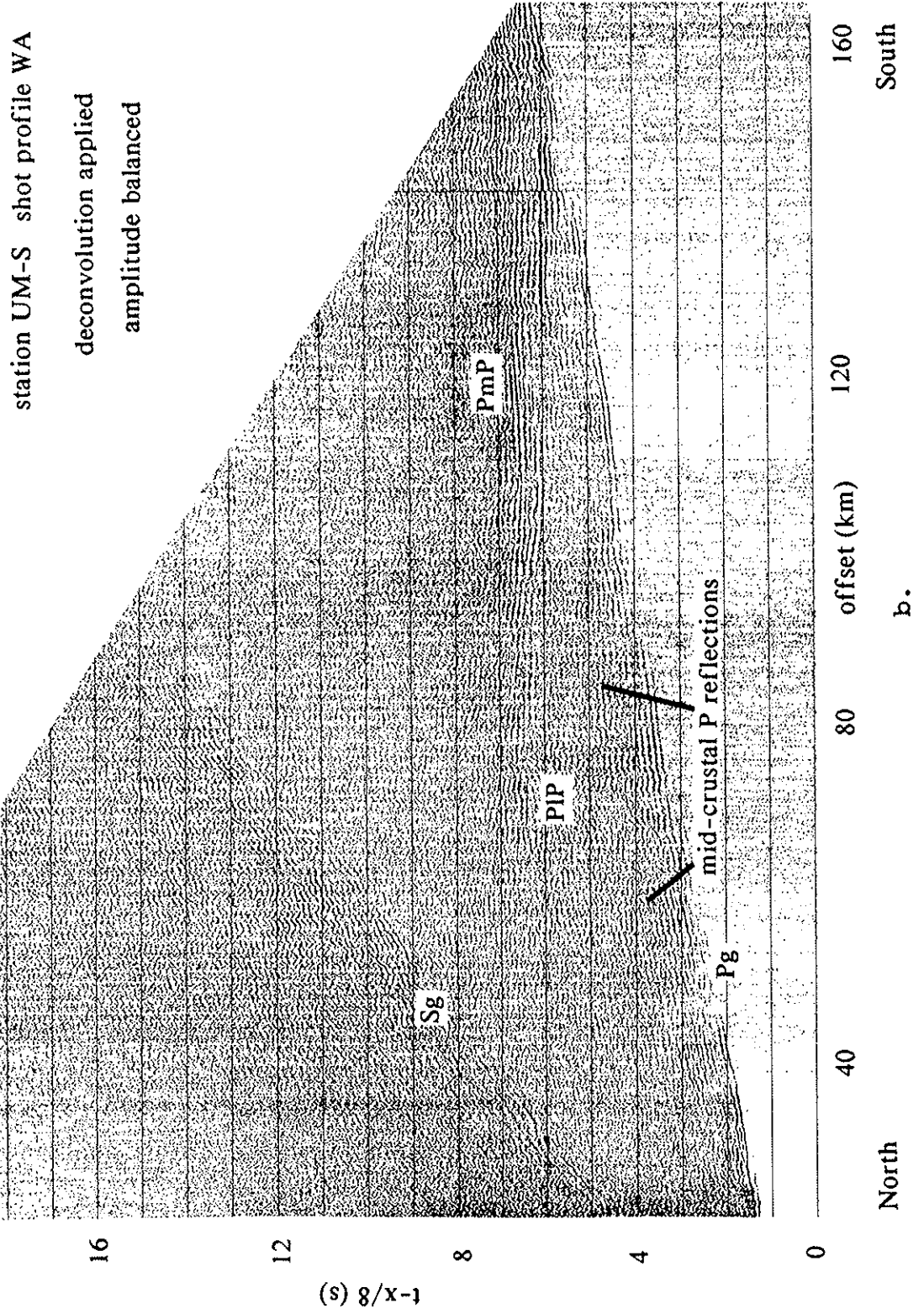
Figure 1.5. Receiver gathers of WA profile, vertical component, deconvolution applied, no coherency filter applied, a) UM-North, b) UM-South, c) KA, d) IK, e) GR. Note the high-amplitude lower crustal (P_1P) and Moho (P_mP) arrivals all of stations. Some recordings show the cross-over of P_1P and P_mP , a result attributed to the dense shot spacing. Several mid-crustal reflections are identified. They are weaker and less continuous than the P_1P and P_mP phases. Station KA contains a high-amplitude S_1S or S_mS phase. A P_n phase is observed in recording IK.

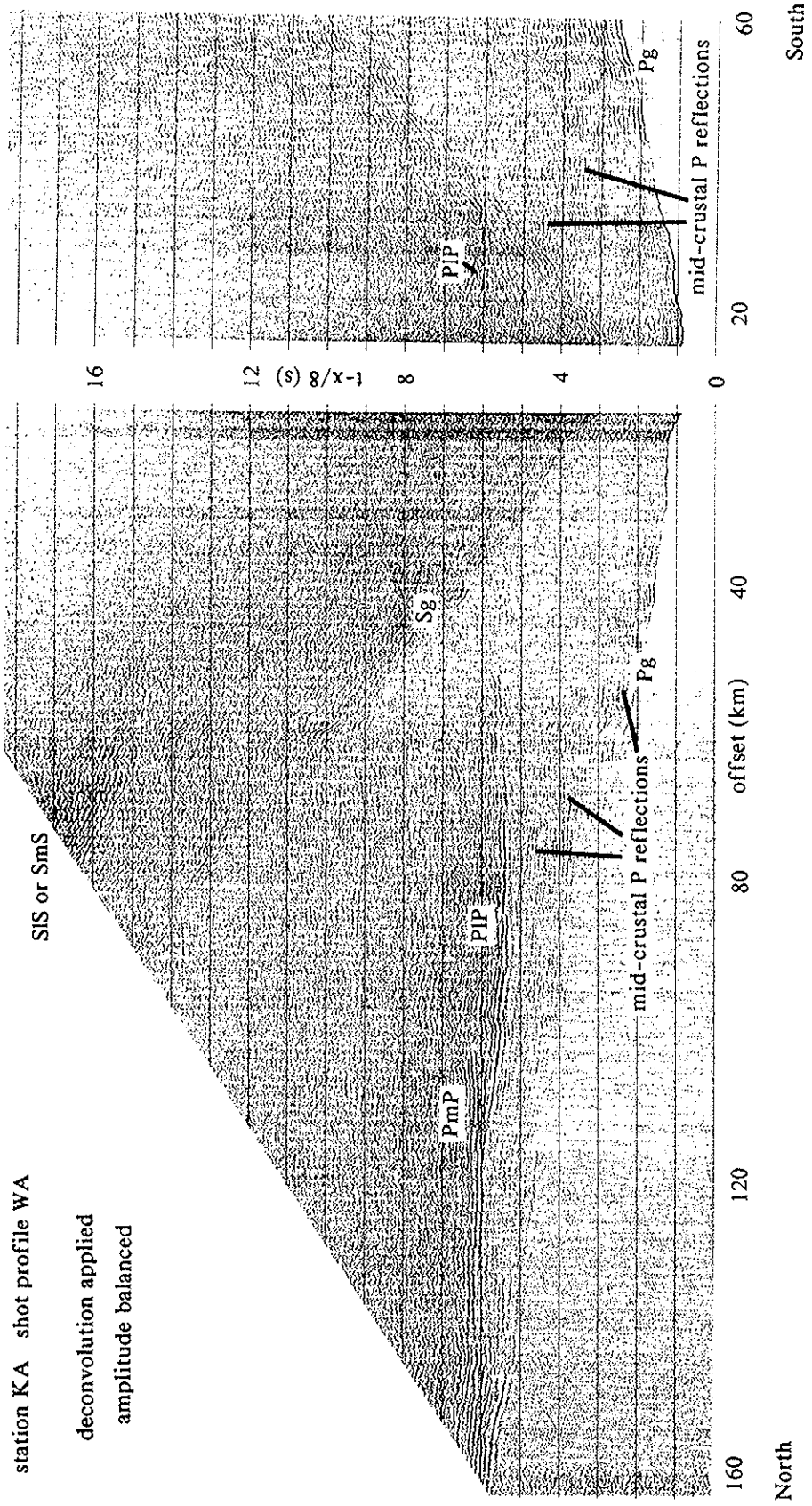
station UM-N shot profile WA

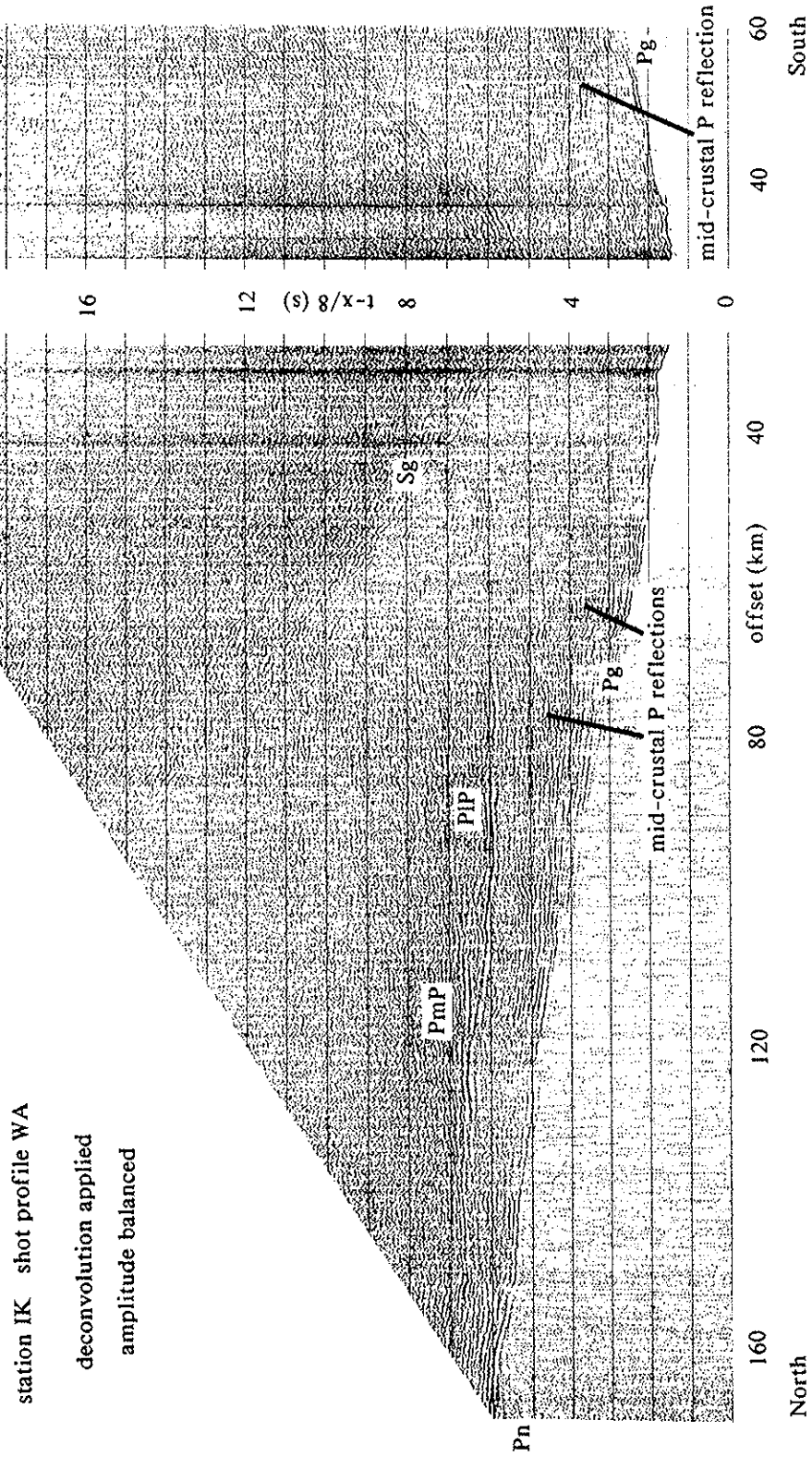
deconvolution applied

amplitude balanced







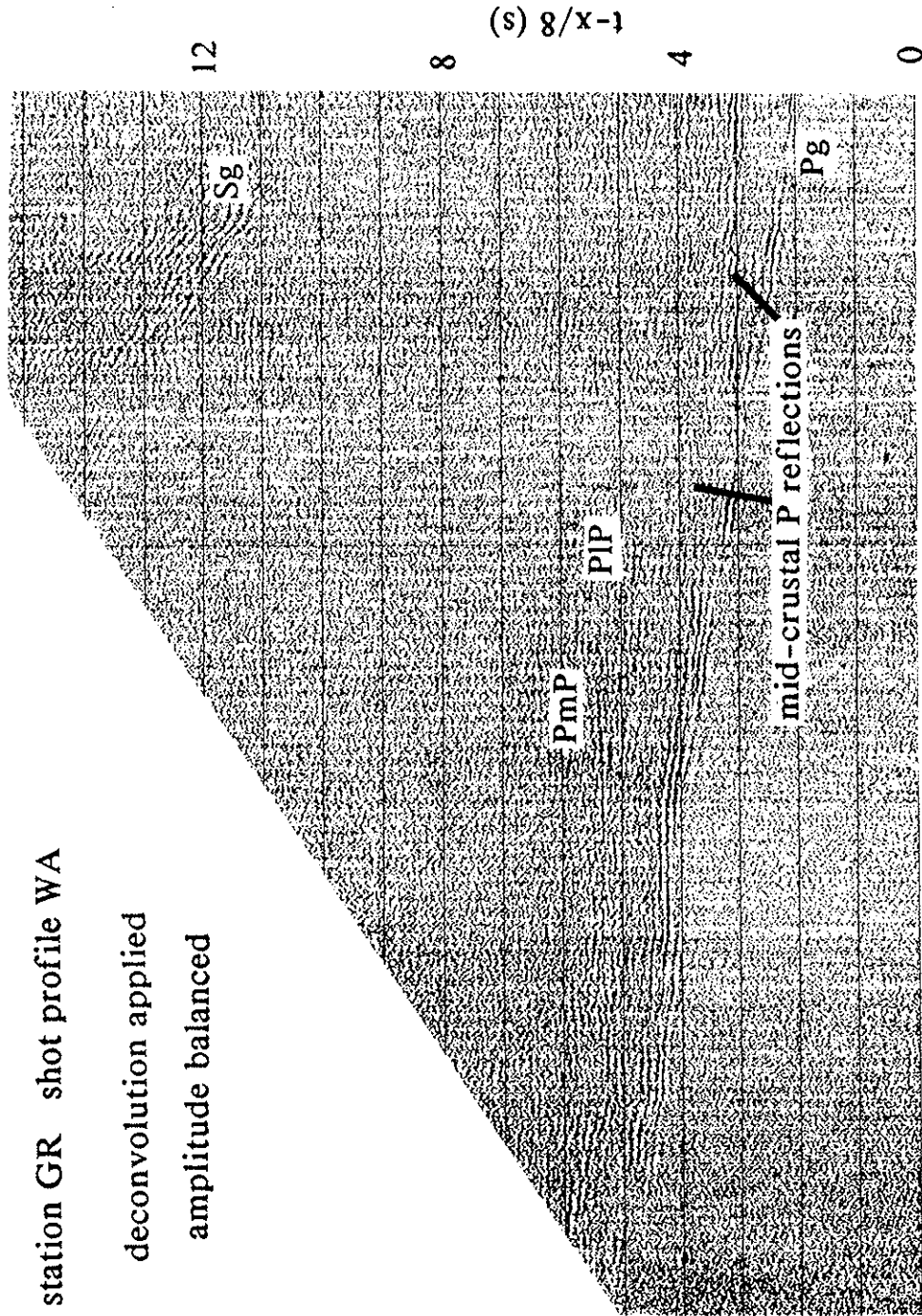


d.

station GR shot profile WA

deconvolution applied

amplitude balanced

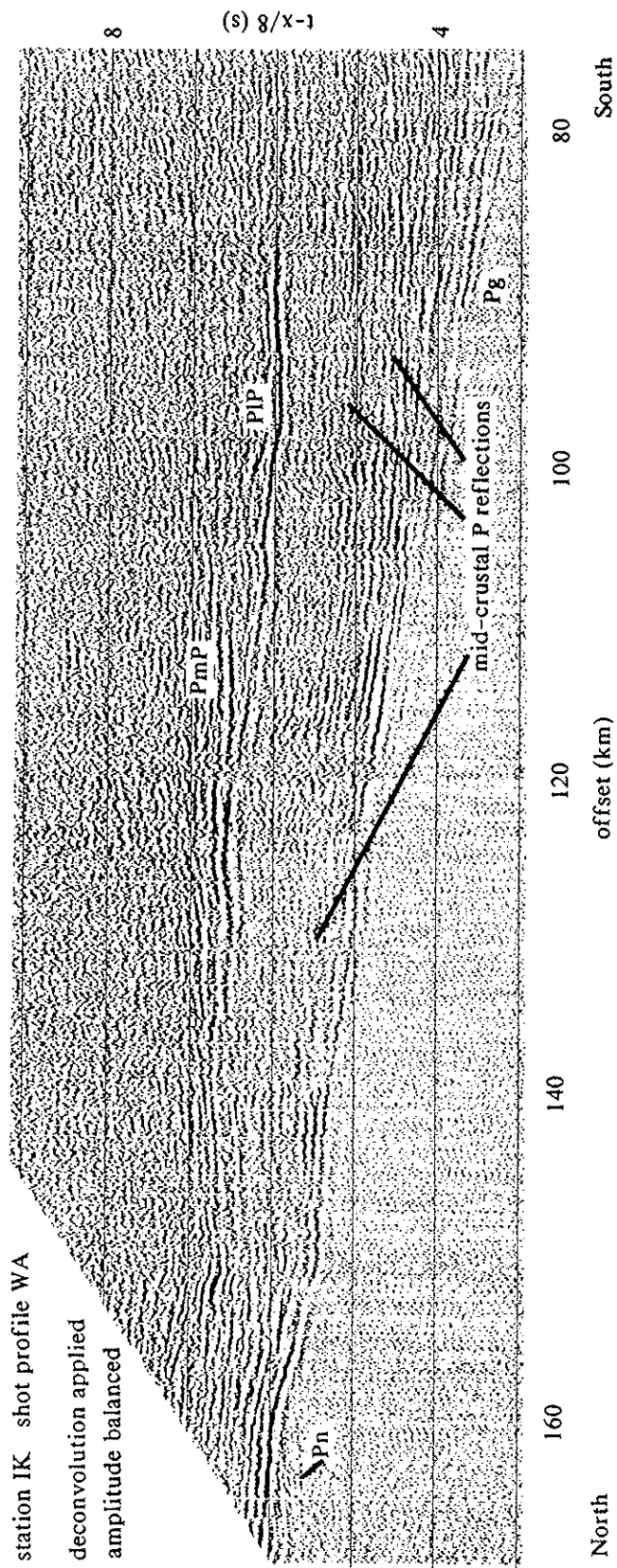


160 North
120 e.
80 South
offset (km)

Figure 1.6. Receiver gather of station IK (WA profile), vertical component, deconvolution applied, reduction velocity 8 km/s, window for P_lP and P_mP phases. Note the cross-over of the high-amplitude P_lP and P_mP phases at 120 km offset and the P_n phase.

station IK shot profile WA

deconvolution applied
amplitude balanced



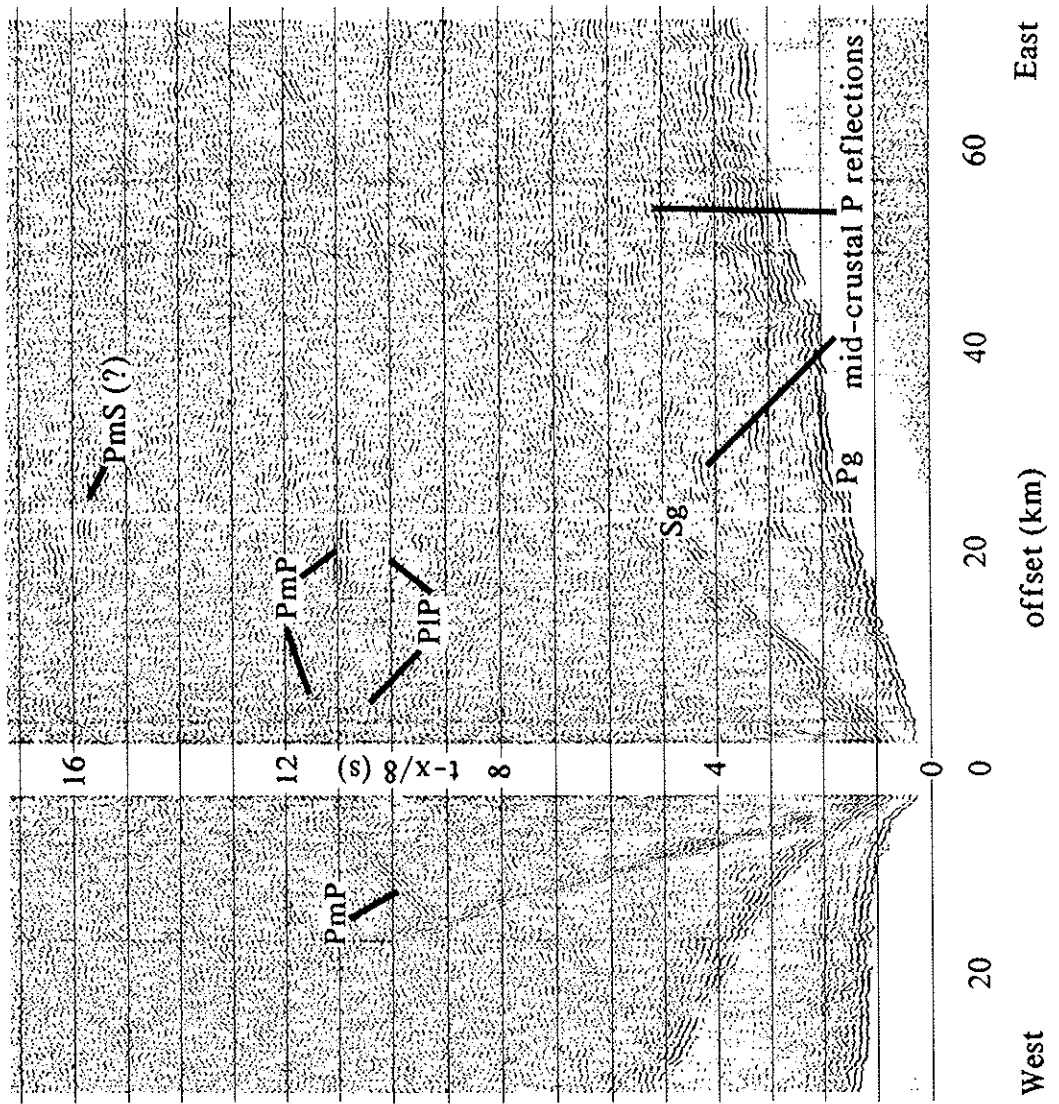
topography and, possibly, the crossing of several gneiss, granite, and anorthosite complexes (Fig. 1.2).

Many mid-crustal reflections were observed in the coast-line recordings UM, KA, IK, and GR [Fig. 1.5 a-e and 1.6]. The coherency and amplitudes of these phases are low at pre-critical distances and increase with larger offsets. One of the most prominent features of the vertical component of these coast stations is a strong, continuous lower crustal pre- and postcritical reflection (P_1P) that is crossed by an equally high-amplitude Moho reflection (P_mP) [i.e. Fig. 1.6]. Despite interruptions of its coherency at pre-critical distances, the P_1P event is traced to near-offsets. The observation of two distinct lower crustal phases (P_1P and P_mP) in the recordings of the northern section of UM [Fig. 1.5 a] is not as obvious as it is for KA and IK. A strong P_1P phase follows continuously through the section into the coherency-filtered near-offset range, while the P_mP arrives a few seconds later in a few places. Within the southern section of that recording [Fig. 1.5 b], however, both phases cross at a distance of 100 km, a rare observation in deep crustal seismic recordings that illustrate the improvement of seismic data with dense shot spacing.

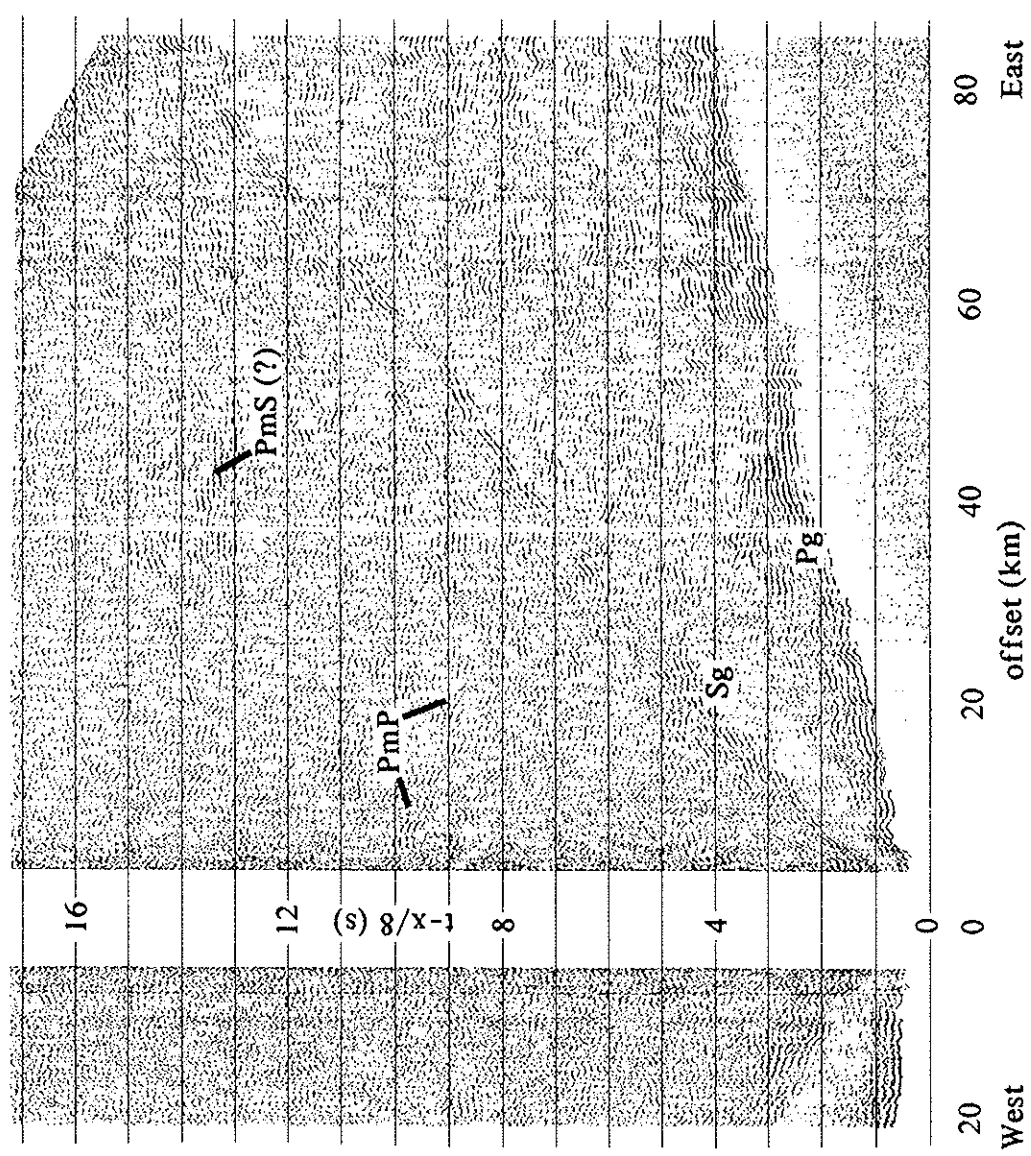
Station IK recorded an upper mantle refraction (P_n) with an apparent velocity of 8.1 to 8.3 km/s. A portion of that phase is seen through the reverberations and coda of the first arrival between offsets of 140 to 160 km [Fig. 1.6].

Figure 1.7. Receiver gathers of AM profile, vertical component, AGC 3 sec., no coherency filter applied, reduction velocity 8 km/s, a) KA, b) IK, c) AM1, d) AM7. These recordings perpendicular to the continental margin contain steeply dipping Moho arrivals inferring a dip angle of 25 to 30 degrees to the east. A low-amplitude lower crustal (PlP) phase is observed in recordings IK and AM1.

station IK shot profile AM AGC 3 sec

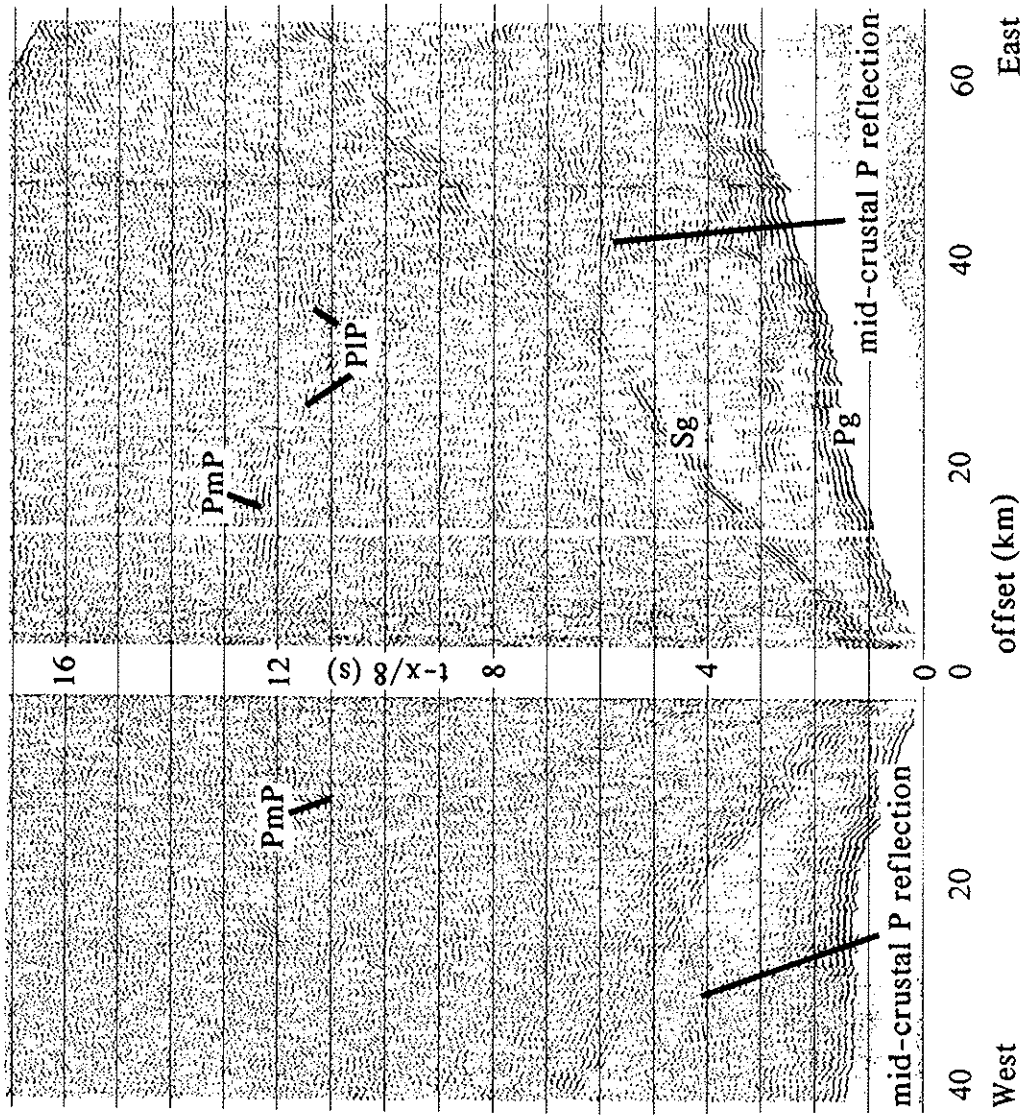


station KA shot profile AM AGC 3 sec



b. West East

station AM1 shot profile AM AGC 3 sec



c.

station AM7 shot profile AM AGC 3 sec

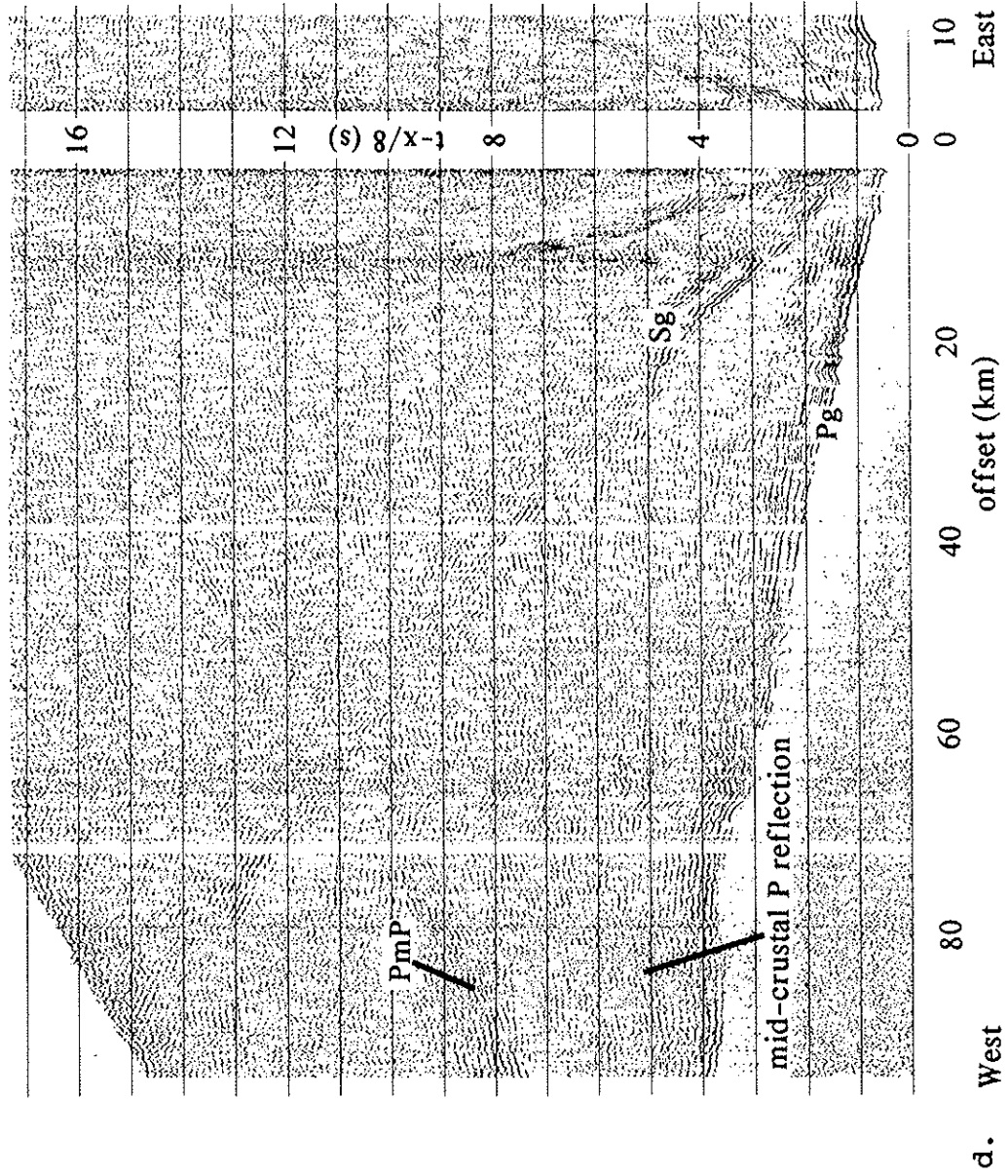
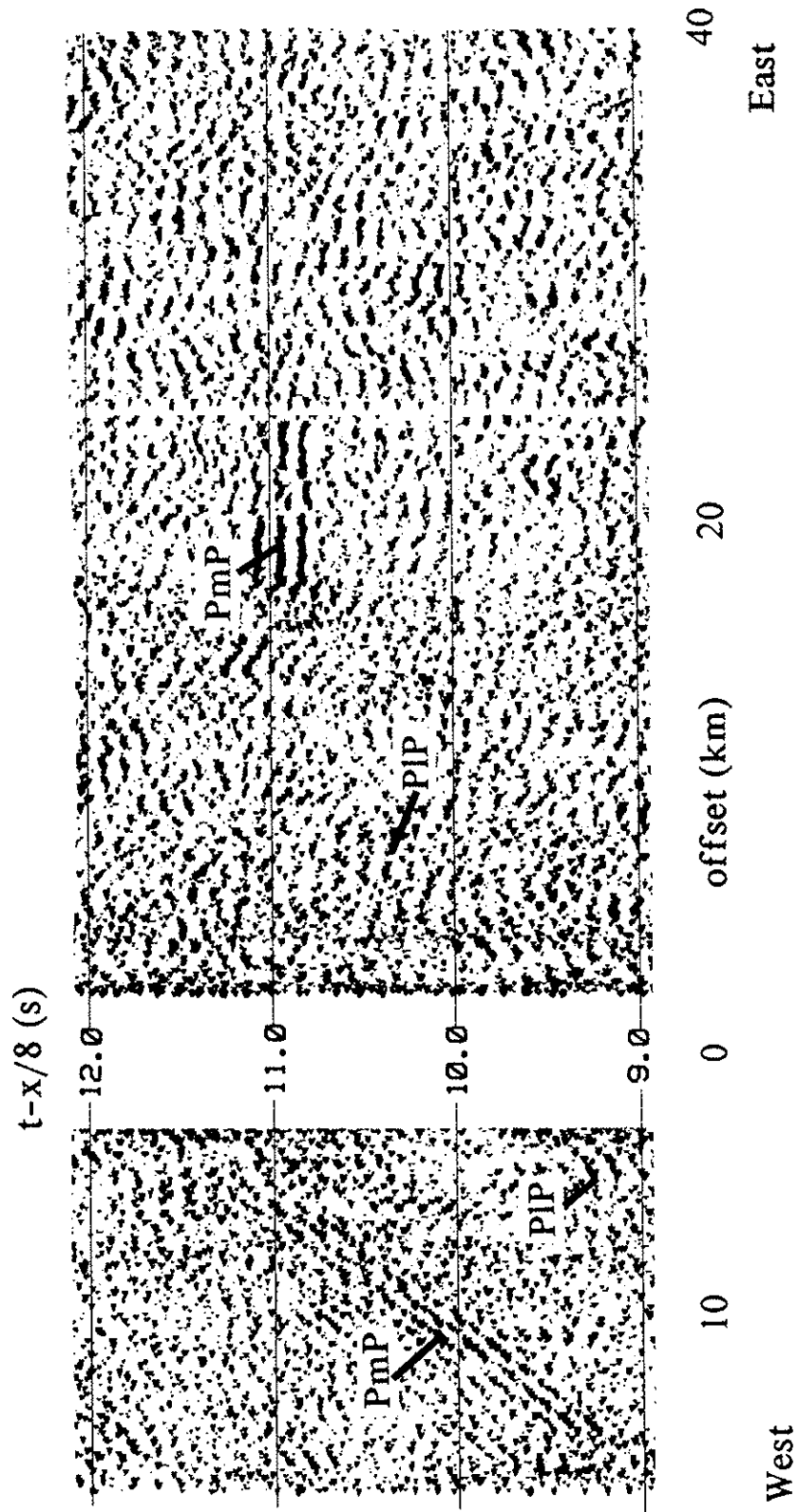


Figure 1.8. Receiver gather of station IK (AM profile), vertical component, AGC 3 sec., reduction velocity 8 km/s, window for P_tP and P_mP phases. Note the strongly eastward dipping Moho reflection.

station IK shot profile AM AGC 3 sec



The Ameralik recordings [Fig. 1.7 a-d] contain a few mid-crustal phases and, from the western stations, continuous Moho arrivals with locally large amplitudes at near-vertical offsets [Fig. 1.8]. The dip-moveout of the P_mP phases indicates a strongly eastward dipping Moho. Stations farther east recorded P_mP as well, but it consists of weaker amplitudes. Some stations recorded a low-amplitude phase slightly earlier in time than the P_mP . This phase is identified as P_lP . Note that the offset range of all fjord recordings is pre-critical for lower crustal and Moho reflections that explains the low amplitudes.

S-WAVES AND CONVERTED ENERGY. Conversion of P-energy at the water-seafloor contact generates downgoing converted S-wave energy. A strong, multi-cyclic direct wave (S_g) phase is easily observed on all sections. Station KA shows a band of coherent S-wave energy reflected from the lower crust (S_lS) or Moho (S_mS) [Fig. 1.5 c]. Continuous recording allowed energy from the previous shot to arrive in the present recording window. Within the window of 60 to 90 seconds, at offsets of 200 to 280 km, recordings of stations IK, KA, and GR reveal coherent energy within a multi-cyclic band. The apparent velocity of 4.5 to 4.7 km/s identifies this phase as a refracted shear-wave from the upper mantle (S_n) [Fig. 1.9 a,b]. A series of coherent, low-amplitude arrivals observed after the P_mP -phase on stations UM, KA and IK are possibly

Figure 1.9. Horizontal components of station KA from shot profile WA showing the Sn phase as transverse (a) and radial (b) components. The arrival is extremely multi-cyclic.

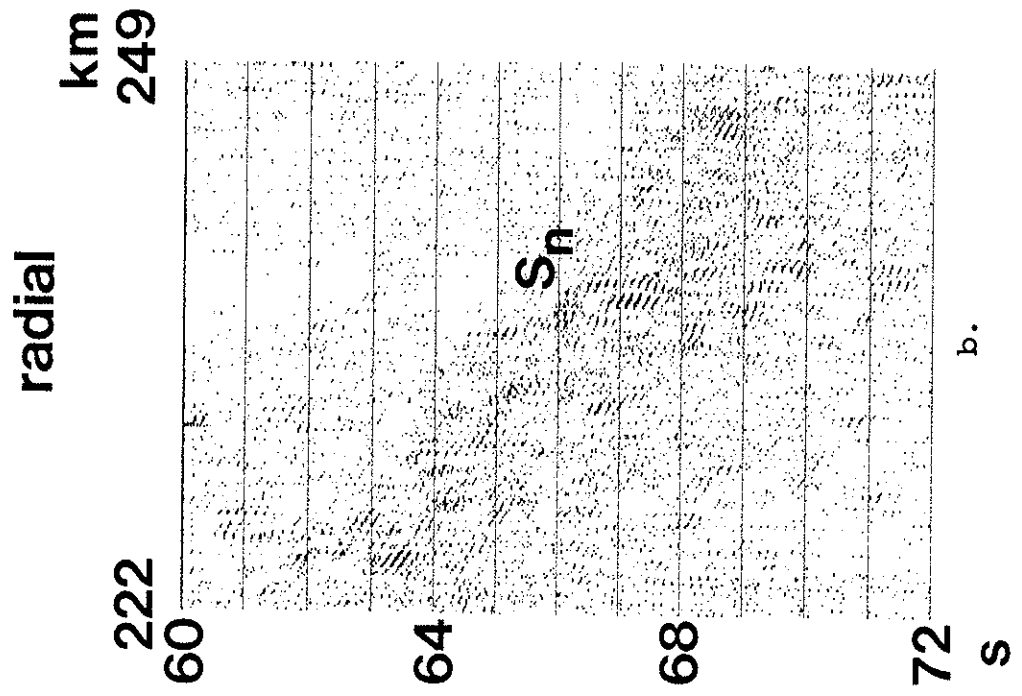
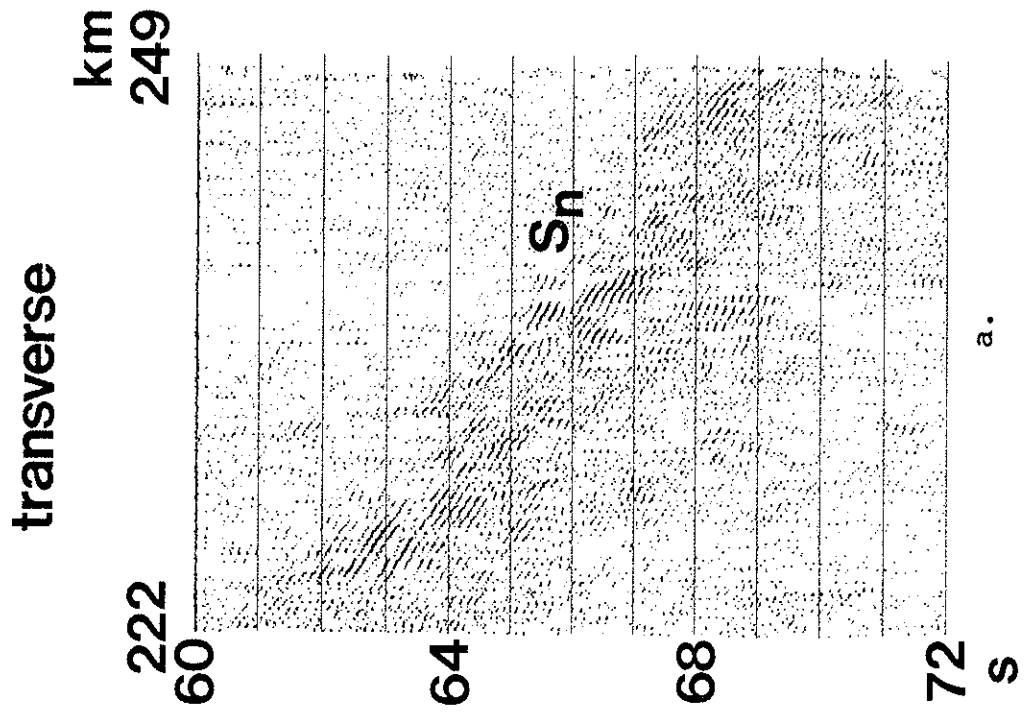
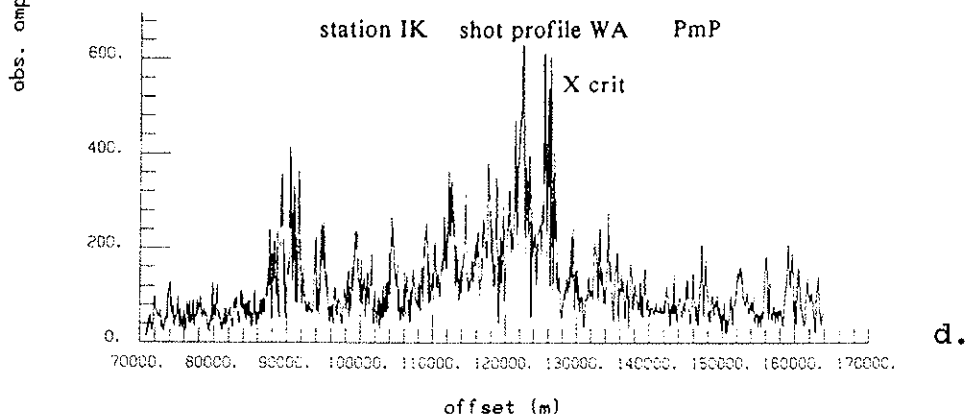
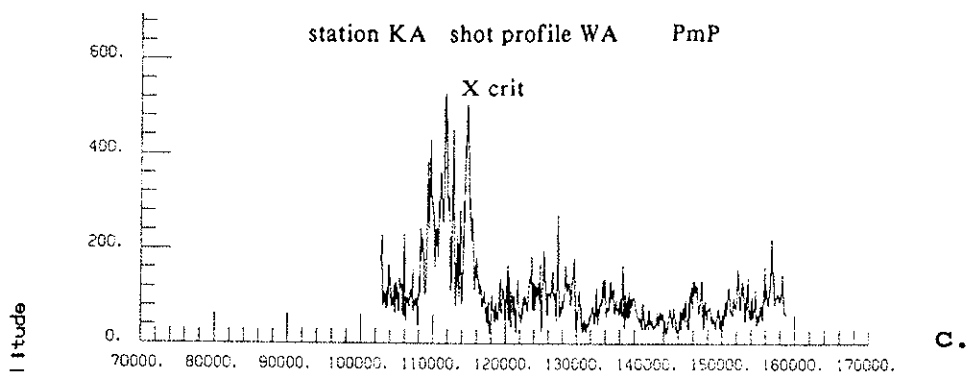
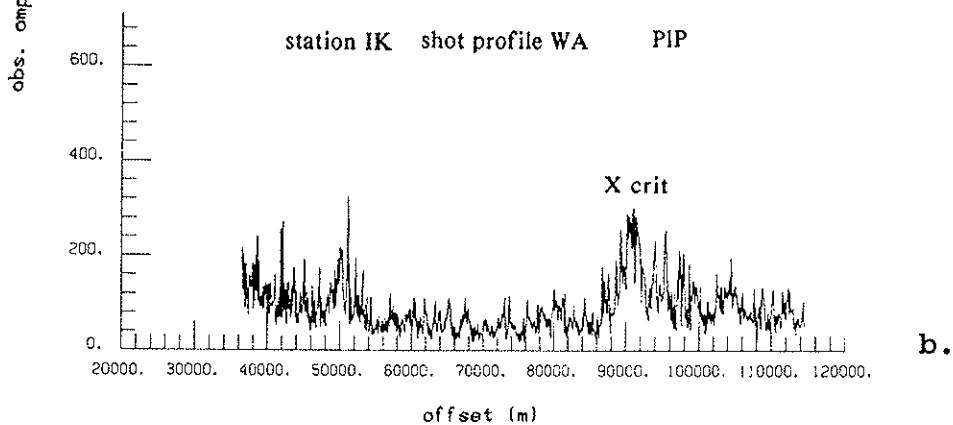
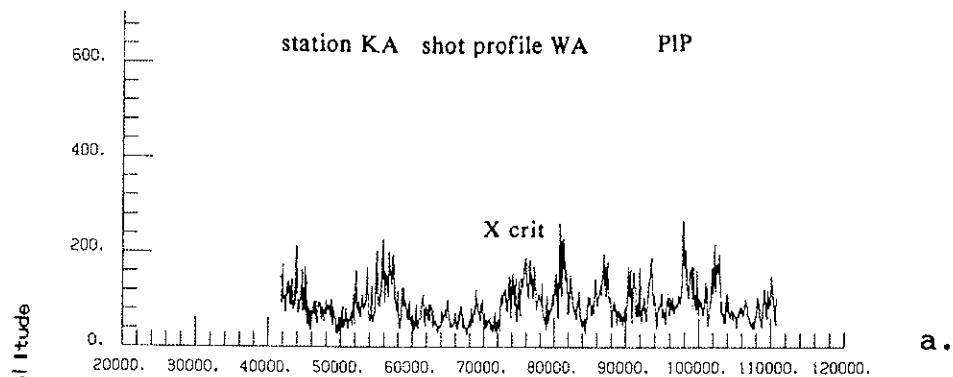


Figure 1.10. Amplitude versus offset for P_1P and P_2P phase of recordings KA (a+c) and IK (b+d). The maximum amplitudes were plotted from a time-window of 1 second following the principal arrival. The high amplitudes at smaller pre-critical offsets of a, b, and c represent the superposed direct S-wave phase. Amplitudes increase at smaller critical distance for station KA, indicating a thinner crust.



converted PS and/or SP-phases from the Moho or lower crustal layers.

FREQUENCIES AND AMPLITUDES VERSUS OFFSET. Frequency spectra over the entire offset range of single phases show an almost constant frequency of about 8 Hz for all phases. Maximum absolute amplitude versus offset plots generated over a window of 1 s for the dominant P_1P and P_mP phases of recordings KA and IK [Fig. 1.10 a-d] show that amplitudes increase approaching the respective critical distance, as expected. Notice that higher amplitudes appear at smaller offsets for station KA, which is located 12 km closer to the continental margin. Measured amplitude ranges along a single phase are valuable for later modeling and interpretation of interfaces, because coupling of air-gun source and receivers for this experiment is almost constant over all offsets.

TAU-P PROCESSING AND 1-D INVERSION

A preliminary step in the interpretation of the densely spaced, large offset wide-angle reflection data from the coast station recordings was the inversion of individual receiver gathers to estimate local depth bounds for the equivalent 1-D structure. Although the bounds are biased to some extent by local dip effects, the inversion results provide useful starting values for deriving more realistic models. The 1-D

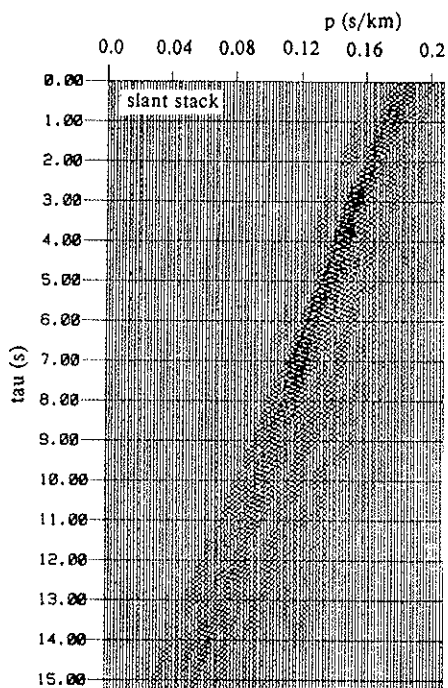
inversion method uses data chosen in the intercept-time - ray-parameter (τ - p) domain.

SLANT STACKING AND COHERENCY-FILTERING. The linear transformation of seismic data from the time-offset (t - x) domain into the τ - p domain, called slant stacking, is described in detail by McMechan and Ottolini (1980), Clayton and McMechan (1981), Diebold and Stoffa (1981), Phinney et al. (1981), and Stoffa et al. (1981). The slant stacking procedure provides an immediate estimate of apparent velocities of arrivals and identifies pre- and postcritical reflections and refractions while retaining their true amplitudes (Fig. 1.11 a-b). The signal-to-noise ratio of arrivals in the τ - p domain is enhanced by the square root of the numbers of traces in the stacking process. A muting process can be performed in the τ - p domain to eliminate arrivals within a defined slowness range (i.e. water-waves and direct waves).

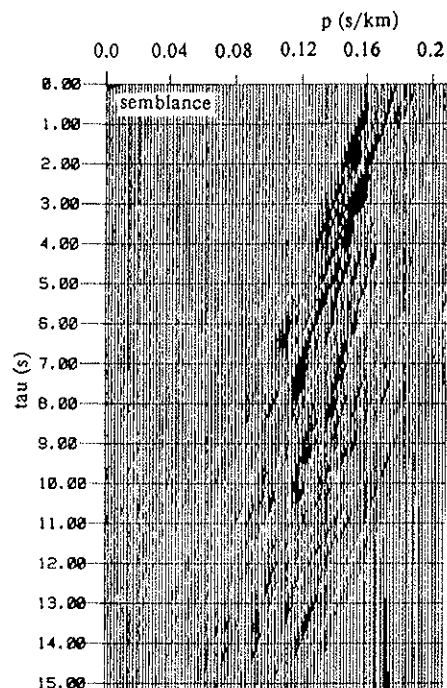
By applying a coherency filter (Stoffa et al., 1981) using the semblance calculation, regions with low coherency were zeroed out and aliasing along with other incoherent noise was suppressed. A threshold value, ranging from 0 to 1, determined what percentage of the maximum semblance value of a gather each sample had to reach to be retained in the slant stack. Otherwise, it was rejected. Figures 1.11 c-d show the isolation of high-amplitude arrivals using the coherency filter with decreasing threshold.

Figure 1.11. Slant stack (a) of offset window (92 - 115 km) of recording KA, b) semblance, c) coherency-filtered slant stack (envelope) with semblance threshold 0.98, and d) 0.90. This figure sequence shows how coherency filtering using the semblance calculation (Stoffa et al., 1981) enhances seismic signal and eliminates random noise and low-amplitude multiples. Pre- and post-critical phases are identified by their tau and ray-parameter.

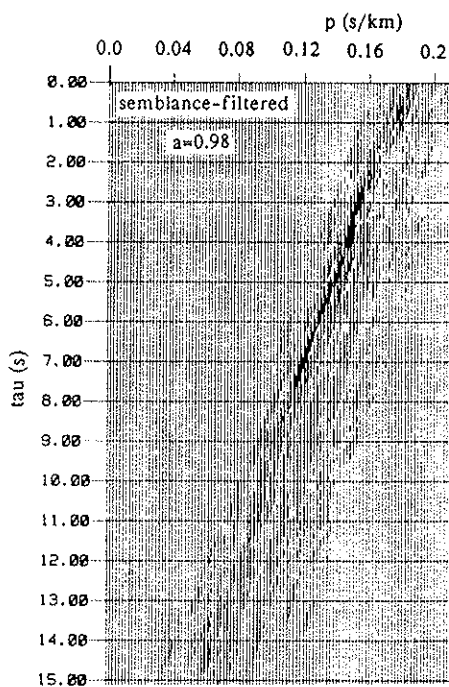
station KA shot profile WA offset window 92-115 km



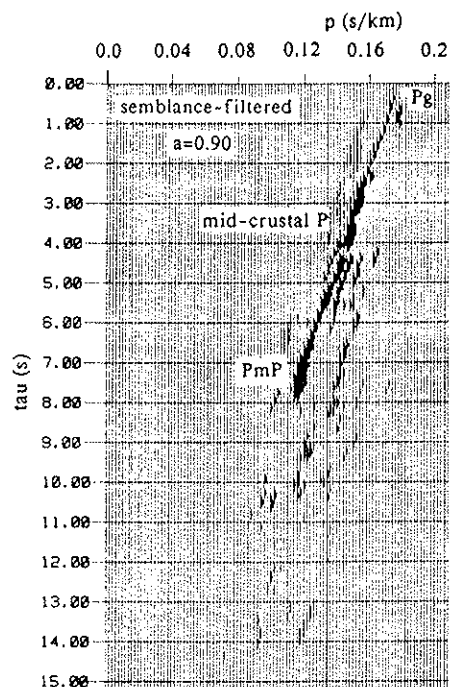
a.



b.



c.

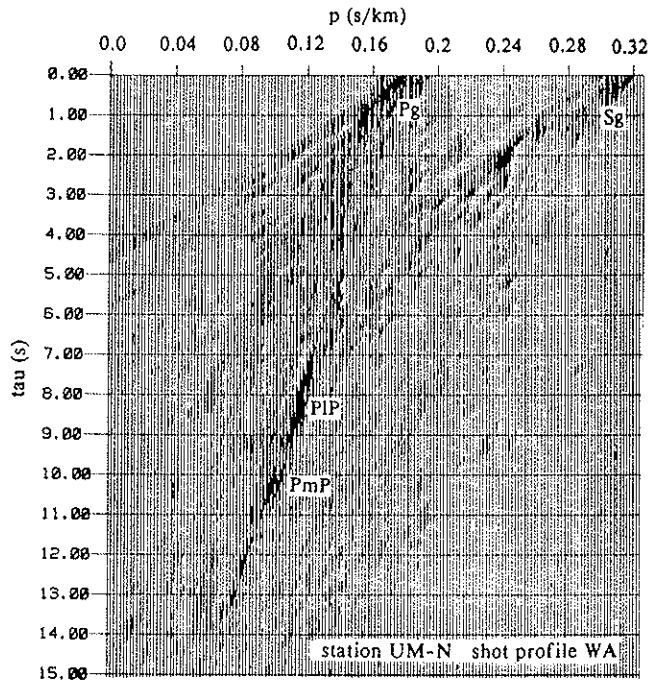


d.

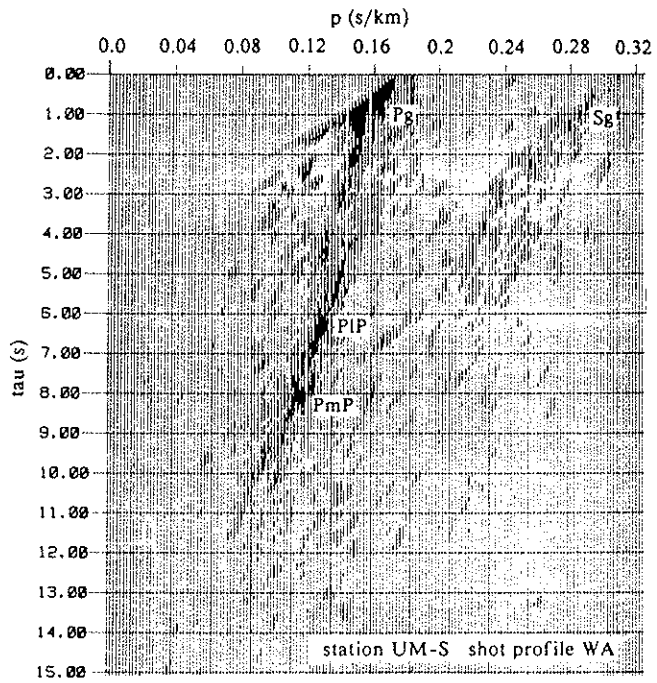
Every receiver gather was split into overlapping windows of about 20 km aperture and each window was transformed into the tau-p domain. A ray-parameter window ranged from 0.0 to 0.35 s/km to include S-wave arrivals. An increment of 0.002 s/km was chosen to include as many arrivals as possible for the inversion, which is necessary to obtain a finer resolution of the tau-p trajectories. The coherency-filtered windows of one shot direction with respect to the receiver location were subsequently summed. Splitting the shots into several windows before slant stacking has the advantage of obtaining control of unavoidable averaging effects by transforming data from a large offset range. Each window in the tau-p domain can be interpreted individually which is important in areas of intense heterogeneity. Also, coherent arrivals are roughly linear when the chosen window aperture is small enough, which increases the value of the semblance.

TAU-P ARRIVALS. Plots of coherency-filtered and vertically stacked slant stacks show a strong P-wave branch and a weaker S-wave branch [Fig. 1.12 a-e]. Several arrivals are matched with the respective time-offset gather. The P_g -phase consists of several high-amplitude clusters between ray-parameters 0.185 and 0.14 s/km (apparent velocities of 5.4 and 7.14 km/s) reflecting the variations in the first break alignment of the offset gather. Several mid-crustal phases show strong amplitudes at critical to post-critical angles

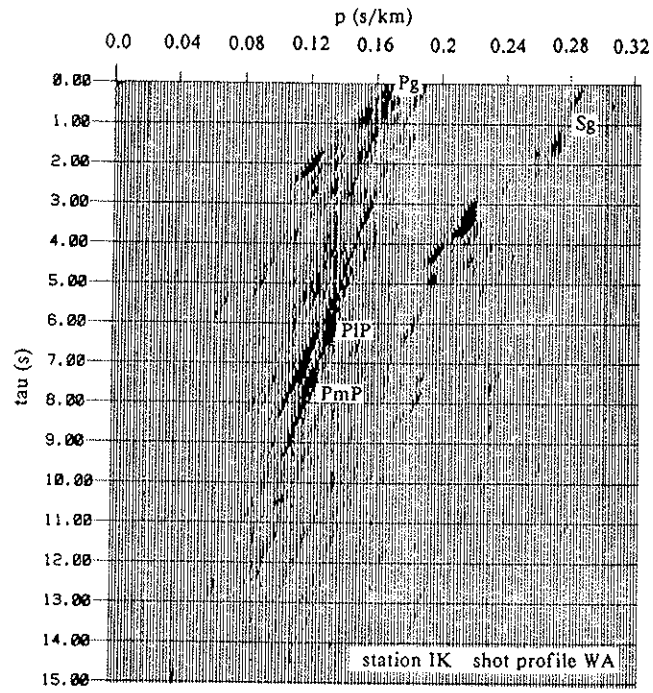
Figure 1.12. Coherency-filtered, vertically stacked tau-p gathers (envelope), a) UM-North, b) UM-South, c) IK, d) KA, e) GR. Recordings UM, KA, and IK contain high-amplitude P_1P and P_mP arrivals. The strongest mid-crustal phases appear in recordings KA and GR, indicating localized mid-crustal discontinuities. The S-wave branches contain mostly S_g and, in case of station KA, a S_1S or S_mS phase.



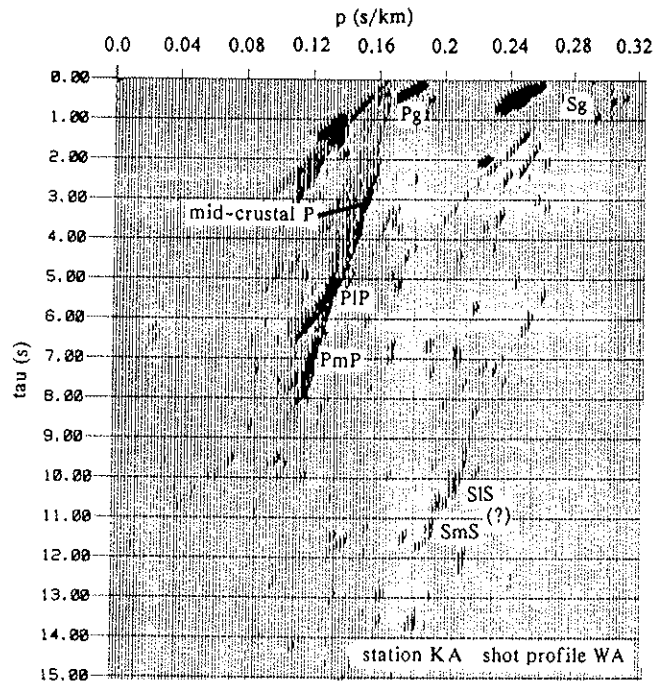
a.



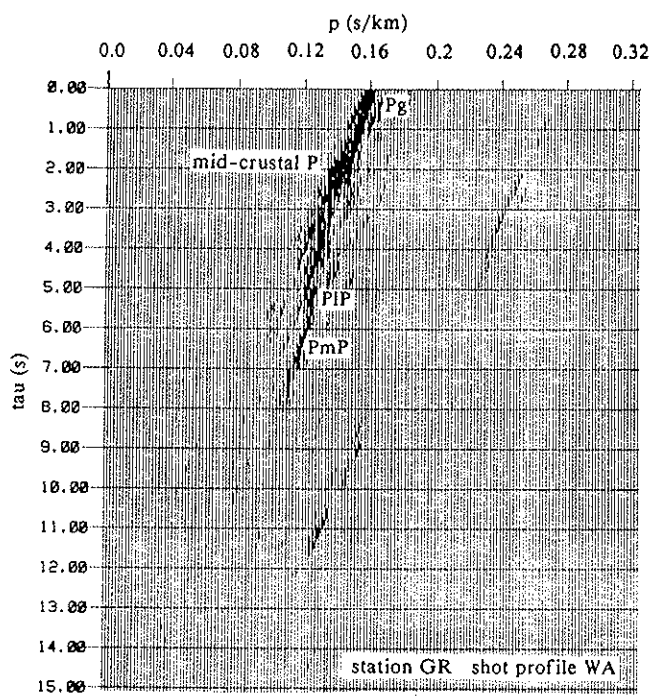
b.



c.



d.



e.

indicated by their ray-parameters of 0.16 to 0.14 s/km (apparent velocities of 6.25 to 7.14 km/s). Local dipping structure possibly generates a smearing effect of mid-crustal phases in recording GR [Fig. 1.12 e] which makes an identification difficult. Tau-p gathers of stations UM, IK, and KA show clear images of pre- and post-critical reflections from the lower crust and Moho [Fig. 1.12 a-d]. The P_1P and P_mP phases appear as high-amplitude events, corresponding to the relatively high energy returning from those interfaces at critical and post-critical distances.

1-D INVERSION. I used an extremal inversion method (Bessonova, 1974; Dorman, 1979; Garmany, 1979; Hawman et al., 1990; Hawman and Phinney, 1991) based on picks in the tau-p domain to invert for minimum and maximum depths of horizontal layers of constant slownesses. Picks in the tau-p domain were made at the onset of each arrival. Uncertainties assigned to intercept-time picks were based on the signal bandwidths (Kennett and Orcutt, 1976) and S/N ratio of the arrivals. They did not incorporate scatter due to local dip effects. These uncertainties ranged between 0.08 and 0.2 s.

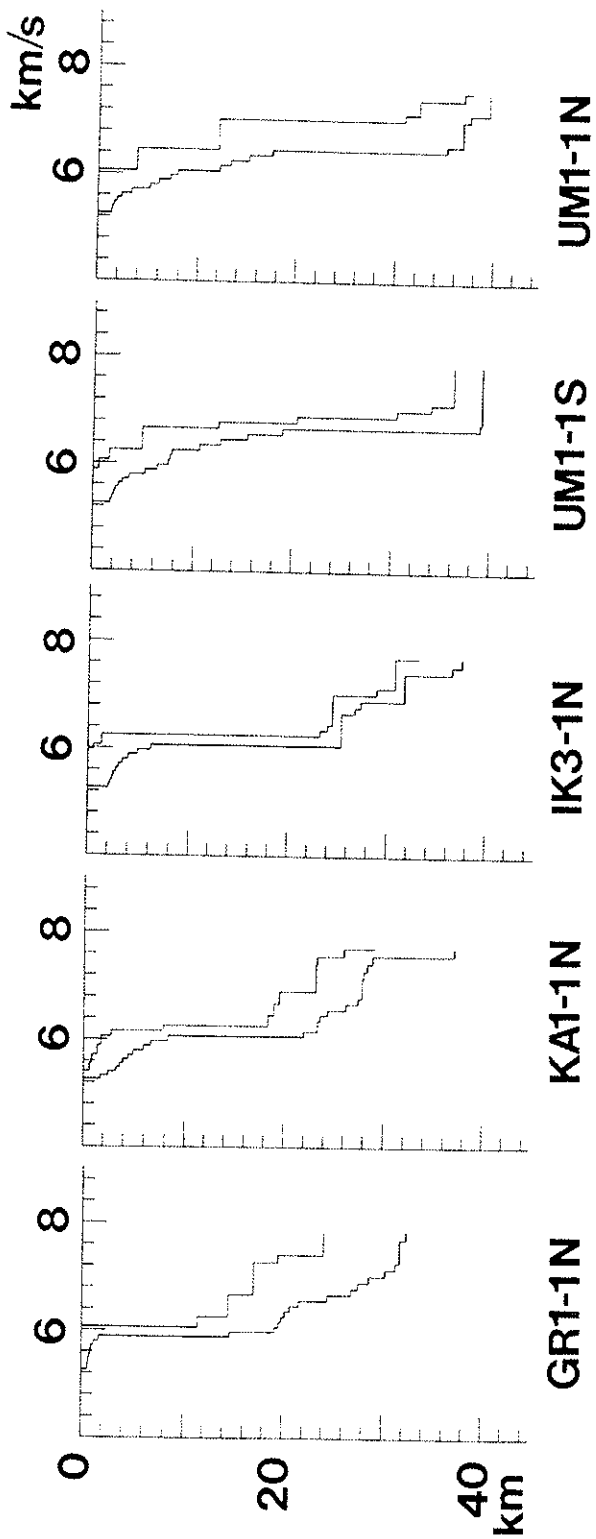
The model parameterization consisted of a stack of layers of constant slownesses (slowness increment: 0.001 s/km) with slownesses decreasing (velocities increasing) with depth. The slowness for the uppermost layer was chosen from the near-offset first break velocities. The minimum slowness was chosen

to allow for the possibility of high velocities near the base of the crust. The model is parameterized such that the number of layers is larger than the number of data picks to more closely approximate the real earth. Tau-p picks from refracted as well as pre- and post-critical reflected phases went into the inversion routine. By choosing as many pre- and post-critical reflections from a single interface as possible, the depth bounds are better constrained.

The extremal method produced a 1-D inverse model [Fig. 1.13] that incorporates data from a large offset range of a crust that is probably extremely heterogeneous and structured in a 3-D sense. However, this analysis serves as a preliminary but valuable step to estimate crustal depths. Several mid-crustal discontinuities appear with varying depths, indicating a complex structure with lateral inhomogeneities at mid-crustal levels along the mid-points of the recordings. A first order discontinuity or a strong, narrow gradient zone, 6 to 8 km above the Moho, is derived from the strong, coherent P_1P -phase from stations KA and IK. Results from the inversion infer a crustal depth of 30 to 40 km that increases northward. The uppermost crust contains a high velocity gradient. Velocities exceed 6.0 km/s below depths of 4 to 6 km for most recordings, but, thereafter, the gradient remains low for the remainder of the crust. The bottom of the crust consists of a zone with velocities between 7.2 and 7.8 km/s.

The profiles were located near the passive continental

Figure 1.13. Results of extremal inversion. Curves illustrate minimum and maximum depth bounds for each layer of constant slowness. Slowness is displayed as layer velocity. Note the increase in crustal thickness from station GR to station UM. Inversion models of stations KA and IK show clearly the high-velocity zone (> 7.2 km/s) above the Moho.



margin where the crust/mantle boundary becomes shallower toward the oceanic crust. Therefore, the results of the inversion are biased by a slope of the Moho perpendicular to the profile. However, results from extremal inversion place useful constraints on starting models for more complete analyses in terms of 2-D and 3-D structure.

2-D INVERSION AND FORWARD MODELING

METHODS AND PARAMETERS. The 2-D travel-time inverse modeling scheme (Zelt and Smith, submitted paper) used in this study applies a fast generalized linear inversion that provides estimates of model parameter uncertainties, resolution, and non-uniqueness. The iterative character of the method involves the forward steps of the inverse approach, such as the ray-tracing algorithm (Cerveny et al., 1977) and an adjustment of model parameters by applying a damped least-square inversion of the travel-times. A detailed description of algorithm and parameters is given in Zelt and Smith (submitted paper).

A model for the inversion is parameterized as a set of layers consisting of trapezoidal blocks with velocities and depths defined for each corner. Block boundaries can be smoothed to avoid scattering and focussing of ray-paths. Take-off angles for the ray-tracing part of the inversion are calculated automatically. A damped least-square method is used

to update the interpolated boundary and velocity nodes for each iteration. To quantitatively evaluate the best approach, RMS travel-time residuals and parameter resolution are calculated allowing estimation of the reliability of the model with respect to real data. The stability of the inversion scheme is increased by reducing the number of independent model parameters, i.e. by keeping the velocity gradient or thickness of a layer fixed or by maintaining a zero velocity discontinuity at a layer boundary, if there is evidence for that in the data. Another technique to increase stability is to first invert for the uppermost crust, then invert arrivals from the middle and lower crust, keeping the parameters for the overlying layers fixed.

INVERSION OF AMERALIK PROFILE. The Ameralik profile was modeled for four principal groups of arrivals, the Pg phase, mid-crustal, lower crustal, and Moho P-wave reflections. The observed travel-time picks were equally spaced with a 1 km horizontal increment and assigned with uncertainties in time of 0.1 to 0.25 s. These uncertainties are rather large, but the variations of the first arrival due to static shifts and the multi-cyclic character of most arrivals prohibit smaller error bounds. Static shifts could not be incorporated into the model, because receivers, located on land, were not in line with the sources. I used a layer stripping approach as opposed to simultaneous inversion of all arrivals from all recordings.

Modeling began with arrivals of the uppermost crust and proceeded with middle and lower crustal phases.

The uppermost crust was initially modeled with two layers, each consisting of 6 boundary and velocity nodes with velocities increasing from 5.5 to 5.8 km/s for the first layer. The uppermost velocity was determined by near-offset apparent velocities of the first arrival and the replacement velocity of the water body for static correction. The first arrival does not provide clear evidence for a reflection from an interface a few kilometers below the surface, but the gradual change in apparent velocities implies a rapid decrease of the velocity gradient with depth. To better model the velocity change, I inserted a second layer at a depth of 1 km in the westernmost part of the section and 2 km in the central and eastern portion. This layer was given a velocity of 6.0 km/s increasing to 6.3 km/s vertically. The RMS travel-time residual reached a minimum of 0.185 s after the 4th iteration. Because of small-scale changes of apparent velocities of the first arrival due to static problems and lateral heterogeneities, the number of boundary and velocity nodes was doubled to a block length of 10 km to provide better resolution. In that case, the best fit was reached after the 5th iteration with a travel-time residual of 0.185 s. Another increase of boundary and velocity nodes, however, did not improve the result. Note, that the RMS travel-time residual was reduced from 0.246 s for the starting model to 0.185 s for

the final upper crustal model, which lies within the uncertainty of 0.2 s for the first arrival. The final upper crustal model consists of lateral velocity variations ranging from 4.7 to 5.6 km/s for the surface and 5.6 to 5.9 km/s for the bottom of the first layer at 2 km depth. Velocities of the second layer increase slightly to about 6.2 km/s at the western portion.

For inverting the travel-times for mid-crustal arrivals, the model parameters of the uppermost crustal model were held constant. The initial model consisted of a layer boundary between 10 km deep at the western end and 30 km deep at the eastern end of the model. Evidence for this dipping layer was derived from the intercept-time and dip move-out of the arrivals. The velocity gradient obtained from the inversion of the first arrivals was adopted, but it could vary through the iterations. After obtaining results from the first iteration, the number of nodes was doubled. A final model was obtained after the 4th iteration in which all travel-times fit within the observed uncertainties. The RMS travel-time residual reached 0.026 s, well within the uncertainty range.

The lower crust is represented by weak, very localized reflections from the top of a lower crustal zone and strong arrivals from the Moho. Again, the model parameters of the final model for the middle and upper crust were maintained. A total of 6 boundary and velocity nodes as independent parameters for the lower crustal layer was implemented. The

initial velocities for the 3rd layer increased vertically from 6.5 to 6.8 km/s. The initial depth increased from 23 km at the western end of the model to 50 km at the center (80 km distance) and remained constant toward the eastern end. I doubled the number of nodes after the first iteration process. Because of the dipping structure in the west and the observation of arrivals from that dipping interface, nodes in that part of the model were denser to allow for more variations. The final model converged after three iterations with all travel-times matched with the picks and a resulting RMS travel-time residual of 0.063 s. Velocities within the 3rd layer increased slightly, ranging from 6.6 to 6.8 km/s for the western half. Due to a lack of arrivals from layer 3 of recordings AM4 to AM7 (east), the nodes of the eastern half of the model did not change.

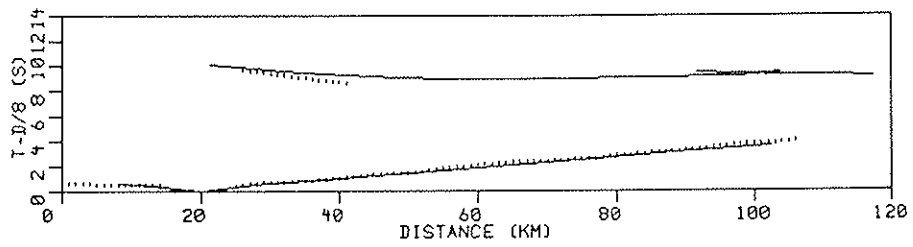
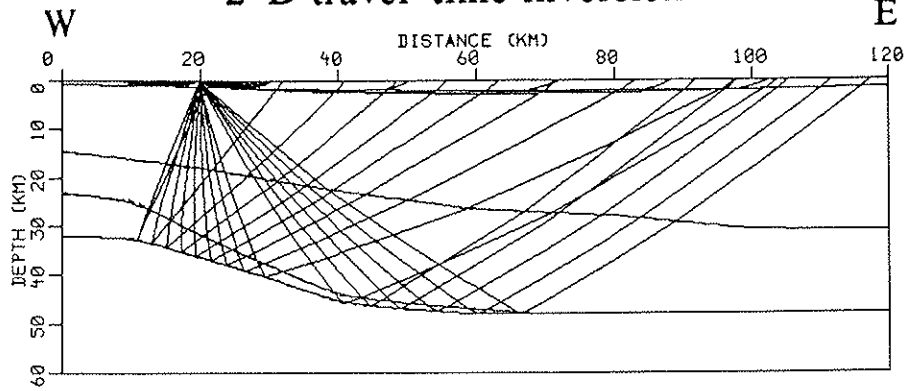
The initial boundary nodes for the Moho reflector were set deep enough to avoid possible crossings with the bottom of layer 3 during the iteration process. The number of nodes were the same as for the layer above. As already detected in the 1-D inversion of the coast-line data, a high-velocity zone at the bottom of the crust can be inferred at least for the western part of the Ameralik profile. Initial velocities for that zone range from 7.4 km/s at the top to 7.7 km/s at the bottom. After 5 iterations, the RMS travel-time residual reached 0.17 s. The depth of the Moho interface decreased to a depth of 32 km at the westernmost end and 48 km at the

bottom of the Moho slope. The depth of 48 km was held constant toward the eastern boundary of the model, due to lack of arrivals. Note that the initial velocities of 7.4 to 7.7 km/s did not change significantly. I tested the inversion by inserting lower velocities into the initial model. Regardless of the initial velocities the inversion continued to converge to higher velocities indicating that these high velocities are well controlled within an estimated uncertainty of 0.2 km/s.

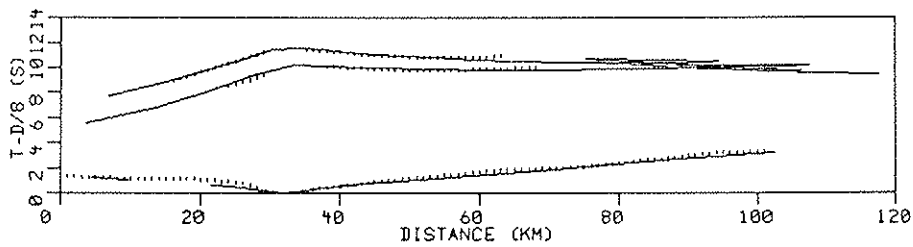
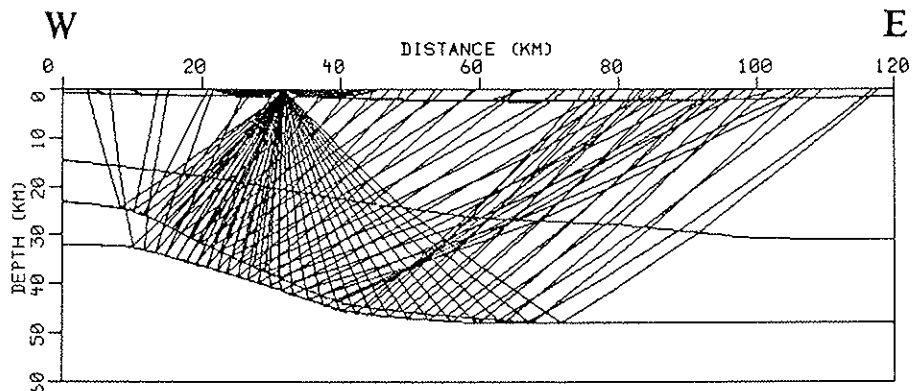
Plots of rays that were shot through the final model as well as observed and calculated travel-times of individual receiver locations [Fig. 1.14 a-h] show the good fit of the mid- and lower crustal phases. The final crustal velocity model [Fig. 1.16 a] contains steeply eastward dipping mid-crustal and lower crustal structures for the western half of the model. Thick lines on the layer interfaces illustrate the spatial coverage of the reflection midpoints. A high-velocity zone (7.4 to 7.8 km/s) of 2 to 8 km thickness exists above the Moho discontinuity. The Moho dips with a maximum of 25 to 30° eastward. High vertical velocity gradients were modeled for the uppermost crust and for the bottom of the crust in the western half of the model. Velocities of the middle crust increase slightly with depth from 6.4 to 6.9 km/s. Note, that the lower crustal depths and velocities of the eastern half are held constant toward the eastern edge of the model. A lack of arrivals prohibited better constraints.

Figure 1.14. 2-D travel-time inversion for AM profile. Rays were shot through final model. Stippled lines are observed travel-times, straight line are calculated travel-times. a) KA, b) IK, c) AM1, d) AM2, e) AM4, f) AM5, g) AM6, and h) AM7. Calculated travel-times are continuous and extend over the range of the observed, because an automatic determination of take-off angles was used as opposed to two-point ray-tracing (Zelt and Smith, submitted paper). The inversion, however, is applied only for the offset range of observed travel-times. Although more mid-crustal reflection are observed in the data, only those that could be correlated over at least two stations were included in the inversion.

2-D travel-time inversion

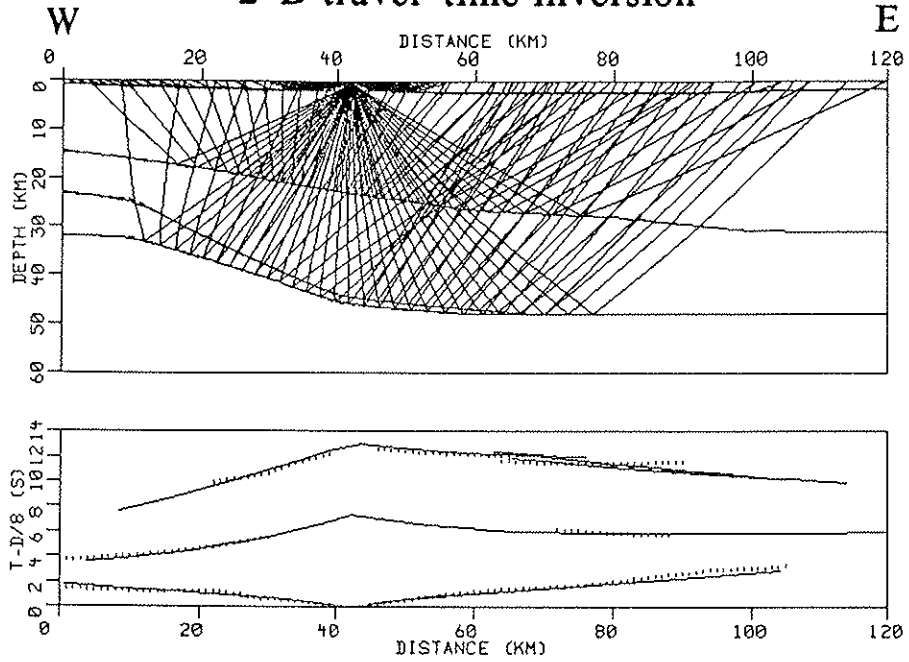


a. station KA shot profile AM

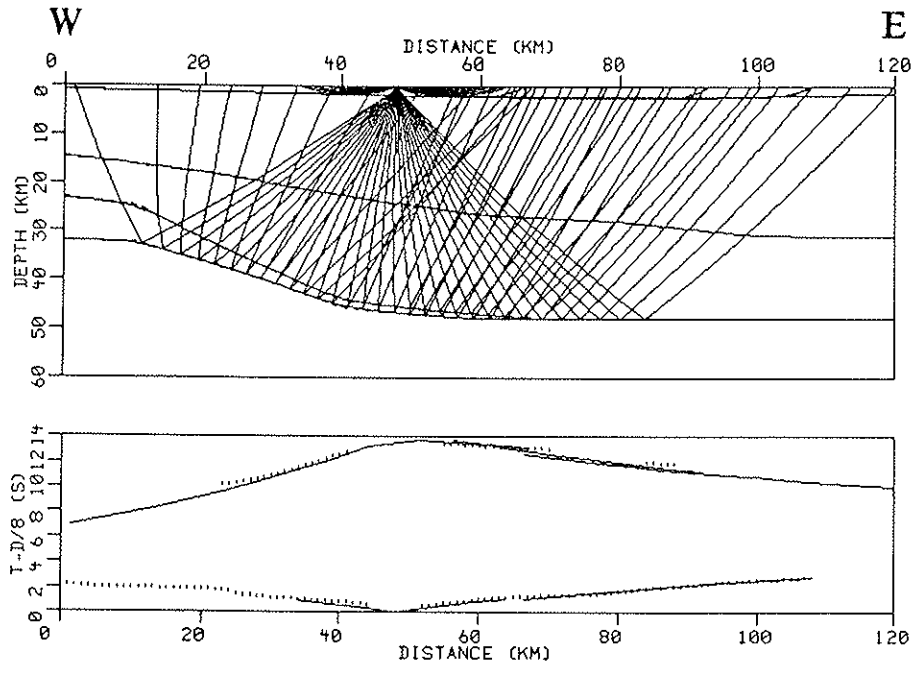


b. station IK shot profile AM

2-D travel-time inversion

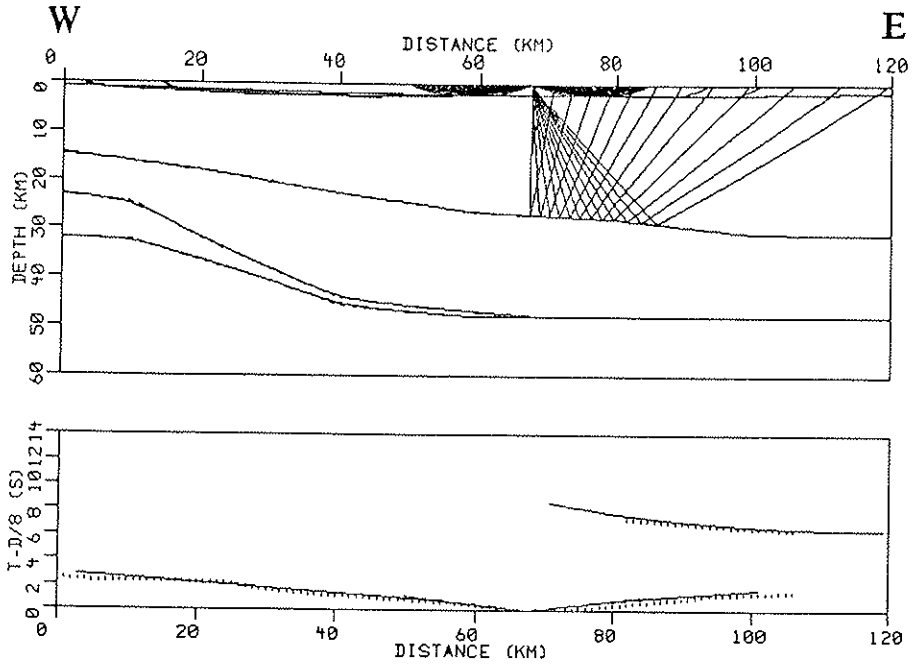


c. station AM1 shot profile AM

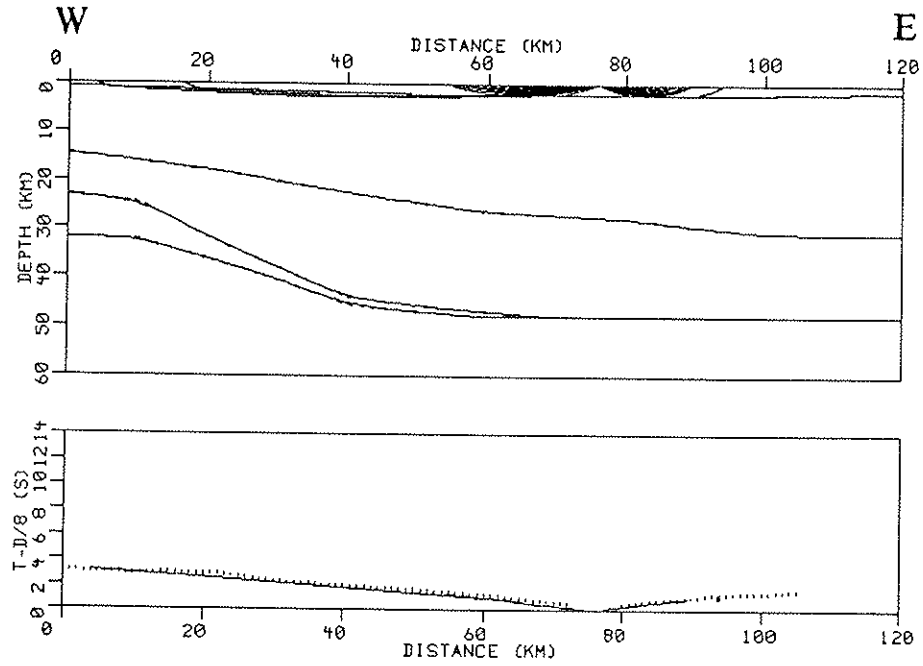


d. station AM2 shot profile AM

2-D travel-time inversion

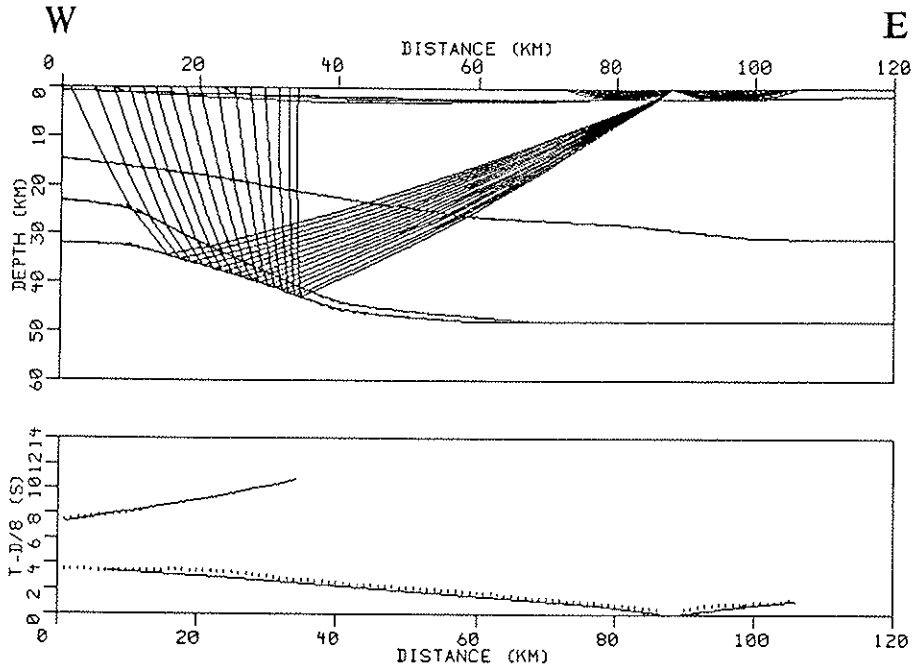


e. station AM4 shot profile AM

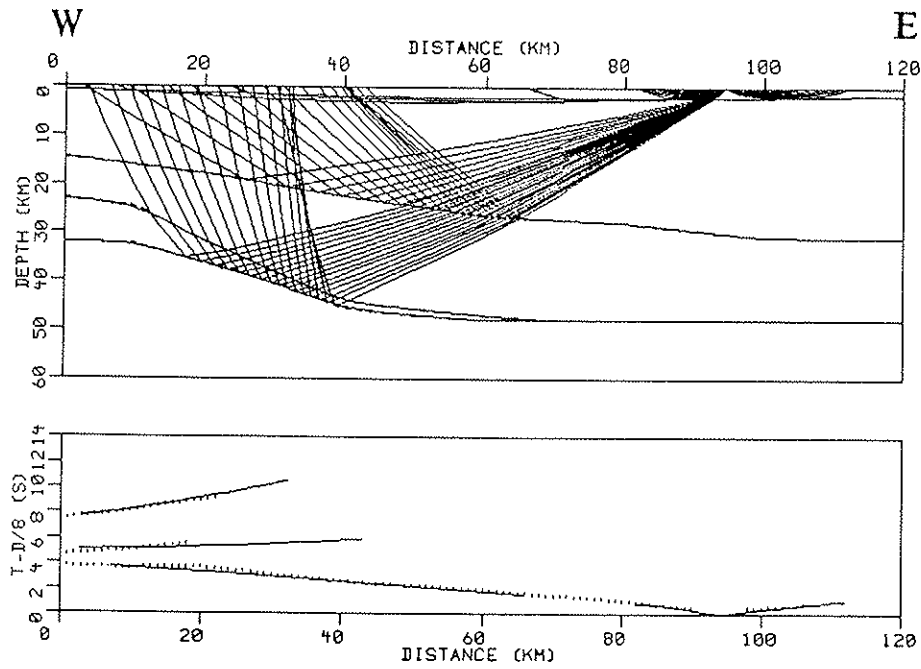


f. station AM5 shot profile AM

2-D travel-time inversion



g. station AM6 shot profile AM



h. station AM7 shot profile AM

INVERSION OF COAST-LINE PROFILE. Because the location and geometry of the coastline profile is parallel to the strike direction of the continental margin, any modeling in a 2-D sense is a rather difficult undertaking. Despite obvious problems, a 2-D inversion was attempted for various reasons. The observation of continuous, high-amplitude lower crustal and Moho arrivals suggest an extended lower crustal feature that can be modeled in terms of its velocity and thickness. The large offset range from near-vertical to post-critical places better constraints on the velocities than for the Ameralik data. Although the calculations of absolute layer depths might be biased to some degree by the east-dipping geometry of seismic interfaces within the transitional crust, a general trend of N-S dipping structures can be estimated. The southern end of profile WA has a 3-D control because it crosses the western end of profile AM.

Any 2-D modeling scheme requires a pure 2-D structure with colinear receiver and sources. A non-colinear acquisition geometry and dipping structures out of plane would violate the principle of geometrical 2-D ray-tracing and inversion. Therefore, the approach taken with the 2-D travel-time inversion was a little different than for the Ameralik line. Also, I did not include arrivals from receiver IK despite their good quality, because this station is located too far out of the plane.

An initial model was created based on the results from

the 1-D tau-p inversion. It included a northward dipping crust-mantle boundary with greatest dip in the southern half of the model, a high-velocity zone at the bottom of the crust and three mid-crustal interfaces with small velocity discontinuities and layers of small velocity gradients. As a first approach, each series of observed travel-time arrivals was modeled by iterative inversion. The model was parameterized with 6 layers, the number of boundary nodes was kept constant with a distance increment of 40 km, except for the northernmost part of the model where the increment was increased to 80 km for layers 2 to 6 due to the lack of observable arrivals. As opposed to modeling of the Ameralik line where the model was derived from un-manipulated inversion, the inversion results in this case were corrected by manual smoothing and straightening of layer boundaries that were obviously affected by the line geometry. It soon became obvious that local dipping structures of interfaces were derived from individual travel-time curves at small offsets. Near-offset arrival curves whose hyperbola caused bending of interfaces that could not be constrained from other stations were rejected thereafter to allow rays to travel to the next interface correctly.

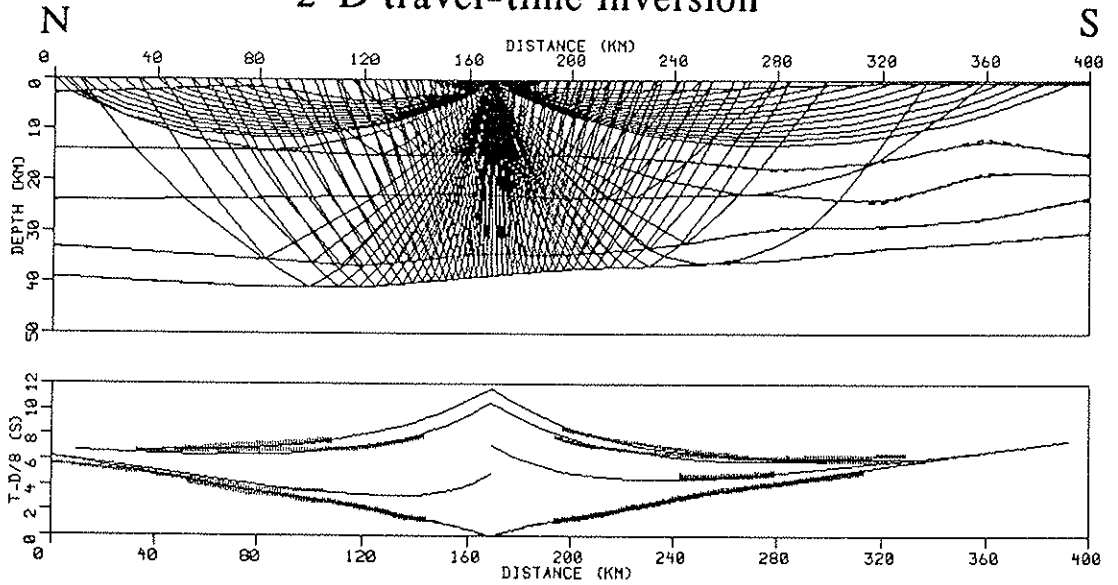
After the inversion was completed for all arrivals of stations UM, KA, and GR, the final inversion model served as a highly improved starting model for the next series of iterations. This time, velocity nodes that were

unrealistically low or high were corrected manually and kept fixed during subsequent iterations. Also, the number of velocity nodes was increased for layers for which far-offset recordings suggest a more alternating depth relief of their boundaries, such as the boundaries of layer 5. Most travel-time branches match the observed data for farther offsets [Fig. 1.15 a-c].

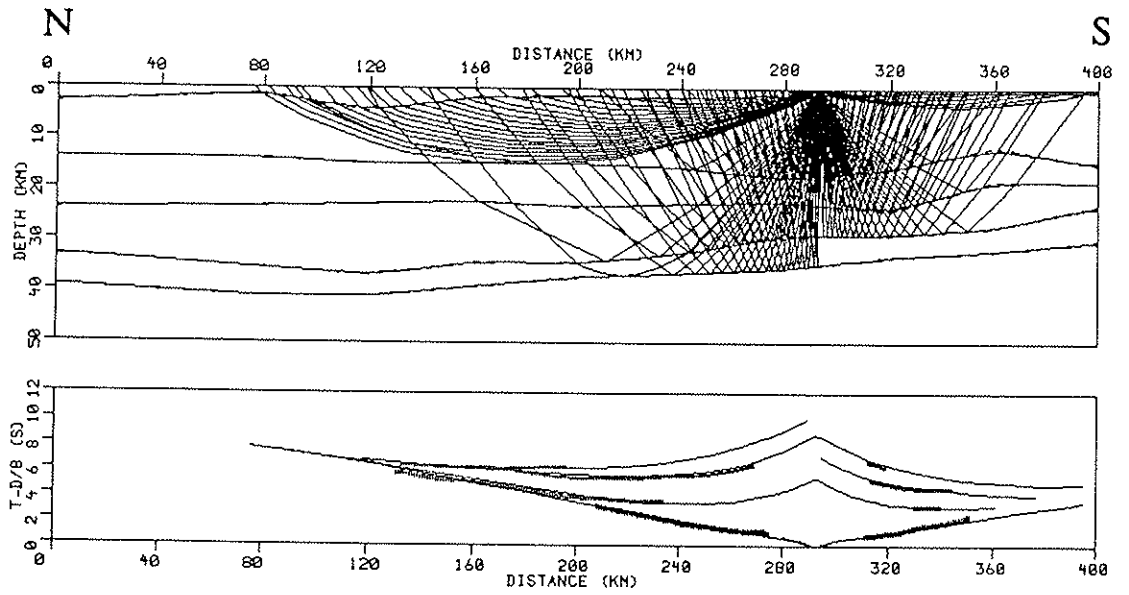
In the final model, the majority of travel-time picks was matched by rejection of near-offset arrivals [Fig. 1.16 b]. The first arrival, modeled as refractions from the first and second layer, was fit even better than for the Ameralik profile, due to fewer problems related to elevation statics. A sedimentary sequence could not be observed in the data. Therefore, velocities of 6.3 to 6.5 km/s represent velocities of the upper basement. A large vertical velocity gradient exists within the uppermost crust with velocities increasing to 6.4 km/s within 1 km depth. The undulating shape of layer 3 in the southern third of the model is possibly due to 3-D related effects. A continuous high-velocity zone with thickness of 3 to 8 km and a velocity of 7.4 to 7.7 km/s, increasing with depth, was modeled. As I did for the Ameralik model, I replaced the high velocities of this layer with lower initial velocities and inverted over several iterations. This test showed that the inversion was most stable at higher velocities. The Moho depth reaches 30 to 41 km with depth moderately increasing northward for the southern two-thirds of

Figure 1.15. 2-D travel-time inversion for WA profile. Rays were shot through final model. For further explanation see figure caption 1.14., a) UM, b) KA, c) GR.

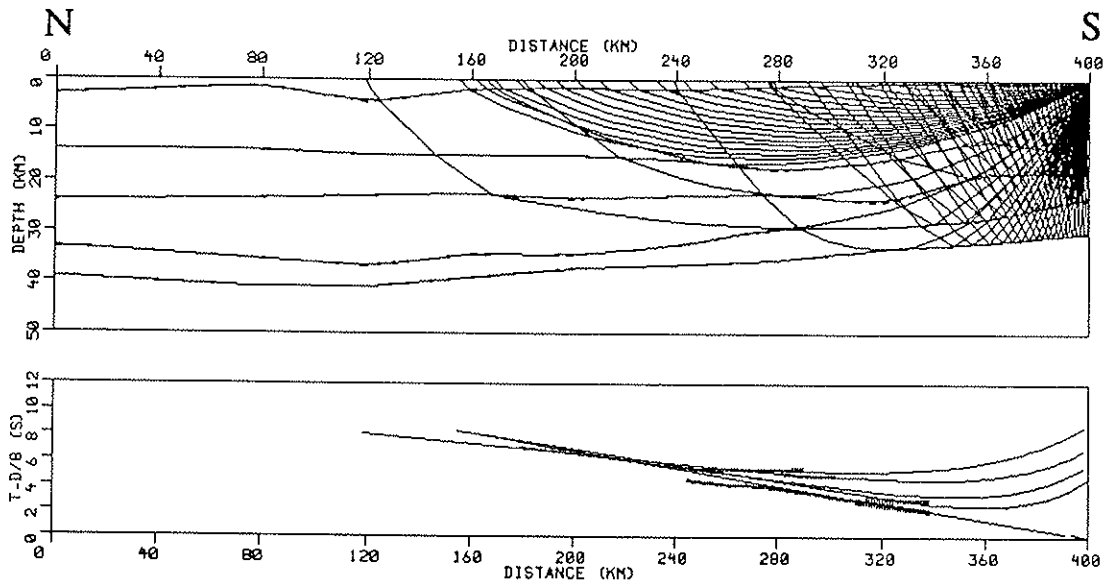
2-D travel-time inversion



a. station UM shot profile WA

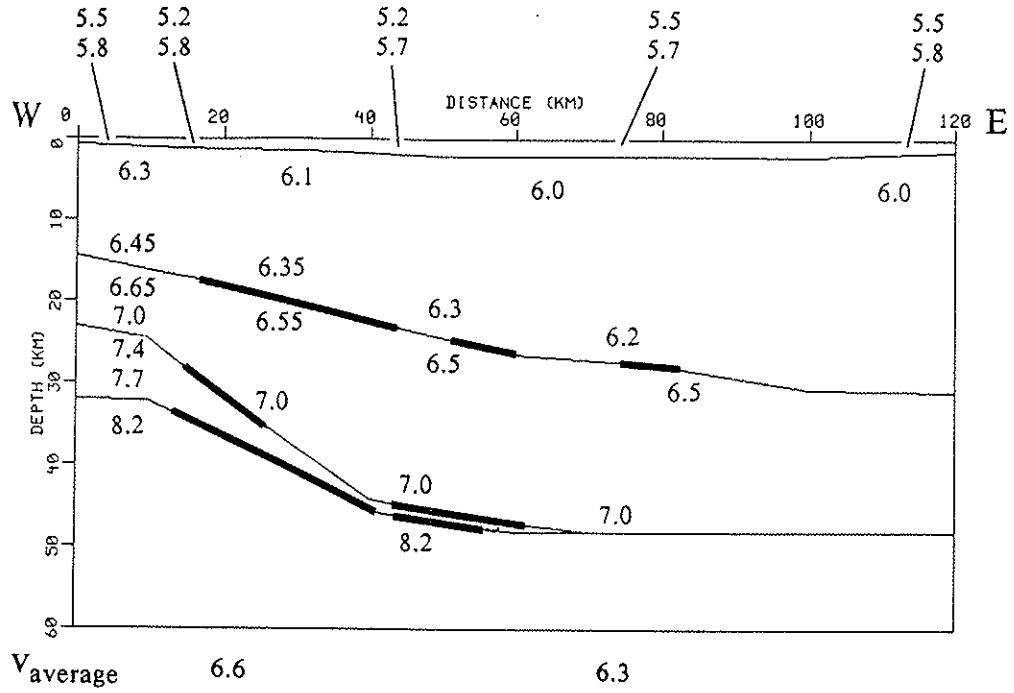


b. station KA shot profile WA

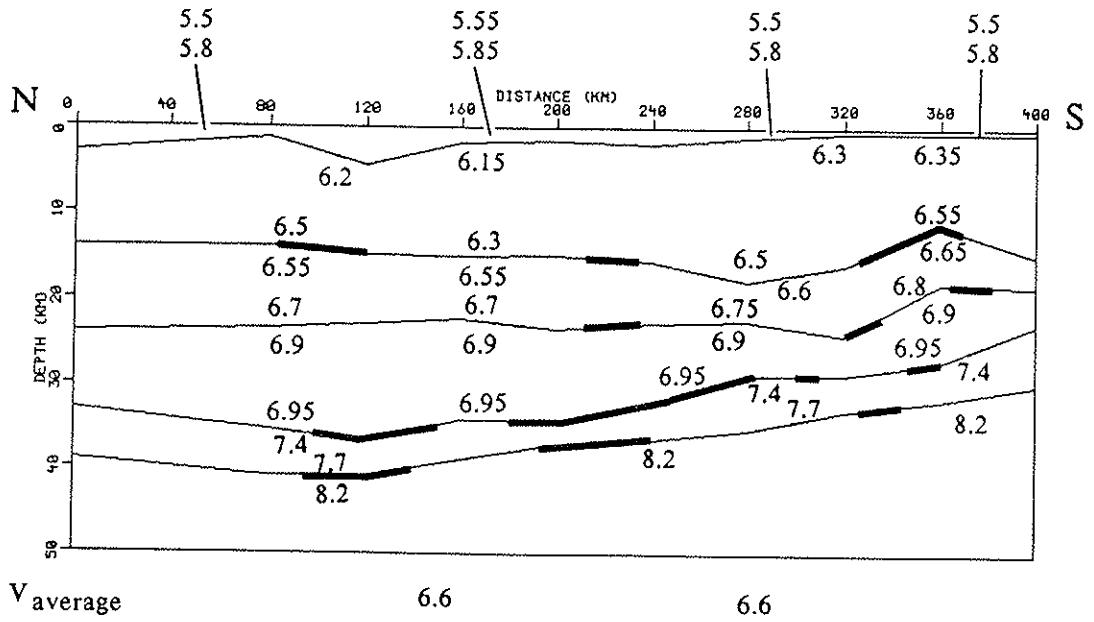


c. station GR shot profile WA

Figure 1.16. Final 2-D P-wave velocity models for profiles AM (a) and WA (b) derived from travel-time inversion. Because of 3-D effects, the inversion of arrivals from the coastline stations were manipulated so that near-offset arrivals were ignored and oscillations of interfaces due to interpolated arrivals was straightened. Actual coverage of interfaces from seismic arrivals is indicated as thick lines. Note the high-velocity zone at the bottom of the transitional crust.



a. velocity model AM



b. velocity model WA

the section and a rather constant depth of 39 to 41 km for the northernmost part.

DISCUSSION OF RESULTS. First, I compare the results from the 1-D extremal inversion [Fig. 1.13] with the 2-D travel-time inversion model of profile WA [Fig. 1.16 b]. As mentioned above, the recordings of station IK were not included in the 2-D modeling process because of its location farther inland over deeper crust than station KA. The depth bounds of dipping lower crustal and Moho discontinuities appear 3 to 5 km shallower in the 1-D models of recordings GR, KA, and UM-North where the shot spread is located in down-dip direction. In this case, the lower apparent velocities and lower intercept-times of the arrivals will force the inversion to shallower depths. The opposite effect is the case in recording UM-South where the shot spread lies in up-dip direction of the Moho boundary. Here, the crustal depth of the reflection mid-points derived from the 1-D inversion is 1-2 km greater than in the 2-D model (36-38 km). The high velocities of 6.9 to 7.7 km/s for the lower half of the crustal 2-D model lie within the bounds of the 1-D models. As a result of this comparison, it can be concluded that inverting for 1-D velocity-depth bounds provides useful initial boundary and velocity nodes for a 2-D inversion. 1-D models from several stations along dipping structure can provide estimates of dip angles.

By comparing the 2-D inversion results of profiles AM

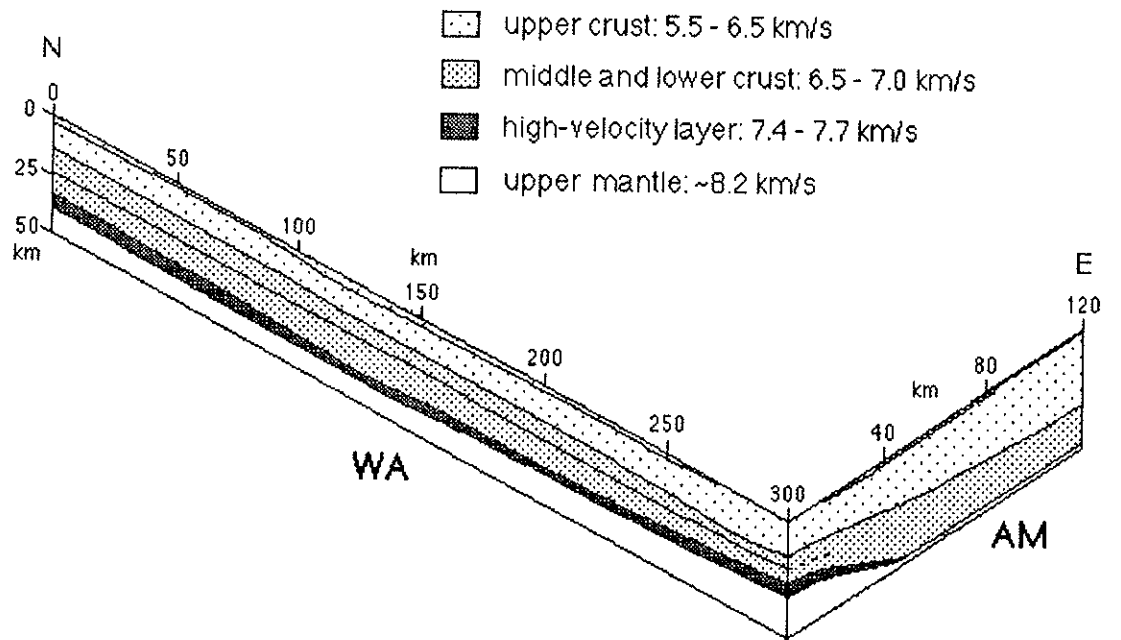
and WA [Fig. 1.16 a,b], one finds that the lower crustal depth boundaries match within variations of 2 km, but the match of mid-crustal boundaries and velocities is poorer. Most arrivals from the middle crust were observed only at critical distances and from stations of the central and eastern part of line AM. Boundaries without returning rays were extrapolated. Also, a perfect fit of the entire arrival curves of profile WA was not achieved because I rejected nearest-offset arrivals in favor of medium- and far-offset phases to minimize the effect of the horizontal offset of source and receivers.

Both the coastline model and the western half of the Ameralik model show similar features, such as a high velocity gradient for the uppermost crust and a moderate increase of velocities for the middle crust [Fig. 1.17]. A 3 to 8 km thick high-velocity zone at the bottom of the crust is a well controlled feature of model WA, while it is less constrained in model AM, due to the lack of high-amplitude arrivals. Lateral velocity variations are on the order of 0.3 km/s at the maximum within a layer, which indicates that assignment of arrivals from different stations to a certain layer boundary is correct.

2-D travel-time inversion is proven to be an extremely useful tool in interpreting this wide-angle data set. Most travel-time picks were modeled within their uncertainties and quantitative information about the quality of the models was given. Accurate phase correlation, however, remains as a

Figure 1.17. Fence diagram of the perpendicular P-wave velocity models. Because of better display, only the northern 300 km of profile WA are included. For more exact velocity information, see Figure 1.16. Velocities for the upper crust exhibit a strong gradient for the uppermost 2-3 km.

P-wave velocity structure of passive margin off SW Greenland



factor of non-uniqueness with every travel-time inversion and forward modeling scheme. The next step is to model amplitudes of seismic arrivals to either confirm or to cause re-adjustments of the travel-time model in terms of impedance contrasts.

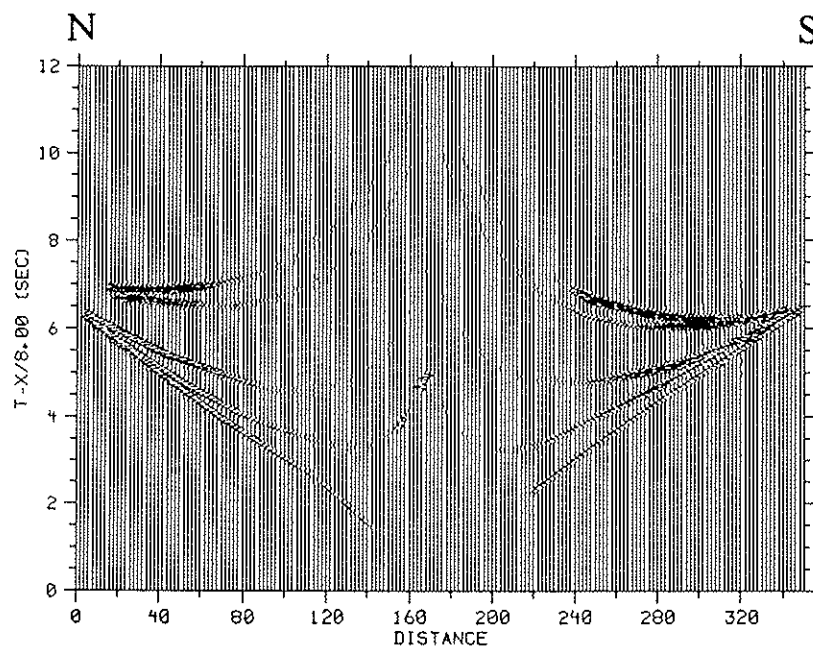
FORWARD MODELING FOR AMPLITUDES. Synthetic seismograms were calculated using an asymptotic ray algorithm (Cerveny, 1977) and the reflectivity method (Fuchs and Mueller, 1971). Amplitudes from ray theory calculated for each arrival are not as accurate (Cerveny, 1979) as from the reflectivity algorithm or a finite difference scheme, but they allow the comparison of synthetic with observed seismograms qualitatively.

Figures 1.18 a,b illustrate the results of ray-theoretical amplitude calculations of recordings UM and KA of shot profile WA for vertical components. The entire range of the final models derived from travel-time inversion was included in the calculation, even zones of interfaces that were interpolated between observed arrivals. Therefore, a lack of synthetic amplitudes from these zones is another indication for the quality of the model. In general, the amplitude distribution of the calculated seismograms follows the observed amplitudes. The fit is better for far offsets reaching critical distance.

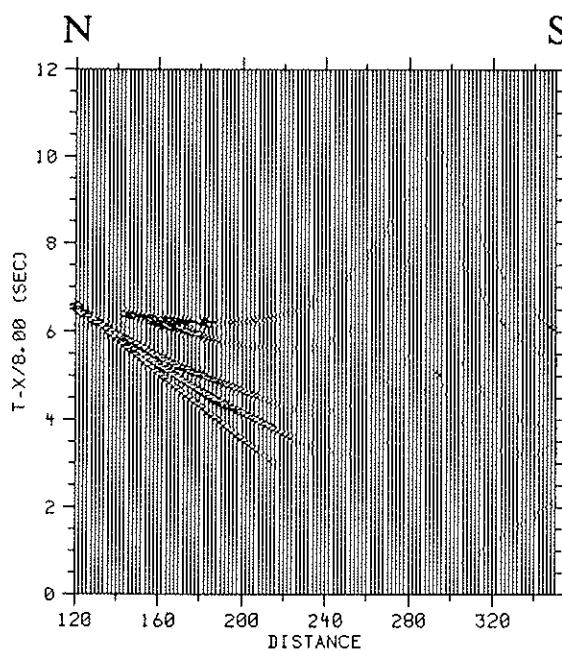
To quantitatively estimate impedance contrasts, I modeled amplitudes of traces at 76 and 104 km offset from

Figure 1.18. Ray-synthetic seismograms of stations UM (a) and KA (b) of shot profile WA. The relative amplitudes are qualitatively in the same order as for the observed data in Figures 1.6 a,b,c.

synthetic seismograms (ray theory)



a. station UM shot profile WA



b. station KA shot profile WA

Figure 1.19. True amplitude plots of averaged five adjacent traces of station KA (profile WA) at 76 and 104 km offset. The smaller offset corresponds to pre-critical distance where P_1P and P_mP are still observed. The offset of 104 km corresponds to the critical distance of the P_mP phase. P_2P and P_3P denote mid-crustal phases from the bottom of layers 2 and 3.

station KA shot profile WA

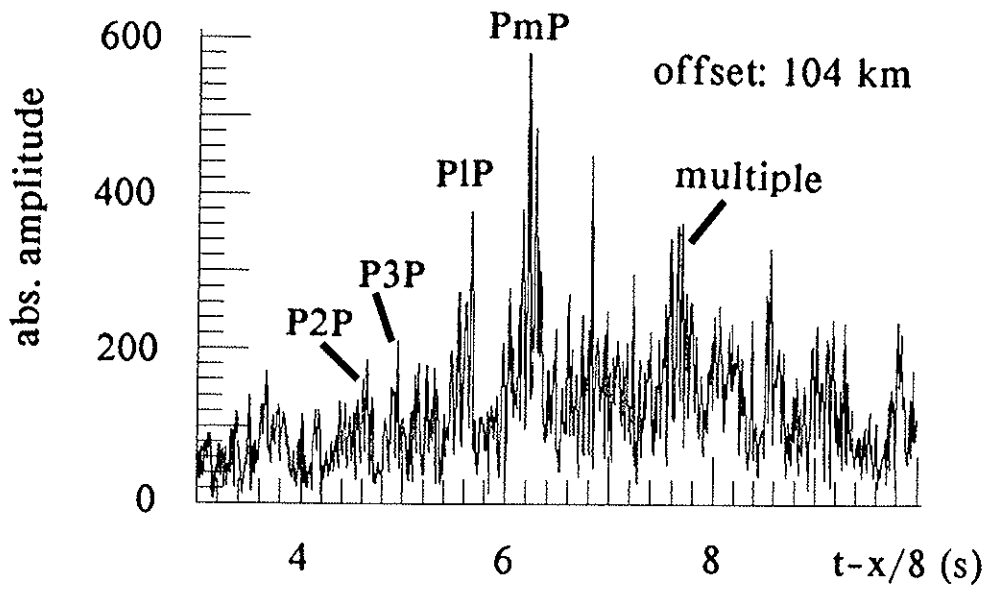
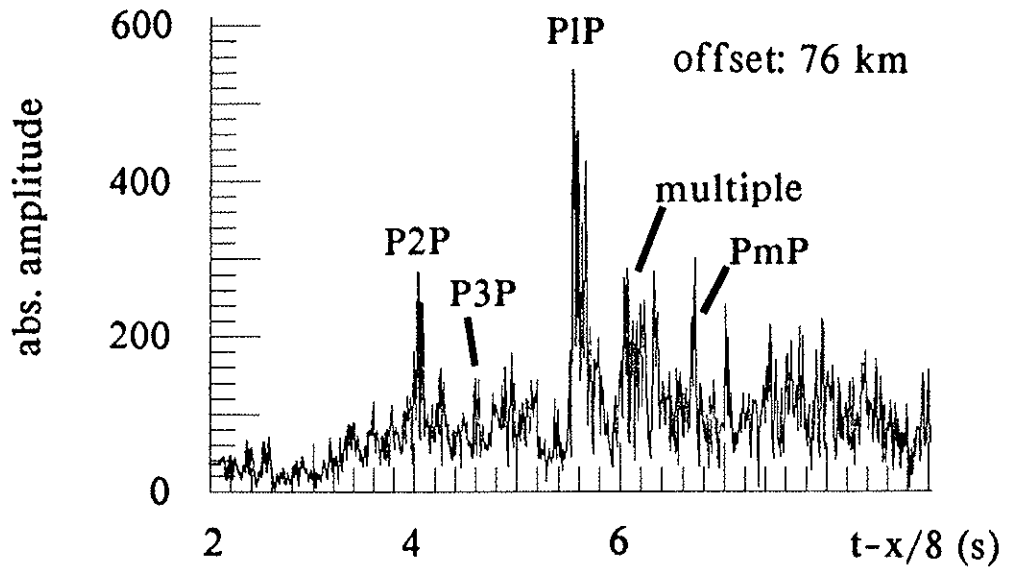
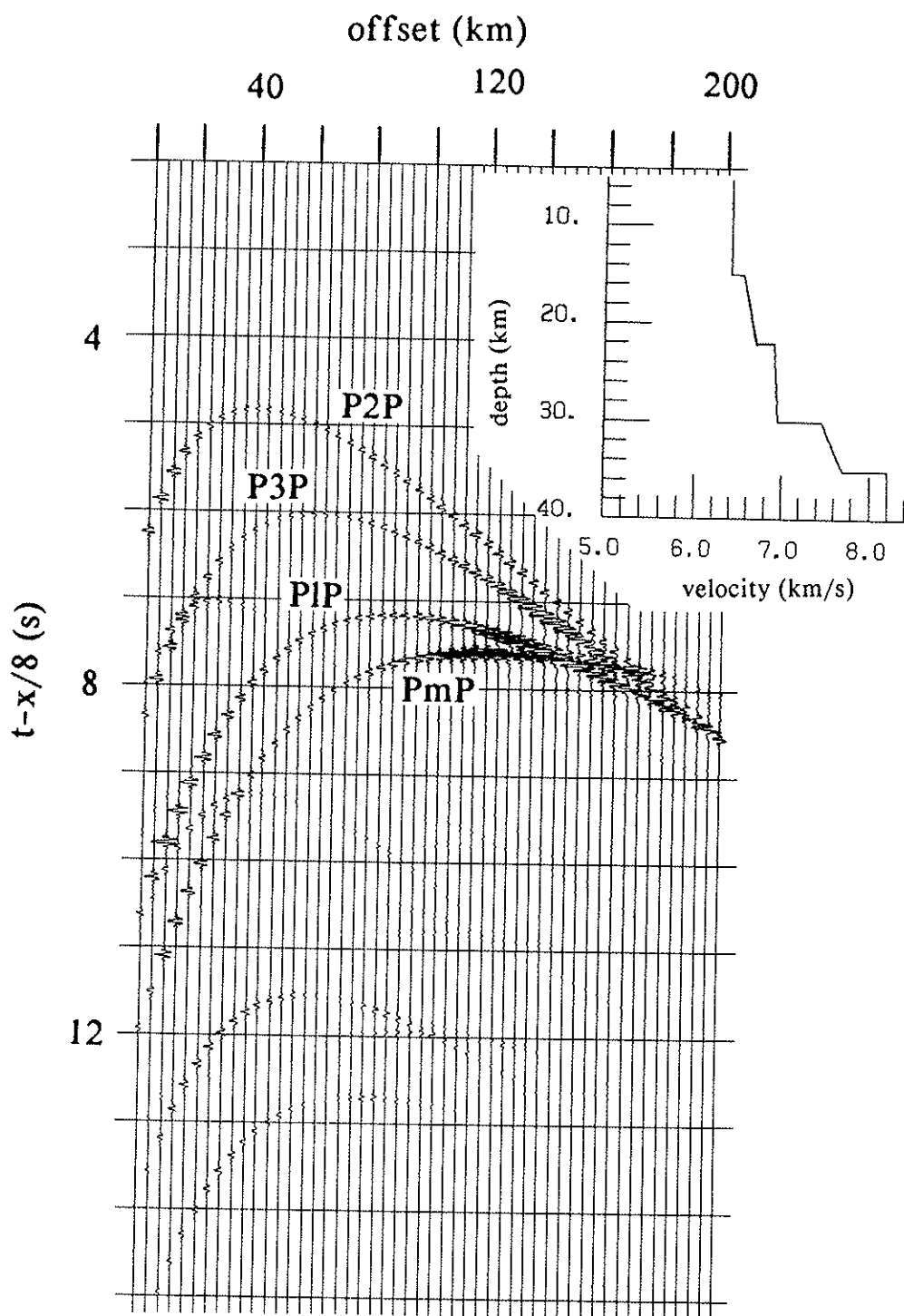


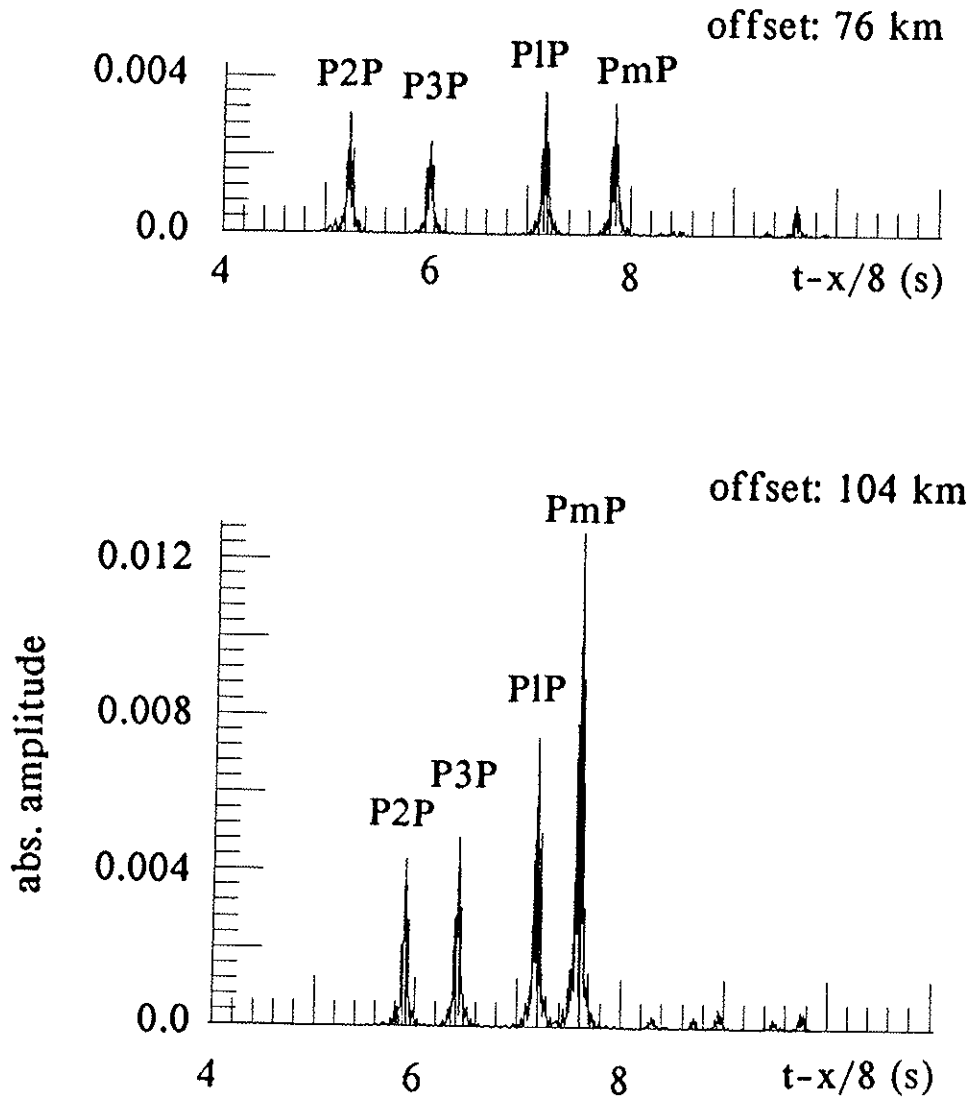
Figure 1.20. Reflectivity seismogram (a) and relative amplitudes for offsets 76 and 104 km (b) to model first-order discontinuity velocity contrasts for P_2P , P_3P , P_1P , and P_mP phases. Amplitudes at critical distance of P_mP (104 km) match observed data, but there is a mis-fit of amplitudes at pre-critical distance.



reflectivity method
1st order discontinuities

a.

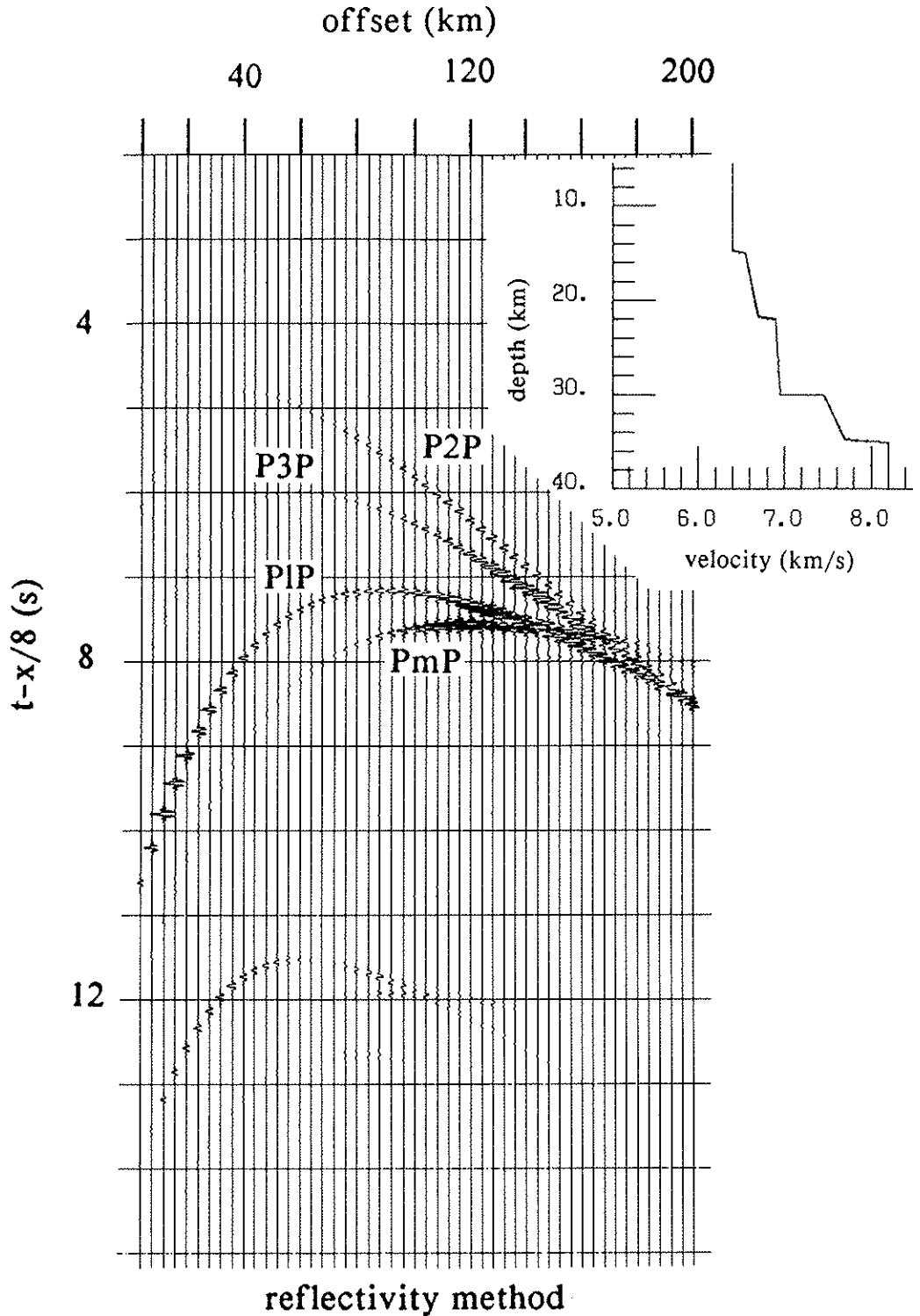
amplitudes of synthetic seismograms



1st order discontinuities

b.

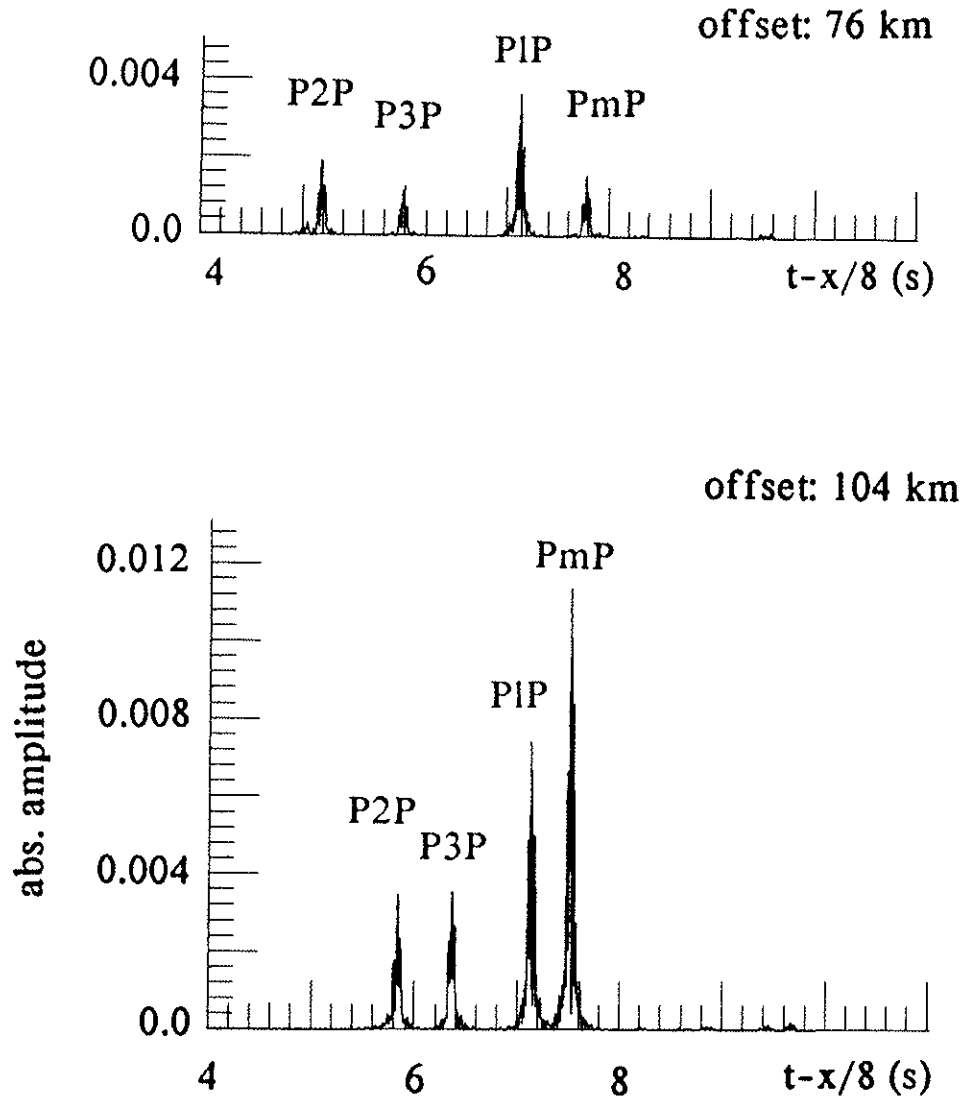
Figure 1.21. Reflectivity seismogram (a) and relative amplitudes for offsets 76 and 104 km (b) to model narrow gradient zones (300 m) for P_2P , P_3P , and P_mP arrivals and a first-order discontinuity for the P_1P phase. This model obtains a better fit for pre-critical distance as well, although the observed P_1P phase [Fig. 1.19] has an extremely high amplitude at 76 km, indicating lateral heterogeneities.



gradient zones (~ 0.3 km) for P2P, P3P, PmP
1st order discontinuity for PIP

a.

amplitudes of synthetic seismograms



gradient zones (< 0.5 km) for P2P, P3P, PmP
1st order discontinuity for PIP

b.

recording KA using the reflectivity method. Amplitudes of these traces [Fig. 1.19] were compared with traces of the synthetic seismogram [Fig. 1.20 a,b and 1.21 a,b]. First, I modeled first-order discontinuities for the four dominant arrivals P_2P , P_3P , P_1P , and P_mP [Fig. 1.20 a]. The best agreement was reached for critical distance of the P_mP phase at offset 104 km with a model that contains P-wave velocity contrasts of 0.2 km/s (P_2P), 0.3 km/s (P_3P), 0.4 km/s (P_1P), and 0.45 km/s (P_mP) [Fig. 1.20 a,b]. Amplitudes at 76 km offset were not matched well enough with this model. To reduce pre-critical amplitudes and to obtain a dominant pre-critical P_1P amplitude, narrow gradient zones of 300 m (approximately one wavelength) width were implemented for phases P_2P , P_3P , and P_mP [Fig. 1.21 a,b]. The amplitudes at critical and post-critical distance do not change much, but better agreement with the observed amplitudes is reached at pre-critical distance. Lateral heterogeneities in impedance contrasts are likely responsible for the extremely high amplitudes of the pre-critical P_1P phase. The modeled velocity contrasts lie in the order of velocity contrasts of the 2-D travel-time model. The one-dimensional character of the reflectivity method limits its interpretive value for a 2-D data set that contains dipping structure and lateral heterogeneities, but it still provides a first order estimate of impedance contrasts.

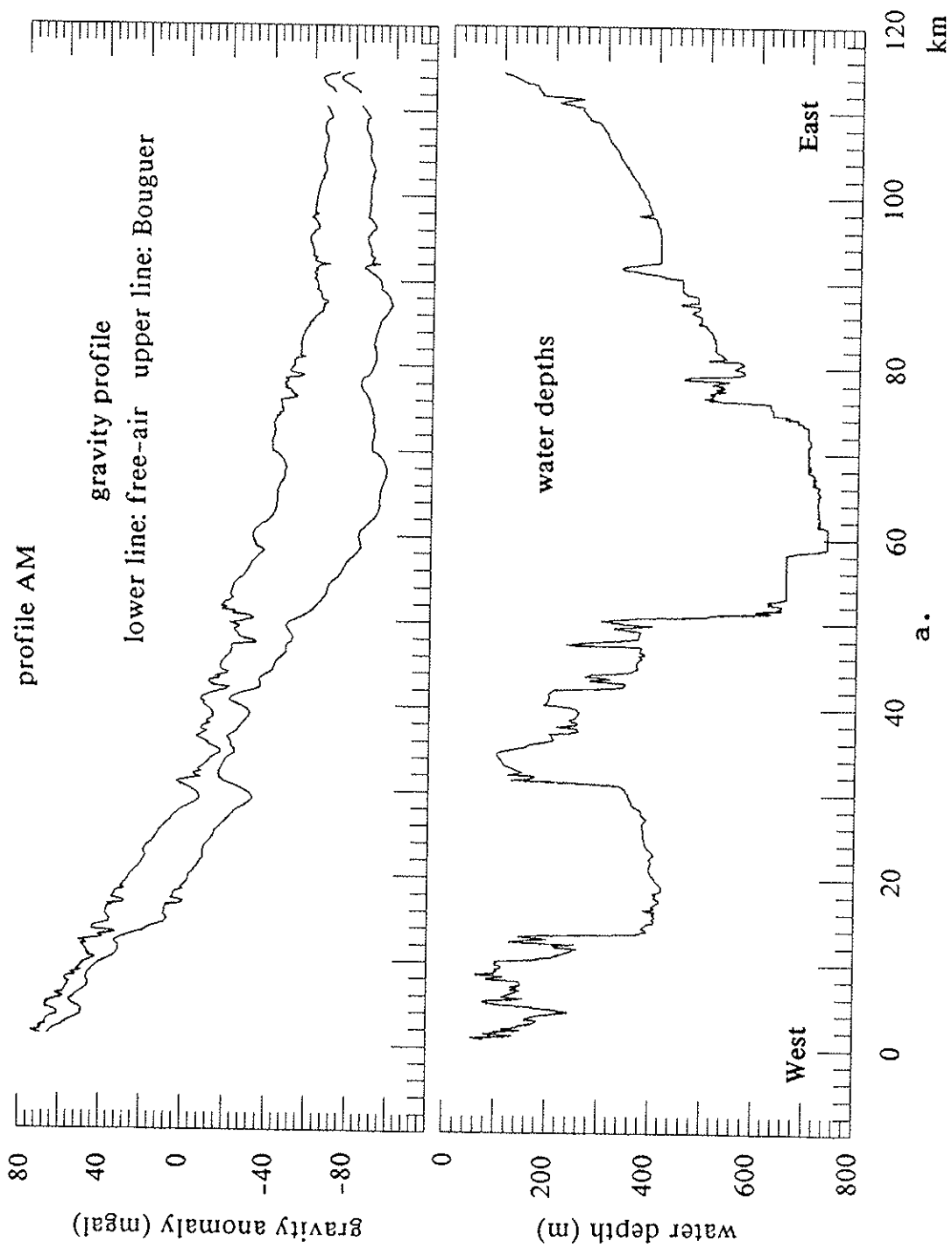
INTERPRETATION AND DISCUSSION OF MODELING RESULTS

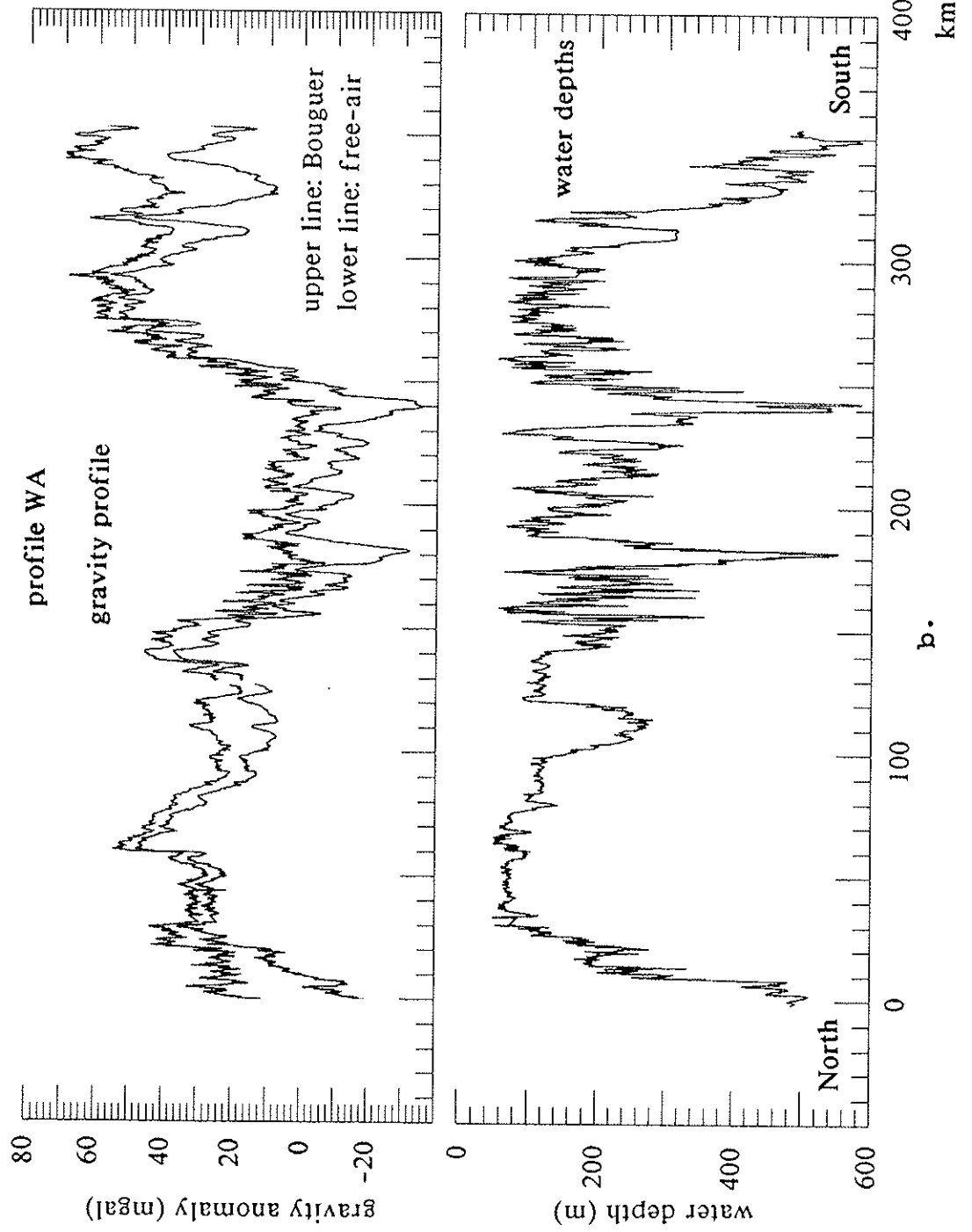
COMPARISON WITH GRAVITY DATA. Our observed Bouguer and free-air anomalies of the E-W profile AM [Fig. 1.22 a] match well with the data obtained by Speece (unpublished data). Gravity data from the N-S profile WA [Fig. 1.22 b] cannot be controlled in a 3-D sense for most of the profile, because of missing coverage. The free-air gravity anomalies reflect the variation in water depth, which changes between 50 and 700 m [Fig. 1.22 a,b]. Therefore, the Bouguer anomaly profiles say more about the effect of the crustal structure and composition, although the Bouguer values are controlled by a constant correction density replacing the water body density.

A westward increase of about 130 mgal of the long-wavelength Bouguer anomaly is observed along the AM profile with the steepest gradient on the westernmost third of the profile. This trend corresponds to a decrease in crustal thickness of about 20 km. The effect of a high-velocity/high-density lower crustal layer does not show in the data, because its long-wavelength gravity effect could also be compensated by a slightly thinner crust.

The lack of 3-D gravity information for profile WA does not permit an accurate comparison with our seismic data. A general trend toward lower gravity values northward, however, is consistent with the thickening of the crust in the Davis Strait.

Figure 1.22. Free-air and Bouguer gravity anomaly and water-depth profiles of line AM (a) and WA (b). The steep gradient of the long wavelength gravity anomaly on profile AM reflects the thinning of the continental crust toward the Labrador Sea (see also Speece, unpublished data). The Bouguer correction was applied with a density of 2.67 g/cm³.





STRUCTURE AND COMPOSITION OF THE MARGIN. Inverse and forward modeling of the wide-angle data reveal new results concerning the structure and composition of the continental and transitional Archean crust in SW Greenland. The portion of the crust close to the margin is highly affected by the rifting event. Lack of seismic wide-angle reflections from the lowermost crust and the Moho indicates that the lowermost crust of the old Archean continent not affected by recent rifting either does not contain interfaces with large impedance contrasts, or compositional changes appear gradually within broad transition zones. Mid-crustal reflectors exist only locally on individual receivers and Moho reflections at near-vertical offsets do not show. The transitional crust, on the other hand, contains numerous mid-and high-amplitude lower crustal reflections both at near-offsets and wide-angle distance, suggesting large impedance contrasts, possibly related to the accretion of high-velocity mafics from the mantle during rifting.

Most lateral velocity variations occur in the uppermost crust. Especially, in the Ameralik model, correlations of velocity variations with geologic observations of Archean subterraneans can be made in some cases. For instance, crossing of the Qorqut granitic complex reveals a lower velocity for the uppermost layer of about 5.2 km/s than seen for the rest of the profile. The wider horizontal range of that low velocity zone suggests a greater extent of the granitic complex than

observed on the surface. The steep vertical velocity gradient within the uppermost 2 to 3 km is probably explained by closure of microcracks with pressure (Birch, 1960; Walsh, 1965).

The middle crust of the eastern AM model is characterized by a low velocity, increasing from 6.0 to about 6.3 km/s, indicating a felsic composition. Mid-crustal velocities within the transitional crust are higher, increasing vertically from about 6.3 to 6.5 km/s. This observation indicates that the transitional crust might have been intruded by mafic material from the mantle during rifting. In general, there is evidence that the oceanic-continental transitional crust has a more mafic composition than the Archean continental crust of SW Greenland indicated by a higher average crustal velocity of about 6.6 km/s (uncertainty 0.1 km/s) as opposed to about 6.3 km/s (uncertainty 0.1 km/s) for the continental crust [Fig. 1.16 a,b]. An addition of 20 % mafic rock (7.3 km/s) into the upper 20 km of a 40 km thick crust and additional 50 % mafic rock into the lower 20 km, assuming pre-existing average velocities of 6.1 km/s for the upper 20 km and 6.5 km/s for the lower 20 km, would increase the total average crustal velocity from 6.3 to 6.6 km/s. Mid-crustal reflections might originate from either intruded and elongated mafic bodies emplaced during an early stage of rifting, or possible shear zones developed as a result of extension. Seismic studies of metamorphic core

complexes in the Basin and Range include interpretations where a combination of mafic intrusions and shear processes might account for high-amplitude reflection zones in the mid-crust (McCarthy and Thompson, 1988).

The most prominent feature of the transitional crust is a high-velocity zone of up to 8 km thickness at the bottom of the crust. This zone exists only within the transitional crust, indicating its emplacement during rifting. Velocities of 7.4 to 7.7 km/s within that zone could be caused by mafic to ultramafic rocks that were intruded or underplated (Furlong and Fountain, 1986; Fountain, 1989). These velocities are higher than those of the lowermost transitional crust of the eastern United States and Canada (LASE Study Group, 1986; Reid and Keen, 1990b). The 7.2 km/s layer of the eastern United States continental shelf is interpreted as being made of plutonic gabbroic rocks (LASE Study Group, 1986). High-pressure laboratory velocity measurements of rock samples from the exposed lower crustal Ivrea zone reveal P-wave velocities from 7.2 km/s to 7.5 km/s for metagabbro, and from 7.4 km/s to 7.6 km/s for mafic granulite (Burke and Fountain, 1990). These velocities were measured between 600 and 1000 MPa (6 and 10 kbar), that corresponds to a depth of 20 to 35 km. Amphibolites and pyroxenites can exhibit P-wave velocities between 7.0 and 7.7 km/s at 600 to 1000 MPa (Christensen, 1965; Burke and Fountain, 1990; Fountain et al., 1990). Based on theoretical calculations of compressional rock velocities

with respect to pressure and temperature, Furlong and Fountain (1986) estimate that underplated olivine-gabbro can reach P-wave velocities of up to 7.8 km/s at 35 to 40 km depth assuming an intermediate surface heat-flow of 60 mW/m². The temperature with increasing crustal depth has an effect on the seismic velocities. Kern and Richter (1981) measured temperature derivatives between 1.6 and 4.9 x 10⁻⁴ km/s °C for a variety of rock samples under 600 MPa pressure. Gneisses, amphibolites, and eclogites exhibit temperature derivatives of only 1.6 to 3.0 x 10⁻⁴ km/s °C. By assuming a surface heat flow of 50 to 55 mW/m², corresponding to extensional basins 80 Ma after the initial rifting event (extension factor of about 4) (McKenzie, 1978), our observed lower crustal velocities are increased by 0.08 to 0.15 km/s to compare them with lab measurements at room temperature. These temperature-corrected velocities, between 7.5 to 7.55 km/s and 7.8 to 7.85 km/s, exceed the range of most observed laboratory data with the exception of eclogite, but lie within the calculated velocity range that might be intermediate between velocities appropriate for crust and mantle materials (Furlong and Fountain, 1986). Considering the great depth of the marginal crust of SW Greenland, it is likely that a portion of the magmatic underplate underwent a phase change from garnet-granulite to eclogite facies during isobaric cooling (Fountain, 1989). A considerable amount of eclogite-facies rocks would increase the seismic velocities to our observed

values.

A high velocity contrast of about 0.4 km/s is responsible for the high-amplitude arrivals from the top and bottom of that underplated zone in profile WA. Inversion of travel-time data reveals that this zone thickens toward oceanic crust. The identification of reflections from the top of a high-velocity zone in profile AM is not as obvious as for profile WA. While the P₁P phase of profile WA can be traced from post-critical distance to smallest recorded offsets, it appears only locally in a few recordings of profile AM (see also Larkin, unpublished data). It is possible that the interface on top of the high-velocity zone changes from a 1st order discontinuity, as modeled with the reflectivity method, to a gradient zone toward the continent, eliminating pre-critical reflections. The thickness of the gradient zone may become small enough (in the order of a few hundred meters) in places to be reflective at small offsets. Depending on the pre-existing rocks of the lowermost Archean crust and their metamorphic grade before the initial rifting event, uprising mantle rocks might have intruded into the lower few kilometers creating a layered or gradational transition zone.

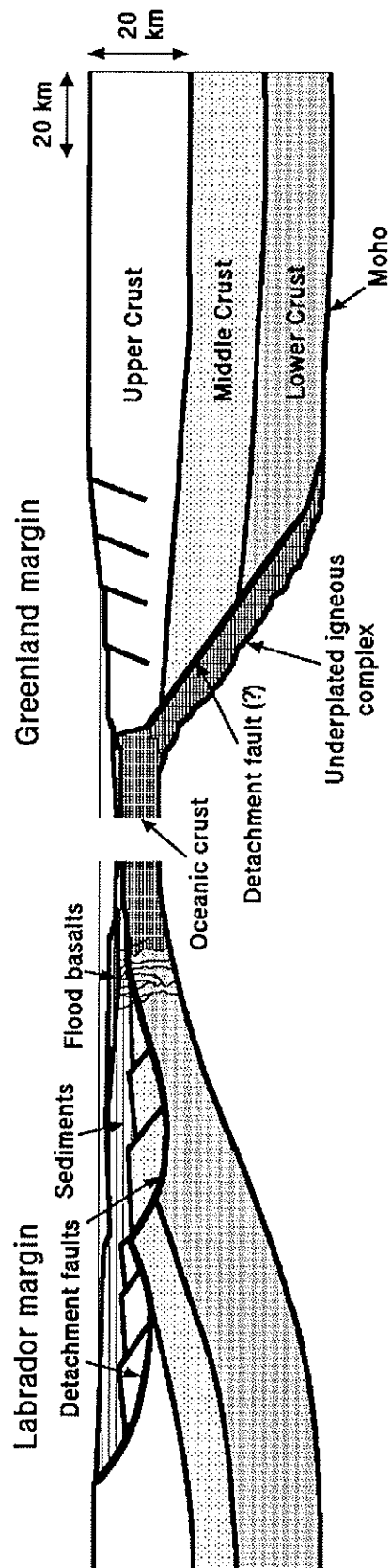
Numerous Moho reflections from the transitional crust show evidence for a steep dip with an angle of 25 to 30°. Such an extreme dip of a crust-mantle boundary within a passive margin has been modeled only on the east coast of Oman, based on travel-times from seismic refraction data (Barton et al.,

1990). Associated with the steep continental slope and the absence of a sedimentary layer, this abrupt change in crustal thickness might be evidence for a continental break-up without much subsidence on the SW Greenland side of the Labrador Sea basin.

IMPLICATIONS FOR EVOLUTION OF LABRADOR SEA

High-velocity layers at the bottom of the transitional crust are observed on several passive margins (Weigel et al., 1982; LASE Study Group, 1986; Keen and de Voogt, 1988; Trehu et al., 1989; Austin et al., 1990; Reid and Keen, 1990a,b). Chian and Loudon (submitted paper), however, do not observe such a zone at the bottom of the transitional crust of SW Greenland approximately 500 km south of our area. The proximity of our data to the Davis Strait where volcanic rocks cover large areas implies that a magmatic layer was emplaced at the bottom of the crust during "active" rifting of the northern Davis Strait but did not reach into the southern Labrador Sea. The absence of volcanics in direct proximity of the observed high-velocity zone, however, suggests that rifting of the Labrador Sea was rather "passive" such that smaller amounts of mafic rocks derived from the hot spot or mantle plume under the Davis Strait intruded and underplated, but did not penetrate the crust completely to be extruded. The high velocities of 7.5 to 7.85 km/s (temperature-corrected)

Figure 1.23. Schematic cross-section of the Labrador Sea conjugate margins. The model illustrates asymmetric margins containing a wide Labrador shelf with a thick sedimentary cover on top of a normally faulted basement. Flood basalts were identified from seismic data (Hinz et al., 1979). The wide-angle data of this study show evidence for a Moho dip of 25 to 30° eastward on the Greenland margin. A high-velocity layer is modeled as an underplated igneous complex along the transitional crust. Whether this mafic to ultramafic complex merges with the oceanic crust, as modeled by Bonatti and Seyler (1987) for the Red Sea, remains unclear due to lack of data. A master detachment fault on top of the mafic underplate might exist according to models by Wernicke (1985) and Lister et al. (1986), but there is no direct evidence in the seismic data.



suggest that the density of the igneous rocks is intermediate between that of continental crust and mantle, and thus would explain why underplated magmatic melts did not penetrate the crust (Herzberg et al., 1983).

Hinz et al.'s (1979) and Srivastava et al.'s (1980) suggestion of asymmetric margins in the Labrador Sea and Davis Strait is supported by the detection of a 25 to 30° dipping Moho on the Greenland margin. The observation of flood basalts on the wide Labrador shelf (Hinz et al., 1979), the existence of a magmatic zone at the bottom of the narrow Greenland transitional crust, and the steep Moho can be explained by extensional models involving simple shear with a possible crustal detachment (Wernicke, 1985; Lister et al., 1986) generated during the pre-spreading phase. A schematic cross-section of the Labrador conjugate margins [Fig. 1.23] is derived from our observations on the Greenland margin and the observed features on the Labrador margin. The cross-section is in agreement in some parts with the model of asymmetric passive margins by Lister et al. (1986), but it contains a zone of underplated igneous rocks directly underneath or interfering with a possible master detachment fault and continuing into the oceanic crust. A model of the Red Sea by Bonatti and Seyler (1987) shows similar features in which the underplated igneous sequence merges with the oceanic crust. In their paper, a crustal detachment fault is illustrated that ends on top of the underplated zone. In case of the Red Sea,

however, the conjugate continental margins are symmetric. Seismic data from the Greenland fjords farther inland lack evidence for an underplated high-velocity zone beneath the continental crust. If the master detachment fault consists of a mylonitic sequence that could cause high-amplitude reflections as observed on mylonitic shear zones elsewhere (Fountain et al., 1984; Hurich et al., 1985), it would contribute to the observed high-amplitude P_1P phases from the top of the igneous lower crustal zone. The existence of a crustal master detachment fault parallel to the Greenland margin is speculative, because of a lack of direct evidence from seismic data. More data acquired on a transect into the oceanic crust are needed to prove the existence of such a crustal detachment and to show whether the lower crustal igneous zone merges with the oceanic crust.

CONCLUSIONS

Densely spaced, large offset wide-angle reflection data from the shelf of SW Greenland reveal a number of upper, mid-crustal, and lower crustal seismic phases. Good correlations of phases from near-vertical to post-critical offsets allowed us to model the structure of seismic interfaces and to perform an amplitude analysis. Recordings from the coastline wide-angle profile (WA), which ran parallel to the continental margin of the Labrador Sea, reveal high-amplitude lower

crustal and Moho reflections identified as arrivals from the top and bottom of a high velocity zone at the base of the crust. The tau-p analysis and 1-D inversion indicated that velocities within the lower crustal zone increase from 7.4 to 7.7 km/s. The results from the extremal inversion served as an initial model for the more detailed 2-D travel-time inversion. The final two-dimensional inverse and forward model includes a Moho with a 25 to 30° dip toward the continent, and a high-velocity zone at the bottom of the crust thinning toward the deepest detectable crustal depth. A low average crustal velocity of about 6.3 km/s for continental crust, and an average velocity of about 6.6 km/s for the westernmost transitional crust indicate an increase of mafic components in the crustal composition for the transitional crust.

Isobaric cooling of the 30 to 40 km deep crust after rifting can bring portions of underplated mafic lower crustal rocks from the garnet-granulite into the eclogite stability field (Fountain, 1989). This phase change might be responsible for the high velocities (7.5 - 7.85 km/s, temperature-corrected) observed from the lowermost crust underneath the margin. The evidence of a high-velocity zone at the base of the transitional crust contradicts interpretations of a "non-volcanic" passive margin in SW Greenland. A lack of such a zone at the bottom of the transitional crust along the southern Archean block (Chian and Loudon, submitted paper) indicates that such an igneous layer is associated with the

magmatism of the Davis Strait. Our seismic data suggest that the magmatism related to the rifting of the Labrador Sea and Davis Strait reached much farther south than previously thought.

A model was developed in which the asymmetry of the Labrador Sea basin can be explained. In leaning toward the model of asymmetric passive margins by Lister et al. (1986), our model contains a possible master detachment fault that lies in contact with the top of an underplated igneous layer. Direct evidence does not exist from seismic data, but a mylonitic fabric of such a detachment fault could cause high-amplitude reflections in addition to the impedance contrast between the mafic to ultramafic rocks of the underplated layer and the more intermediate to mafic rocks of the middle and lower crust. The detachment fault might have been also overprinted by the intruded and underplated igneous complex. This model explains the abrupt transition from continental to oceanic crust inferred by the steeply dipping Moho on the Greenland side, high-amplitude reflections from a lower crustal layer parallel to the Moho, and observations of a different character of the margin off Labrador by other workers.

CHAPTER II
SEISMIC CHARACTER OF EARLY ARCHEAN CRUST IN SOUTHWESTERN
GREENLAND AND SOUTHERN MINNESOTA

INTRODUCTION

A few locations worldwide where early Archean crust is exposed include both southwestern Greenland and southern Minnesota, two ancient Archean terranes that are comparable in age. Little is known about the formation of continental crust during the Archean. Important questions include the initial composition of the early Archean continental nucleus, its alteration during tectonic events in geologic history, and, in particular, the nature of the Moho beneath these terranes in comparison with younger crust.

In an attempt to address some of these questions, the University of Wyoming conducted seismic experiments in SW Greenland and S Minnesota using normal-incidence/wide-angle recordings of controlled sources. Large offset, densely spaced recordings from an air-gun array were obtained over the Greenland margin and along two fjords farther inland on continental crust. Densely spaced vibroseis and quarry blast recordings were obtained on the gneiss terrane in S Minnesota. In this paper, I focus on the analysis of the wide-angle

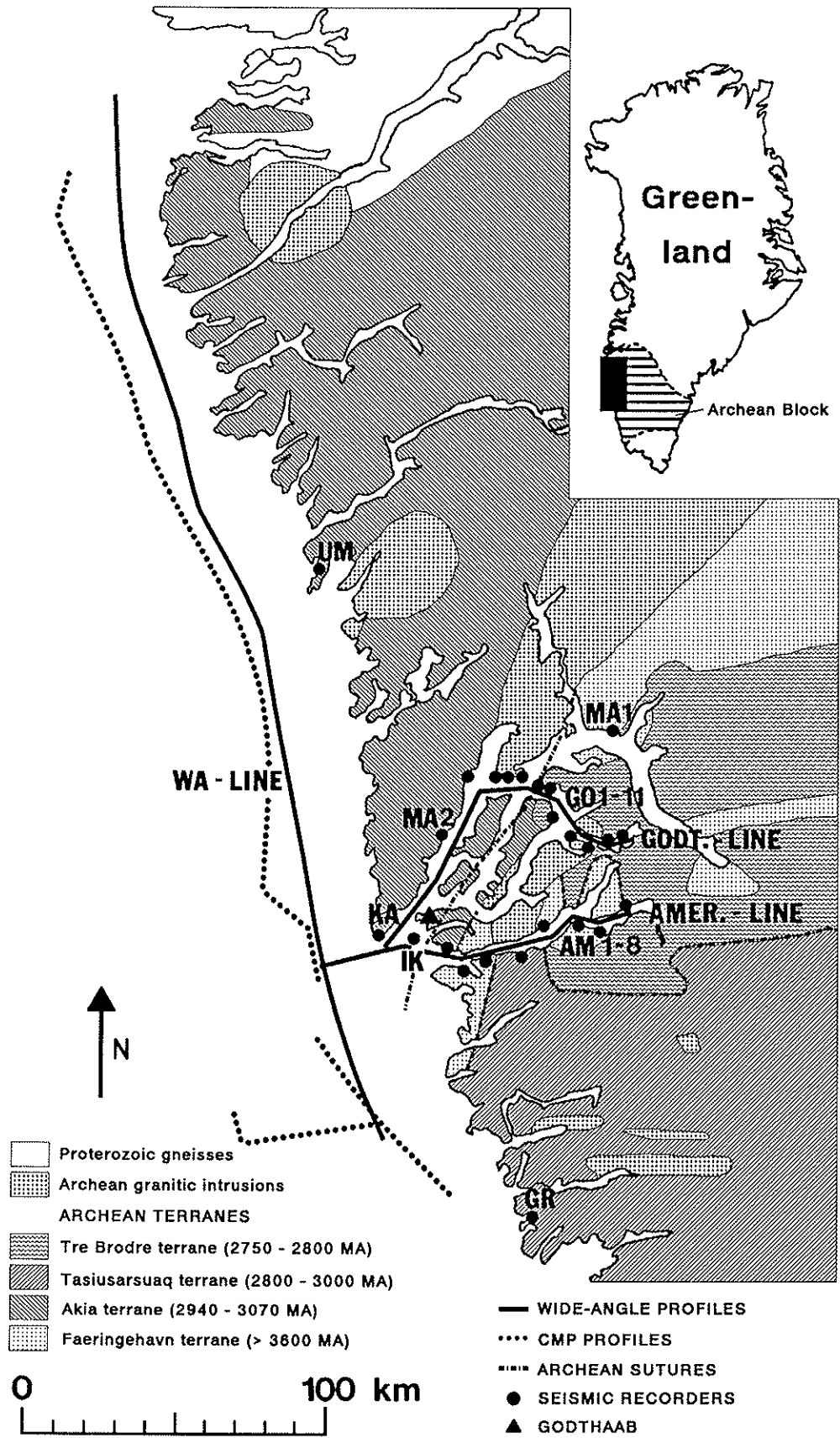
reflection recordings.

The dense shot/receiver spacing permits processing steps similar to pre-stack processing of multi-fold CMP data. Subsequently, I inverted and forward modeled the data to estimate local velocity structure. The lack of Moho reflections at pre-critical distance from the Archean continental crust seems to be in agreement with observations from other Archean cratons. Pre-critical wide-angle recordings from the Archean in Minnesota, however, reveal high-amplitude Moho arrivals. To qualitatively determine the reflectivity character of Archean crust-mantle boundaries from near-vertical to post-critical offsets, I modeled two Moho types using the reflectivity method (Fuchs and Mueller, 1971).

ARCHEAN TERRANES

SW GREENLAND. The coastal strip of SW Greenland [Fig. 2.1] consists of several gneiss, granite, anorthosite and supracrustal complexes (McGregor, 1973,1979; Bridgwater et al., 1976; Brown et al., 1981; McGregor et al., 1986; Nutman et al., 1989). The oldest complexes, the 3800 MA old Isua supracrustal belt and the 3700 MA old Amitsoq gneiss are some of the oldest exposed rock formations on earth. The Isua sequences are dominated by interlayered meta-sedimentary rocks, derived from volcanic sources, and banded basic rocks of igneous origin, such as amphibolites (Nutman et al., 1984).

Figure 2.1. General geologic map of study area in SW Greenland including seismic source and receiver locations. Map includes Archean terranes and sutures (from Geological Survey of Greenland, 1982; Nutman et al., 1989). Seismic land-stations recorded air-gun shots from profiles along the coast and fjords.



Nutman et al. (1984) favor a model that describes the deposition of the Isua sequence in a predominantly submarine volcanic environment at shallow depth. Several tectonic events in the Precambrian deformed the supracrustal sequence. Various authors (McGregor and Mason, 1977; Nutman et al., 1983; Baadsgaard et al., 1984) suggest a correlation between the Isua sequence and several isolated fragments in SW Greenland and northern Labrador. These sequences might have evolved as an early version of a greenstone belt (Nutman et al., 1984) and fragmented during the addition of granodioritic rocks to the crust.

Several large gneiss complexes were emplaced in the Archean between 3700 and 2800 Ma. The tonalitic, granodioritic, and trondhjemitic gneisses [3100 - 2900 Ma] of the Nuuk complex cover most the region northwest of Godthaabfjord. The area surrounding Godthaabfjord and Ameralik includes several smaller gneissic, granitic, supracrustal, and gabbro-anorthositic complexes, such as the Amitsoq gneisses (c. 3700 Ma), the Amitsoq iron-rich association (c. 3600 Ma), the basic Ameralik dykes (3400 - 3100 Ma), the Malene supracrustal rocks (2500 - 2960 Ma), the granitoid and pegmatitic Qarusuk dykes (2600 - 2700 Ma), and the Qorqut granite complex (c. 2530 Ma). Various deformational events and associated amphibolite and granulite facies metamorphism affected all gneiss complexes (McGregor et al., 1986). Bridgwater et al. (1974) and McGregor et al. (1983) described

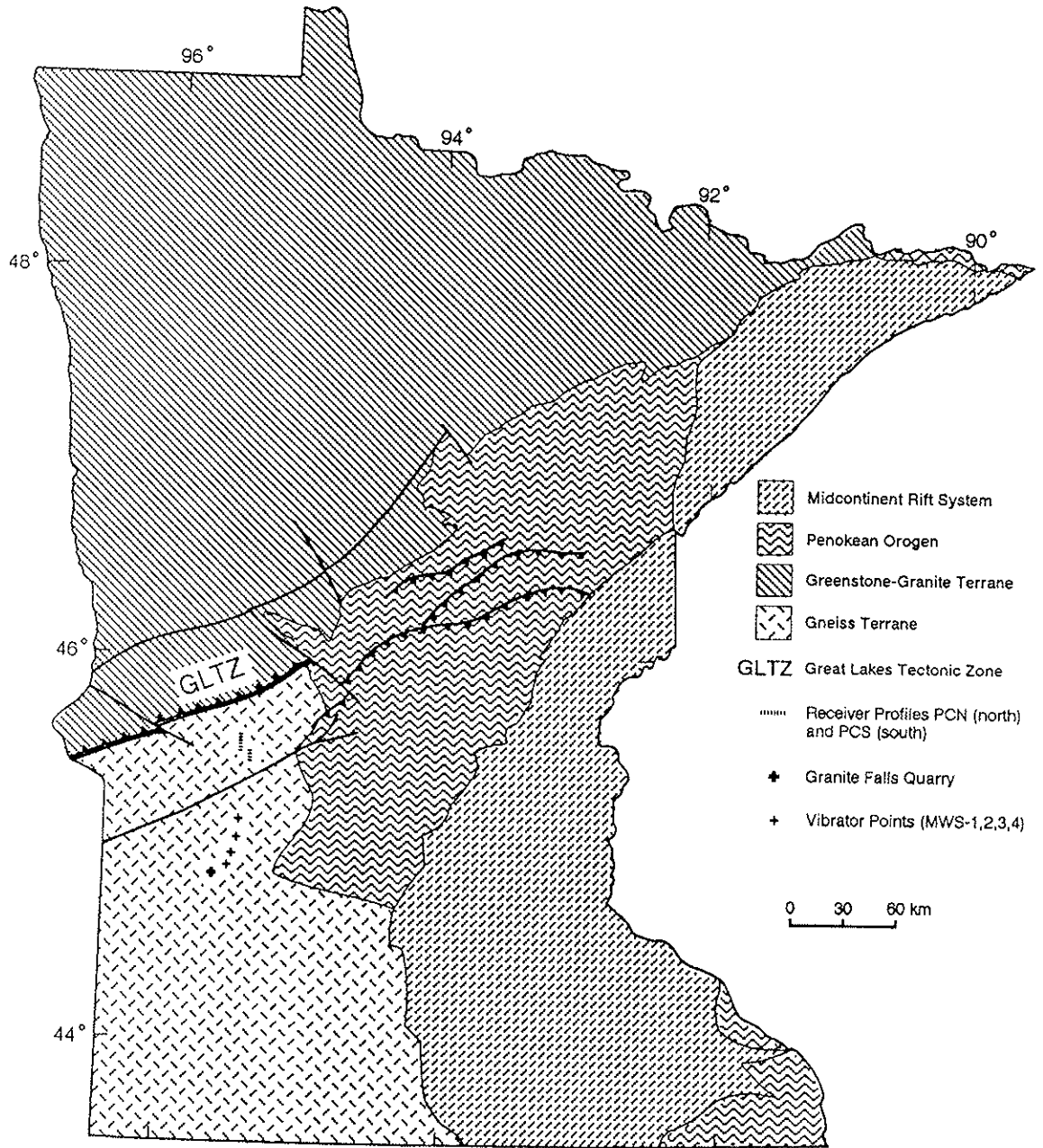
the evolution of the Archean block as a sequence of depositional and tectonic events within a single region. Dominant events in the Archean were the deposition of extrusive volcanics coincident with or followed by intrusions of voluminous tonalitic-granodioritic magmas, the injection of basic pegmatitic or granitic sheets and dykes, ductile deformation and metamorphism, and the final emplacement of granites as a NNE-SSW trending belt of the Qorqut complex.

Nutman et al. (1989) developed the concept of a possible assembly of independently evolved Archean terranes. They based their arguments on the existence of steeply dipping, 10 to 50 m wide mylonite zones at the terrane boundaries, that developed during accretion of contrasting terranes. The Faeringehavn terrane [Fig. 2.1] includes the Amitsoq gneiss complex, the Amitsoq iron-rich suite, and the Akilia supracrustal association. The Tre Broedre terrane comprises the Ikkattoq gneiss complex and gabbro-leucogabbro intrusions. Both the Tasiusarsuaq terrane and the Akia terrane formed by the intrusion of tonalitic-dioritic and granitic magma (Nuuk gneiss) into a sequence of supracrustal rocks (Nutman et al., 1989). Granulite-facies metamorphism dominated during deformation. Nutman et al. (1989) postulate that the terranes accreted after 2750 Ma. Subsequent intense folding, amphibolite-facies metamorphism and intrusion of granitic sheets deformed and altered the contacts of the assembled terranes. Robertson (1986) suggested that the crust thickened

by the successive emplacement of quartzo-feldspathic rocks from differentiation of basic material in the lower crust. Nutman et al. (1989) speculated that the assembly of individually evolved Archean terranes is evidence for Archean plate tectonic processes.

S MINNESOTA. The study area in Minnesota consists of two distinct Archean terranes, an older granite-gneiss terrane to the south, and a younger greenstone terrane to the north. The volcanic and sedimentary rocks of the greenstone terrane were metamorphosed to greenschist and amphibolite facies during the late Archean (2750 - 2600 Ma). The 3500 - 3800 Ma old rocks of the gneiss terrane exposed in the Minnesota River Valley (Goldich and Hedge, 1974; Sims et al., 1980) are comparable in age to those in SW Greenland. The Minnesota rocks consist predominantly of quartzofeldspathic and pelitic gneisses and amphibolites and underwent upper amphibolite to lower granulite facies metamorphism. Mafic rocks ranging from amphibolites to komatiites may represent fragments of the earliest crust. Granitic and gabbroic complexes as well as swarms of mafic dykes repeatedly intruded both Archean terranes in Minnesota (Morey, 1972; Morey and Sims, 1976). Aeromagnetic data of the gneiss terrane reveal lineations suggesting subdivisions of Archean crustal units such as the Benson, Montevideo and Morton blocks (Chandler and Southwick, 1990).

Figure 2.2. Schematic geologic map of Minnesota including the seismic source and receiver locations. The receiver profiles were located at the southern edge of the Great Lakes Tectonic Zone (GRLZ). The Granite Falls quarry is located in the Minnesota River valley, the vibrator points north of the valley.



Minnesota

The Great Lakes Tectonic Zone, possibly a major crustal suture, separates the Archean granite-gneiss terrane from the greenstone terrane (Morey and Sims, 1976; Sims et al., 1980; Gibbs et al., 1984). Analysis of aeromagnetic (Smithson and Johnson, 1989; Chandler and Southwick, 1990) and seismic reflection data (Gibbs et al., 1984; Smithson et al., 1986; Smithson and Johnson, 1989; Boyd et al., 1991) suggest that the zone is bounded by several major northward dipping faults. Distinct Moho reflections from normal-incidence seismic data are not identified beneath and in proximity of the Great Lakes Tectonic Zone, but appear farther south in the Minnesota River Valley (Boyd et al., 1991).

ACQUISITION OF WIDE-ANGLE DATA

The University of Wyoming, in cooperation with the University of Bergen, the Geodetic Institute of Denmark, and Incorporated Research Institutions for Seismology (IRIS), acquired large-offset wide-angle data from three shot profiles in SW Greenland. Fifteen REF TEK seismic instruments on 35 locations recorded an 6000 cu.in. air-gun array fired along the shelf and in two fjords [Fig. 2.1]. Stations were placed along the fjords to image possible Archean sutures and continental crust unaffected by the rifting of the Labrador Sea. The instruments recorded shots of up to 400 km offset with a shot spacing of 100 to 150 m. Chapter I includes a more

detailed description of the recording parameters.

Seismic data from southern Minnesota were acquired by the University of Wyoming, the University of Wisconsin, Oshkosh, and the University of Georgia, extending the seismic coverage for the central and southern state from the COCORP seismic reflection survey (Gibbs et al., 1984) and Greenhalgh (1981). We collected normal-incidence seismic data parallel to the southernmost COCORP profile to better image the suggested Precambrian suture. We also acquired data along the Minnesota River Valley to image the Archean crust (Boyd and Smithson, 1990; Boyd et al., 1991). This study evaluates recordings of large offset shots into of the normal-incidence deployments located on the southern boundary of the Great Lakes Tectonic Zone [Fig. 2.2]. The wide-angle data consist of recordings of vibroseis sources as well as quarry blasts into densely spaced (50 m) receivers of the 9.6 km long normal-incidence profiles. Offsets from the sources ranged between 60 and 108 km. Four trucks generated 32-s long, linear sweeps of 10-42 Hz. Each vibrator point consists of 20 to 34 sweeps. The quarry blasts detonated as a series of delayed explosions in 39 to 43 holes per shot with 90-100 kg of explosive per hole. Each blast was about 0.4 s in duration.

PROCESSING AND DATA DESCRIPTION

The wide-angle data from Greenland were corrected for

elevation statics, band-pass filtered (7-20 Hz), deconvolved, and coherency and/or tau-p filtered in cases where direct S- and water waves interfered with reflections. Detailed processing steps are described in Chapter I.

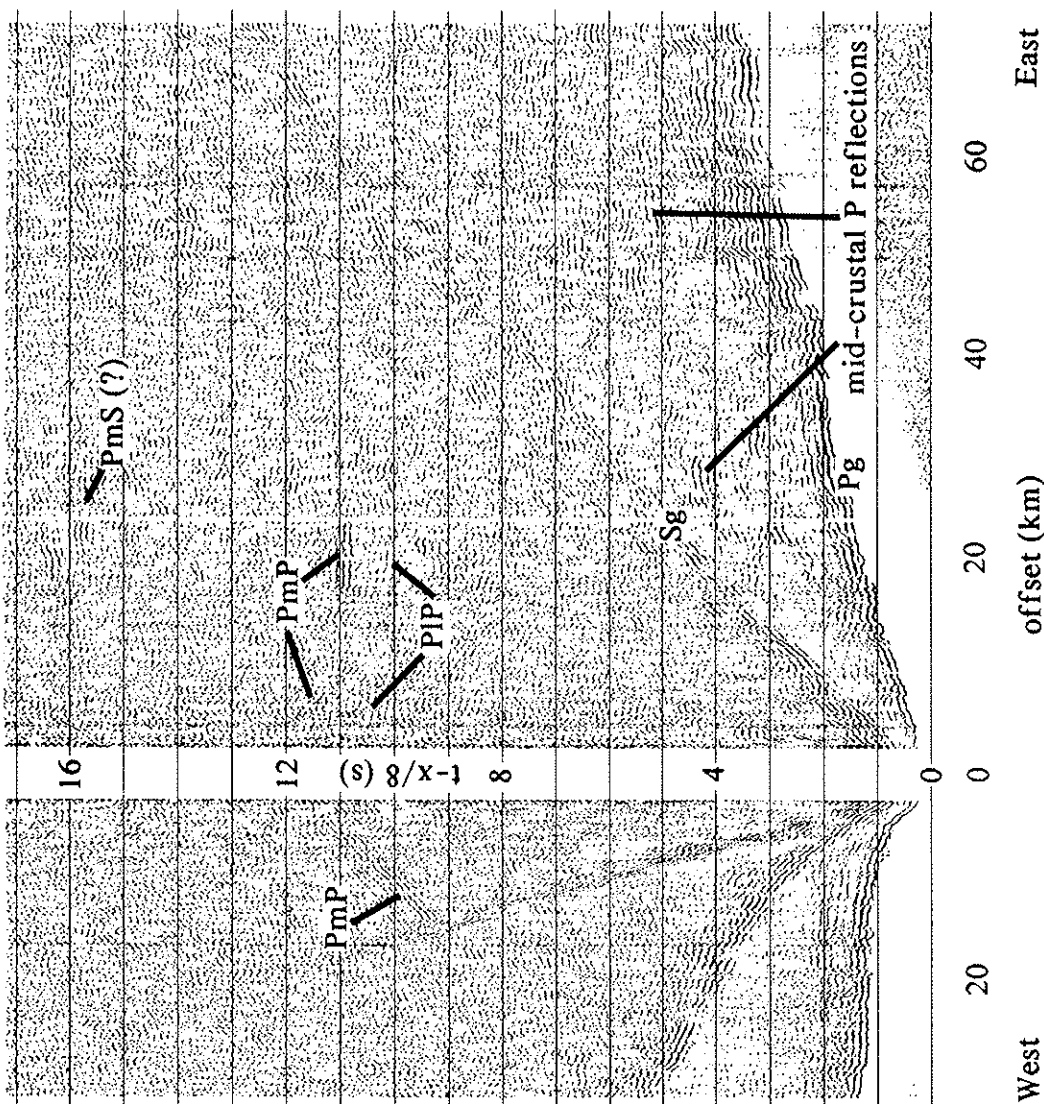
The seismic phases analysed in this study include predominantly mid- and lower crustal arrivals from the Ameralikfjord data. Mid-crustal phases are observed throughout the entire range of the fjord. Lower crustal and Moho arrivals appear with high amplitudes from the transitional crust [Fig. 2.3 a], but are missing from recordings farther inland on the more predominantly continental crust [Fig. 2.3 b].

The vibroseis records from Minnesota were vertically stacked, using a diversity stacking routine, and subsequently band-pass filtered (10-42 Hz). Processing in the tau-p domain was done to obtain one-dimensional velocity-depth information. Also, tau-p processing isolates the delay sequence of quarry blasts (Hawman and Phinney, 1991). In addition to the slant stack, the semblance was computed to design a coherency filter (Stoffa et al., 1981) which was applied to each slant stack to suppress artifacts due to spatial aliasing and other incoherent noise. Because of the limited range of available offsets, I did not sum the individual slant stacks.

Generally, the vibroseis recordings [Fig. 2.4] show arrivals with significantly lower amplitudes than the quarry blasts [Fig. 2.5 a], but they cover a wider range of offsets. Slant stacking and coherency-filtering assisted in identifying

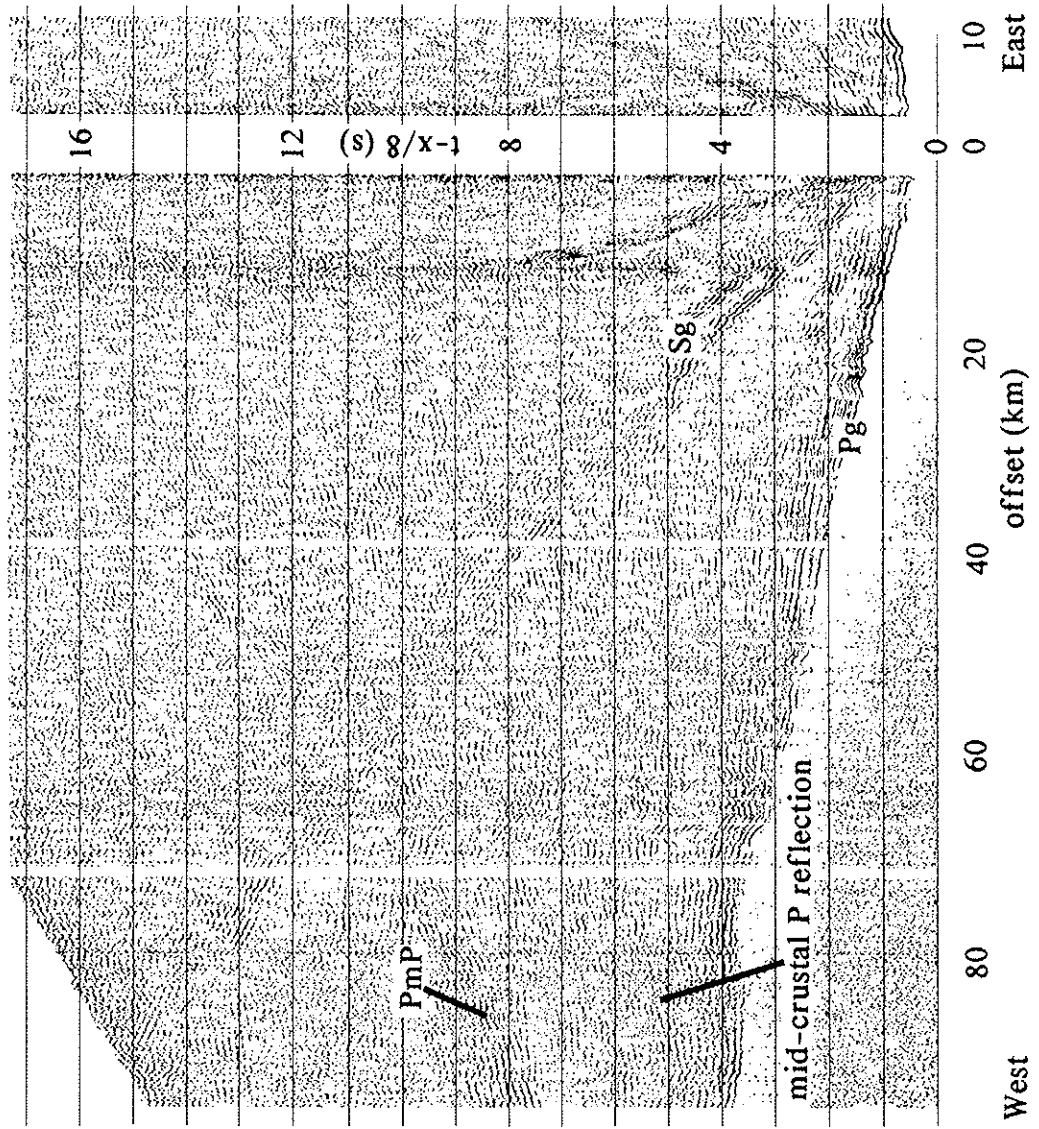
Figure 2.3. Record sections of Greenland fjord (Ameralik) shots, stations IK (a) and AM7 (b), profile AM, AGC 3 sec. Lower crustal reflector and the Moho are identified in the continental-oceanic transitional crust. There is no evidence for a Moho reflection from the Archean continental crust.

station IK shot profile AM AGC 3 sec



a.

station AM7 shot profile AM AGC 3 sec



b.

Figure 2.4. MN vibroseis record from profile PCN, max. offset 79.4 km. This 21-fold record contains low-amplitude P_g and P_m phases that are better identified in the tau-p domain.

MWS-2 vibroseis record

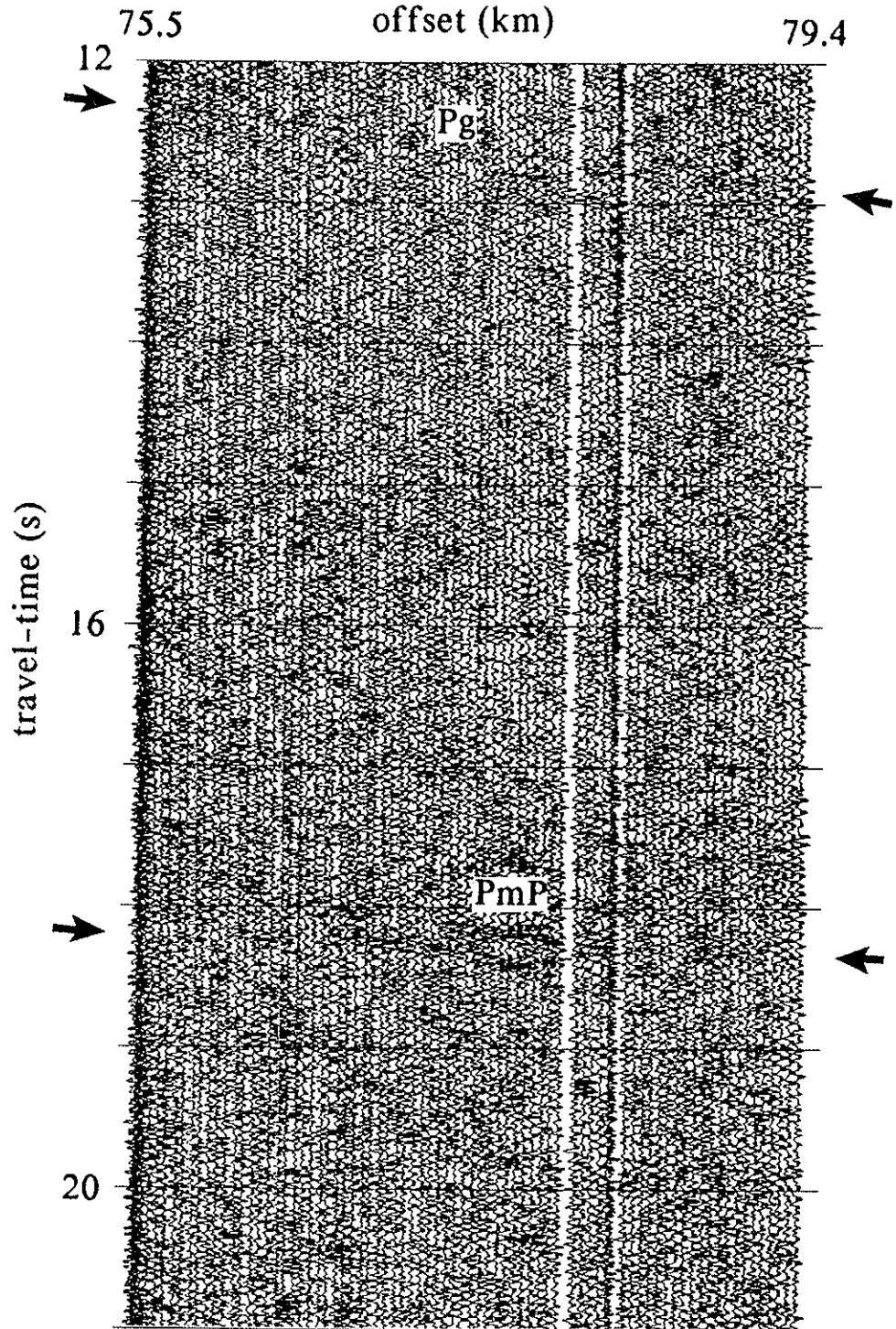
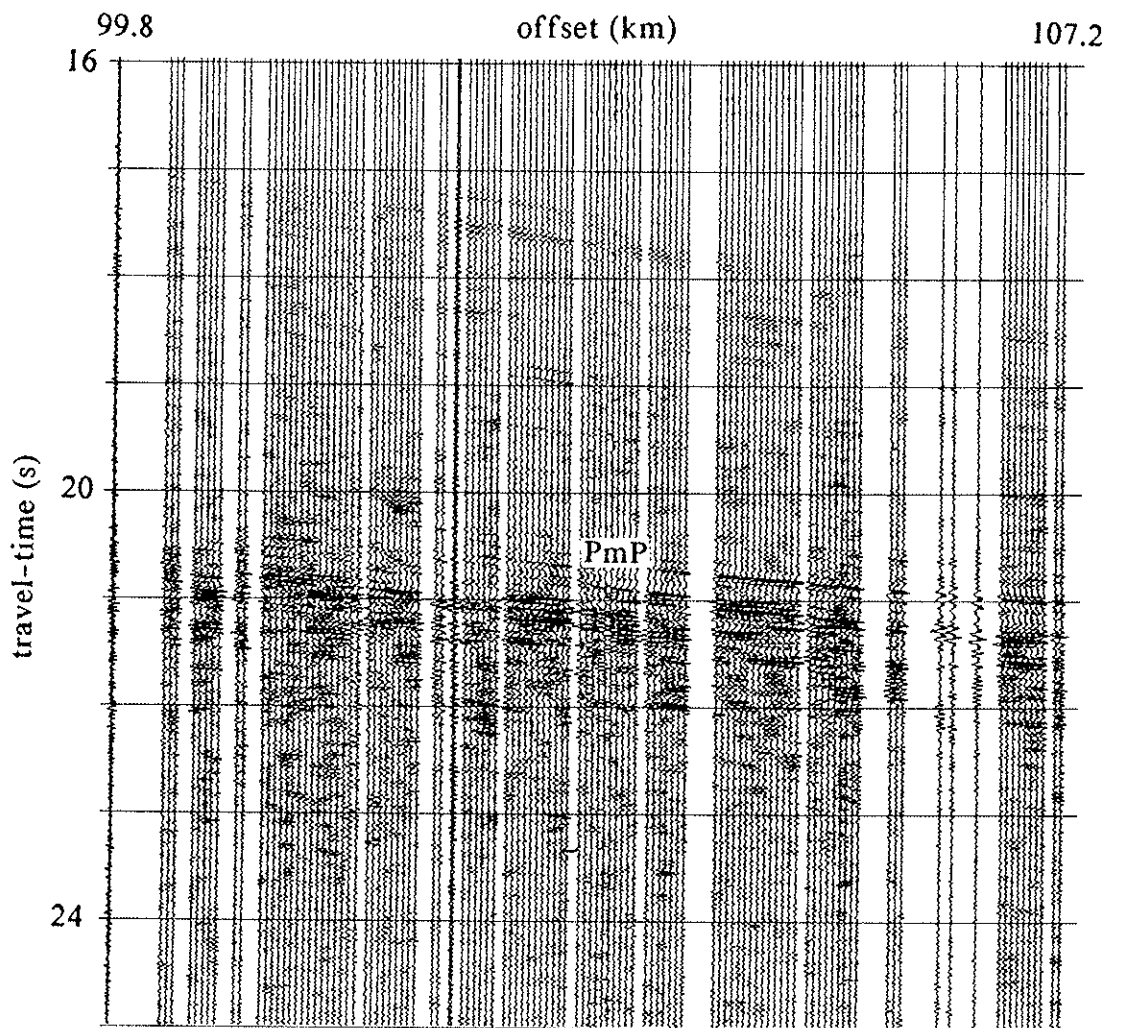


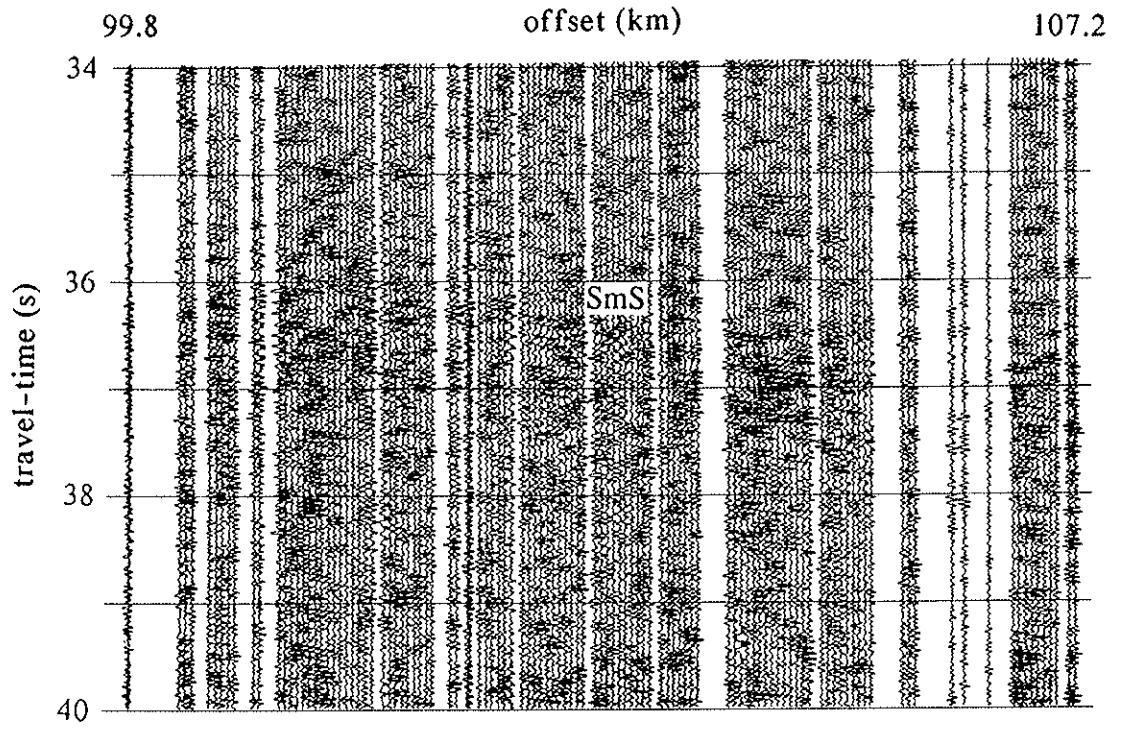
Figure 2.5. MN quarry blast record from profile PCN, max. offset 107.2 km, section containing a) P_mP , b) S_mS phases. Record contains arrivals from a delayed charge_m sequence (duration 0.4 s). Note the remarkably strong P_mP arrivals at pre-critical distance.

PCNQ quarry blast record



a.

PCNQ quarry blast record



b.

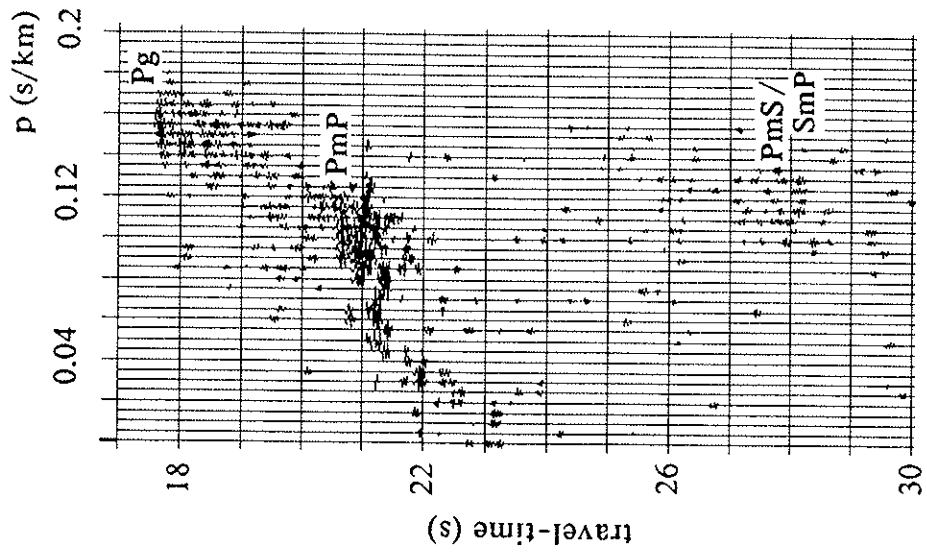
coherent arrivals. The vibroseis data at farther offsets contain reflected arrivals that coincide with the high-amplitude band of multi-cyclic reflection arrivals of the quarry blast data, identified as a pre-critical Moho reflection (P_mP). The quarry blast recordings also reveal reflected S-wave (S_mS) and converted (P_mS/S_mP) phases from the Moho [Fig. 2.5 b]. Figures 2.6 a,b illustrate the separation of S_mS and earlier S-wave arrivals at larger ray-parameters from multiples and P_mS converted phases by zones of low coherency in the slant stack.

INVERSION

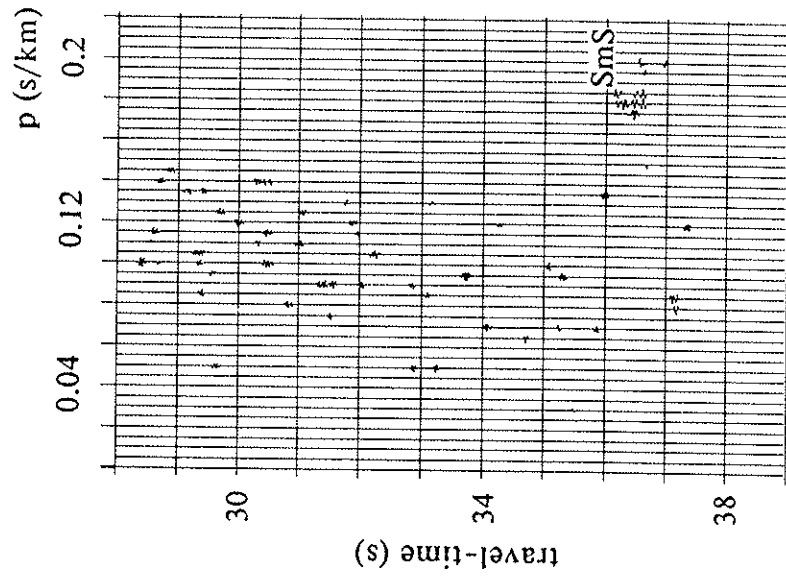
The wide-angle data from Ameralik were modeled by applying a 2-D travel-time inversion (Zelt and Smith, submitted paper), supplemented by amplitude modeling using asymptotic ray-theory (Cerveny et al., 1977), to obtain velocity distributions and depth boundaries for the continental and transitional Archean crust. An initial model was derived from a 1-D extremal inversion method (Bessonova, 1974; Dorman, 1979; Garmany, 1979; Hawman et al., 1990; Hawman and Phinney, 1991) applied to the larger offset coast-line data (Gohl et al., in press; also see Chapter I). The number of independent parameters for the velocity and boundary nodes of the 2-D inversion was reduced by implementing fixed values for impedance contrasts derived from amplitude modeling. The

Figure 2.6. Coherency-filtered slant stacks (t-p) of MN quarry blast record (max. offset 107.2 km), a) P_mP and P_mS , b) S_mS arrivals. The t-p domain enlarges the S/N ratio in aids in identifying phases as converted P_mS/S_mP and S_mS .

PCNQ quarry blast record

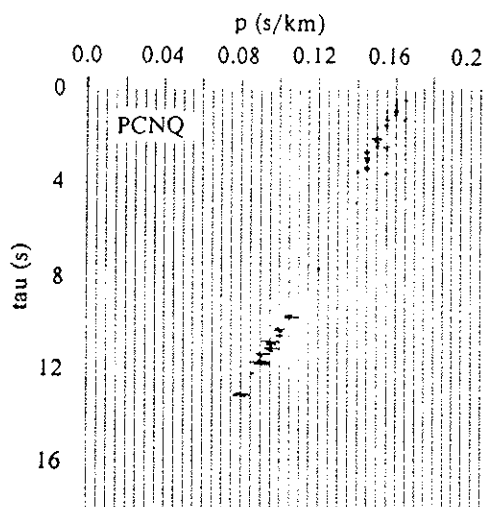
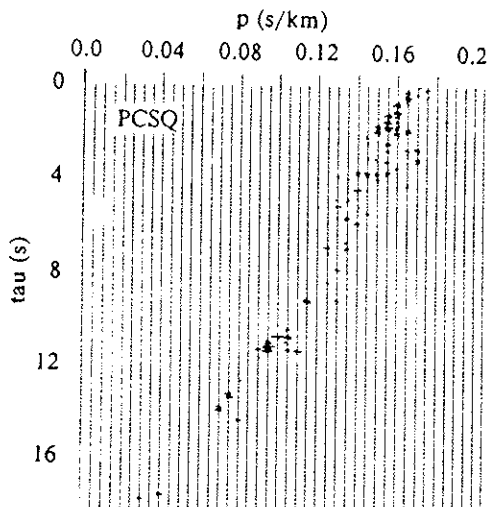
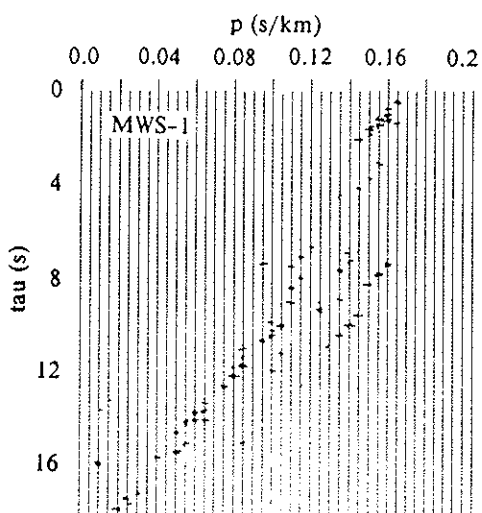
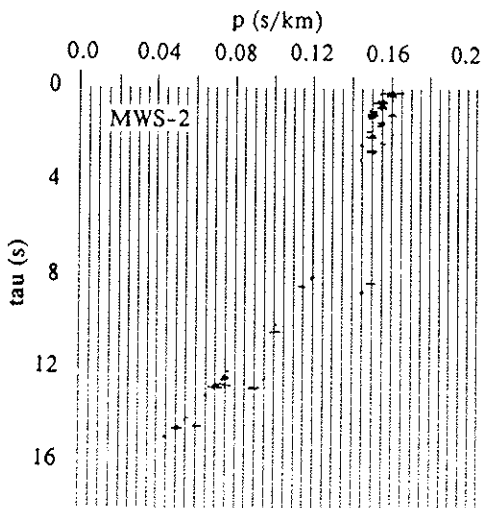
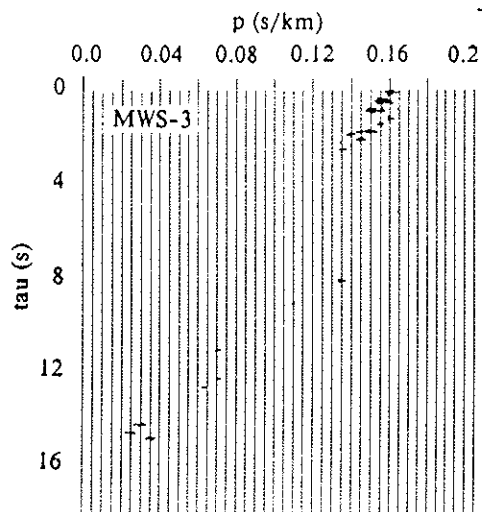
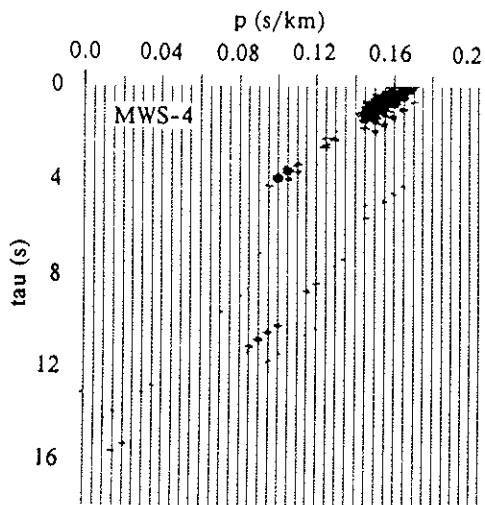


a.



b.

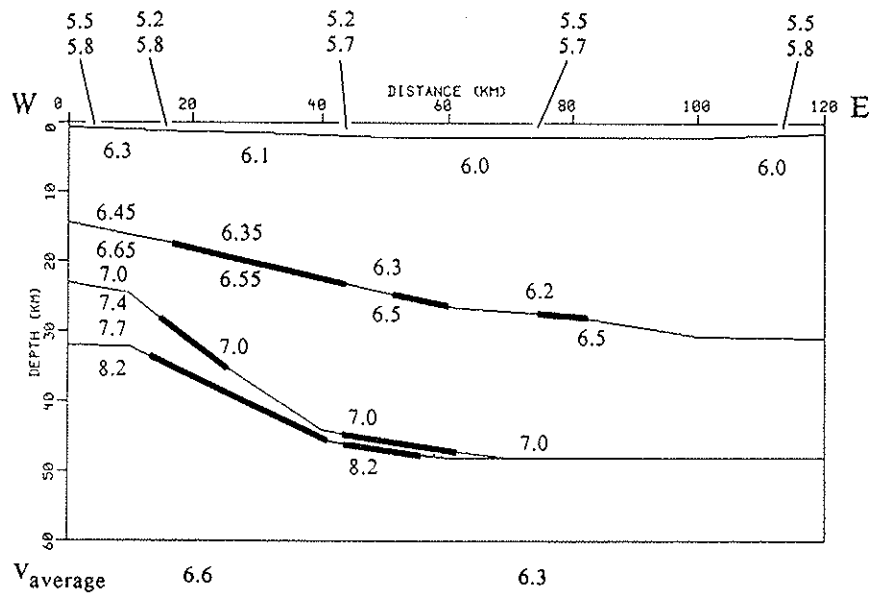
Figure 2.7. Coherency-filtered slant stacks (τ - p) from all MN quarry blast and vibroseis records used to pick arrivals for extremal inversion.



final 2-D P-wave velocity model for the Ameralikfjord profile [Fig. 2.8] contains a continental crust that thins rapidly toward the margin from about 48 km to 30 km depth. The dip is 25 to 30°. The base of the continental crust is poorly constrained due to a lack of reflections from the lower crust and Moho. The complete disappearance of these reflections toward the continent shows variations in reflectivity, possibly due to changing impedance contrasts or the existence of gradient zones. Results of the inverse modeling include an up to 6 km thick high-velocity zone (7.4-7.7 km/s) at the base of the oceanic-continental transitional crust [Fig. 2.8], and a mid-crustal low-velocity contrast reflector (ranging from 6.2 to 6.5 km/s and 6.45 to 6.65 km/s) between 25 km (east) and 17 km (west) depth. The average crustal velocity increases westward from 6.3 to 6.6 km/s (uncertainty 0.1 km/s).

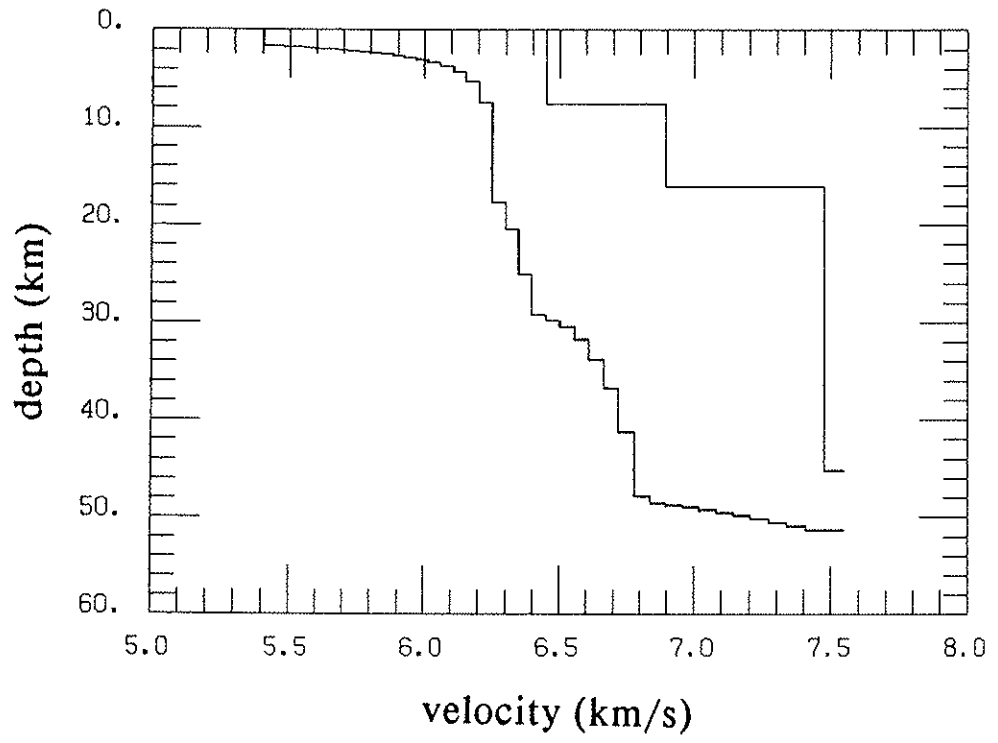
I performed a 1-D inversion on the recordings from Minnesota using the extremal method. Picks from slant stacks of individual shot gathers [Fig. 2.7] were combined into a single composite tau-p section of principal P-wave arrivals from the crust (Hawman and Phinney, 1991). The identification of principal arrivals becomes more reliable as data from larger offsets are included. Uncertainties in tau were assigned to the picks. Second order errors are due to uncertainties in ray-parameter measurements. The depth bounds from the extremal inversion [Fig. 2.9] are rather broad. Smaller ranges of depth bounds are seen for highest and lowest

Figure 2.8. Final P-wave velocity model from the Greenland profile AM. The thick lines indicate the horizontal coverage of the reflections. Note that no lower crustal and Moho arrivals were recorded from the Archean continental crust. On the continental-oceanic transitional crust the Moho dips with about 25 to 30 degrees. The average crustal velocity increases westward from about 6.3 km/s to 6.6 km/s.



velocity model AM

Figure 2.9. Results of extremal inversion of Minnesota wide-angle data; curves illustrate minimum and maximum depth bounds for each layer of constant slowness with slowness displayed as velocity. The depth bounds are wide for the middle crust because of lack of arrivals. Various reflections from the Moho provide good constraints for the crustal depth of 45 to 51 km in southern Minnesota.

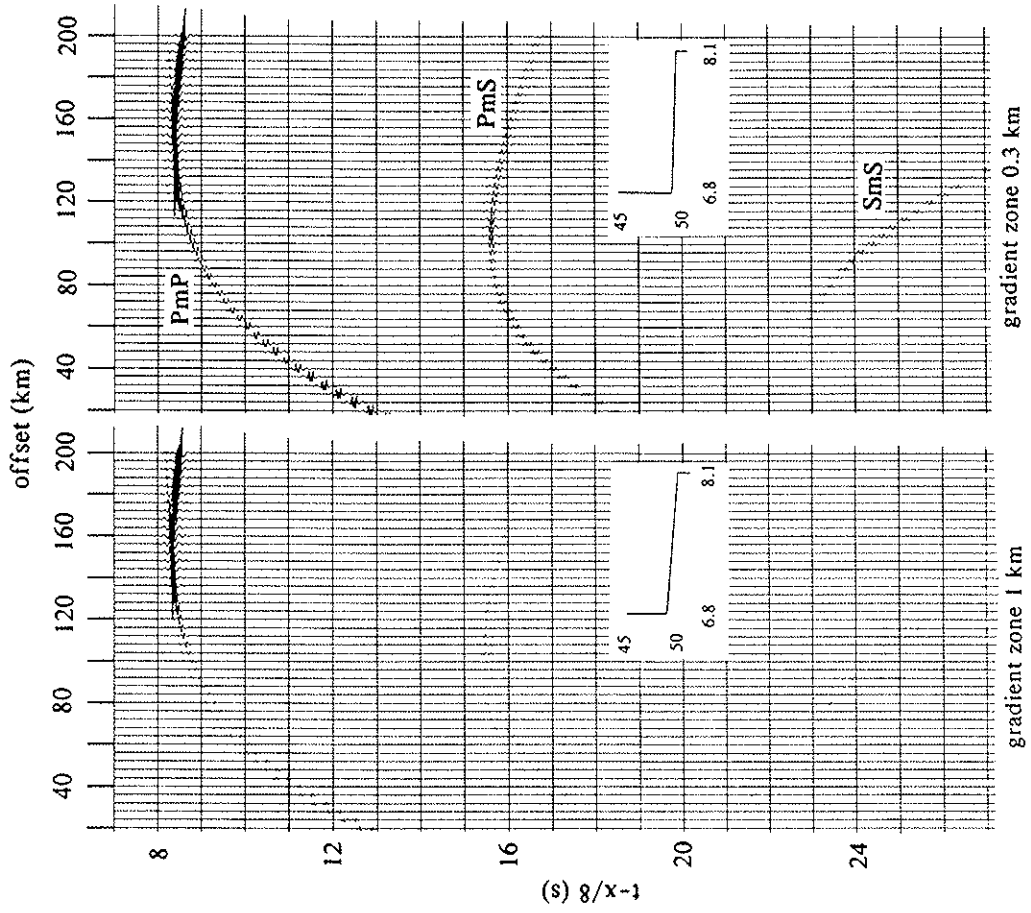


slownesses due to well constrained picks. A total crustal thickness of 45 to 51 km, an average crustal velocity of 6.5 to 7.0 km/s and a velocity of 6.8 to 7.5 km/s at the base of the crust comprise the main results of the inversion. Predicted critical distances for the Moho reflection range from 120 to 180 km which says that our maximum offsets are still in the pre-critical range. The recording of strong pre-critical P_mP arrivals at wide-angle offsets, and the observation of converted Moho reflections imply a first order discontinuity or a layered zone containing small velocity contrasts at the crust-mantle boundary rather than a gradient zone larger than a wave-length.

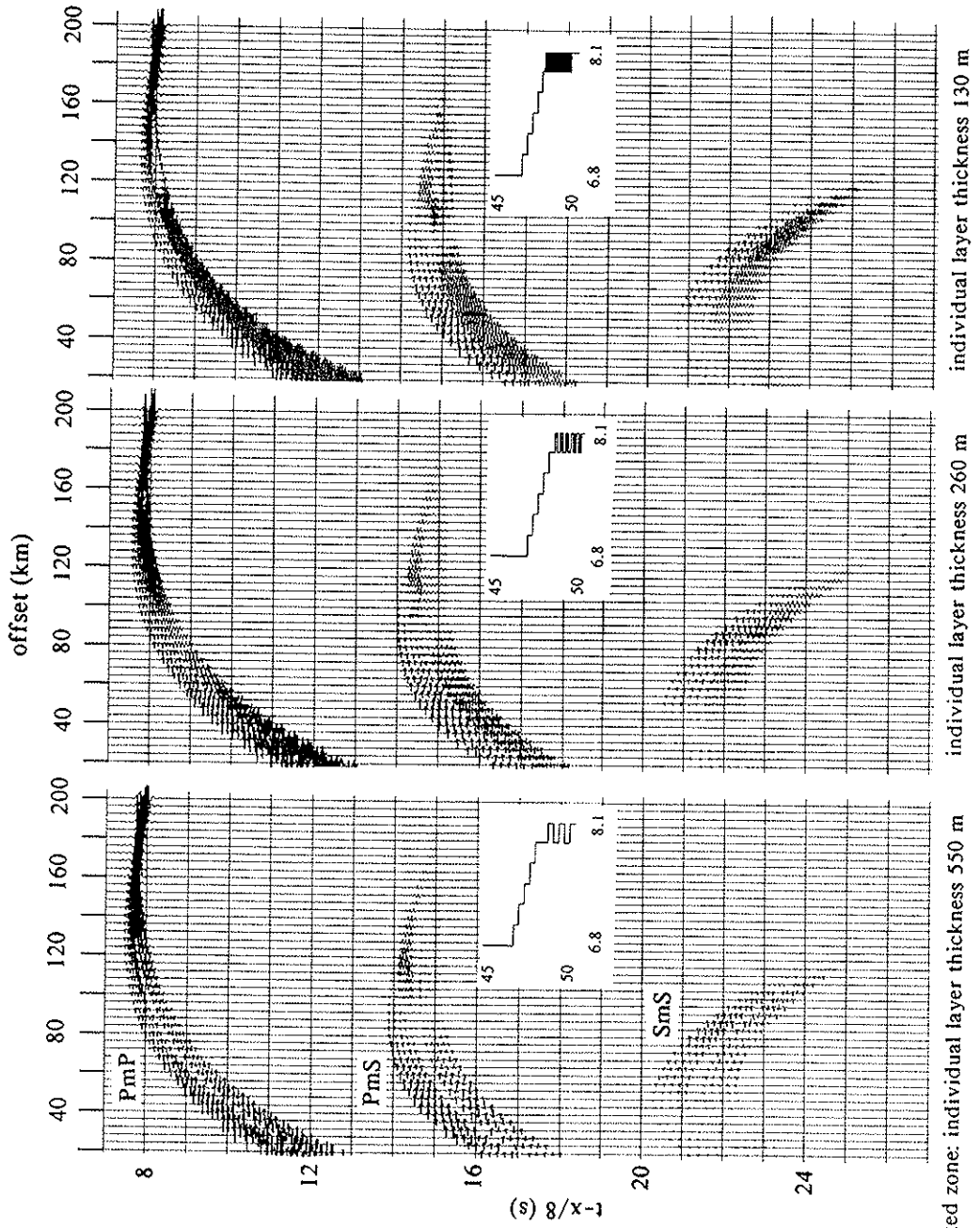
REFLECTIVITY MODELING

I used the reflectivity method (Fuchs and Mueller, 1971) to model different types of Archean crust-mantle boundaries with offsets from near vertical to 200 km. Two groups of Moho models were tested. Each model contains a crust-mantle transition within the depth range of 45 and 50 km with a velocity of 6.8 km above that zone. One type of transition zone [Fig. 2.10 a] consists of linear gradients of increasing velocities up to 8.2 km/s with a total thickness of 300 m (about one wavelength) to 3,000 m. The gradient is approximated by layers of 50 m thickness. The second model group [Fig. 2.10 b] contains alternating low- and high-

Figure 2.10. Reflectivity seismograms with corresponding velocity-depth models for Archean Moho in S Minnesota and SW Greenland. Two types of Moho transition zones are modeled: a) a linear gradient zone with a total thickness of 300 to 3,000 m, gradient is approximated by layers of 50 m thickness; b) a laminated zone of high-velocities, alternating between 7.9 and 8.1 km/s; this zone is gradually approached from above with a stepwise transition; individual layer thickness with the laminated zone ranges from 130 to 550 m; Model (a) reflects the observations from the continental crust in SW Greenland, while model (b) shows bands of high-amplitude arrivals at pre-critical distance as observed in S Minnesota. Amplitudes of the SmS phase are larger than those of the PmS phase at the observed offset of 99 to 107 km when the laminated zone consists of very fine layers.



a.



laminated zone: individual layer thickness 550 m
individual layer thickness 260 m
individual layer thickness 130 m

b.

velocity layers of 7.9 and 8.1 km/s, respectively, with individual layer thicknesses between 150 and 800 m. This zone is gradually approached from above with a step function of 2 km thickness. Variations in total thickness of the alternating layering range from 1.5 to 5 km. A high quality factor of 2000 was chosen to approximate the low seismic attenuation of crystalline crust. Each section is plotted with a reduction velocity of 8 km/s.

Discussion of results. Both types of models show characteristics of seismic amplitudes with respect to offset according to observation either from Greenland or Minnesota. The disappearance of pre-critical Moho reflections toward the Archean continental crust of SW Greenland is best approximated with a wide (> 1 km) gradient zone [Fig. 2.10 a]. Gradually increasing metamorphic grade with depth of mafic to ultramafic rocks can cause such a gradient. Griffin and O'Reilly (1987) and Smithson (1989) suggest a gradational phase change from granulite to eclogite facies, which seems plausible considering the great depth of the Archean crust in Greenland. The Archean Moho in S Minnesota, however, is represented by a model that contains sequences of 1st order discontinuities [Fig. 2.10 b]. A laminated Moho transition would generate a band of high amplitude P- and S-wave as well as P to S converted arrivals even for pre-critical distances as observed in our wide-angle experiment. Such a layered crust-mantle

transition has been suggested by numerous authors (i.e. Davydova et al., 1972; Hale and Thompson, 1982; Braile and Chiang, 1986; Meissner, 1973, 1986; Smithson, 1989), but mostly for younger, Phanerozoic crust and not for the Archean where Moho reflections at near-vertical offsets are not abundant. Our model consists of a layered complex with small velocity contrasts of only 0.2 km/s. The thickness of the Archean crust in Minnesota would bring increasing portions of the lowermost crustal rocks into the eclogite facies field with greater depths. The small velocity contrasts could be caused by interlayering of high-pressure garnet-granulite and garnet bearing eclogites. It is possible that parts of the Archean in Minnesota underwent multiple extension with associated underplating (i.e. Furlong and Fountain, 1986) during younger geologic time. Whether the reflective lowermost crust is related to tectonic events that generated swarms of mafic dykes in the late Archean and early Proterozoic (i.e. Morey, 1972) cannot be excluded but is speculative. Portions of accreted and intruded mafic to ultramafic material could have been brought into the eclogite facies field after cooling (Fountain, 1989) increasing the seismic velocities to be close to those of the upper mantle. This qualitative comparison of seismic observations with simple 1-D models shows that the crust-mantle boundaries of Archean crusts in Greenland and Minnesota are fundamentally different.

CONCLUSIONS

This study shows that Archean crust varies in composition and structure depending how a craton was affected by tectonic events after its initial generation in the Archean. The oldest Archean crust in SW Greenland is characterized by a loss of lower crustal and Moho pre-critical reflections where the crust is thickest (c. 48 km) and probably pure continental. On the other hand, strong pre-critical reflections from the Moho and from top of a high-velocity zone at the base of the transitional crust toward the continental margin indicate that younger extensional tectonic events would bring dense, ultramafic material into the lowermost Archean crust.

A very thin high-velocity lowermost zone is observed from wide-angle data in the 45 to 51 km thick Archean crust of southern Minnesota. Velocities within that zone exceed 7.0 km/s. A significant observation is the existence of high-amplitude P and S wave reflection bands at pre-critical distance (< 107 km) for Moho reflections.

A qualitative comparison of both Archean data sets by using reflectivity modeling over offsets ranging from near-vertical to post-critical shows that a wide gradient zone of more than 1 km thickness can explain the lack of pre-critical Moho reflections from the continental Archean crust of Greenland. The pre-critical Moho arrivals from the Minnesota

experiment are best modeled by implementing a laminated sequence of high-velocity layers, alternating from 7.9 to 8.1 km/s. This laminated zone is approached by a stepwise transition. Depending on the velocity contrast within the Moho transitional zone, such a crust-mantle boundary would generate amplitudes high enough to be observed in vertical-incidence seismic experiments as seen in the Minnesota River Valley (Boyd and Smithson, 1990; Boyd et al., 1991).

These simple reflectivity models show the different character of the Archean Moho. The gradational transition of the Greenland Moho can be explained by a phase change from granulite to eclogite facies at great crustal depths. Multiple extensional tectonic events with associated magmatic underplating and intrusions might have affected the Archean crust in Minnesota during younger geologic time. A connection of magmatic underplating with tectonic events that generated mafic dyke swarms in the Archean and Proterozoic is possible but speculative. Accreted and intruded mafic to ultramafic material could be brought into the eclogite facies field, increasing the velocities to be close to those of the upper mantle. A higher average crustal velocity of about 6.7 km/s for the crust in S Minnesota, as opposed to about 6.5 to 6.6 km/s for SW Greenland, indicates a slightly more mafic character of the Minnesota crust.

This study shows that oldest Archean crusts of similar age can be different in composition, in particular of the

crust-mantle boundary. Tectonic events in their post-Archean history might have affected their crustal composition and character of the Moho. It will be a challenge for the future to identify signatures of these events that may explain our observations.

CHAPTER III

SEISMIC WIDE-ANGLE STUDY OF ACCRETED PROTEROZOIC CRUST IN SOUTHEASTERN WYOMING

INTRODUCTION

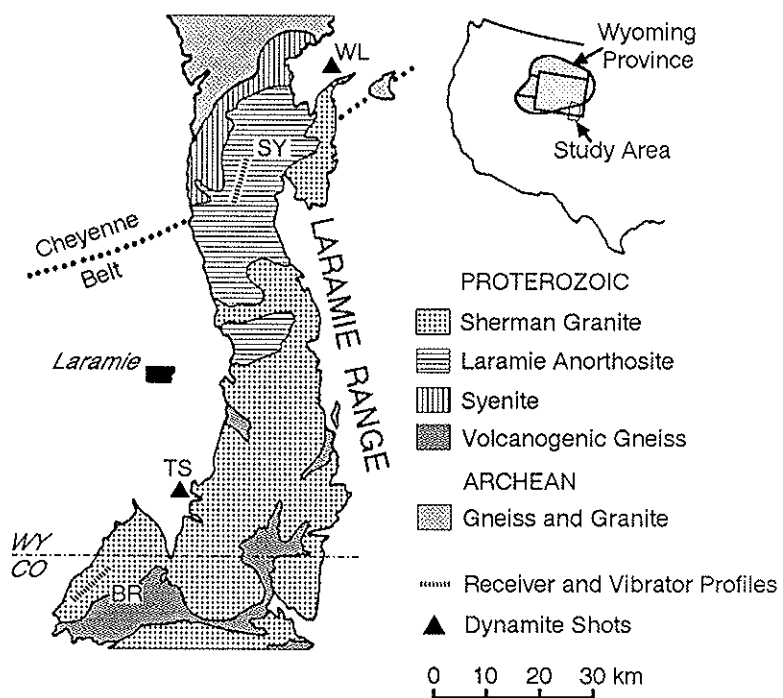
The boundary of the Archean Wyoming Province is considered to be an accretionary feature of a collision between a Proterozoic island arc and the Archean terrane in southeastern Wyoming (Hills and Armstrong, 1974; Condie, 1982; Johnson et al., 1984; Duebendorfer and Houston, 1986, 1987; Houston et al., 1989). Questions that remain open include the structure, the composition of mid- and lower crustal rocks, and the character of the crust-mantle boundary of the deep crust of the Proterozoic belt south of the suture (Cheyenne Belt). To address some of these questions, the University of Wyoming conducted several seismic wide-angle experiments in SE Wyoming. Vibroseis and dynamite shots were recorded into receiver profiles located on the bedrock of the Laramie Range and the northern Colorado Front Range. All the shot gathers were slant stacked to identify pre- and post-critical arrivals. Subsequent 1-D inversion provided estimates of local crustal depths and velocities. By using the reflectivity method, I obtained further models of impedance contrasts of

lower crustal phases and the crust-mantle boundary. The models have important implications for the petrological composition of the accreted Proterozoic terrane.

GEOLOGY AND PREVIOUS GEOPHYSICS

The most prominent geological feature in SE Wyoming is the NE-SW striking Cheyenne Belt [Fig. 3.1], a major shear zone that bounds the Archean Wyoming Province to the north from the lithologically different Proterozoic terrane to the south (Hills et al., 1968; Johnson et al., 1984; Karlstrom and Houston, 1984; Duebendorfer and Houston, 1986, 1987). 2700 to 2500 Ma old exposed basement in the Laramie Range, Medicine Bow Mountains, and Sierra Madre, consists of quartzofeldspathic gneisses, Archean supracrustal rocks, and late Archean intrusive granites. Karlstrom and others (1983) interpreted a sequence of quartz-rich metasedimentary rocks in the Medicine Bow Mountains as rift-deposits within an early Proterozoic basin along the southern margin of the Archean craton. Proterozoic basement rocks south of the Cheyenne Belt are different in composition from rocks to the north. They consist of 1800 to 1600 Ma old highly deformed amphibolite-grade meta-volcanic rocks. The existence of pillow basalts and agglomerates possibly indicates the presence of an early Proterozoic island arc (Houston et al., 1989). Syn- and post-tectonic anorthositic and granitic intrusions, such as the

Figure 3.1. Schematic map of geologic units in SE Wyoming including seismic wide-angle shot and receiver locations. Both wide-angle lines SY and BR served as reversed vibroseis shot and receiver profiles. The dynamite shots TS and WL were recorded on profile BR.



Laramie anorthosite (1400-1500 Ma) and Sherman granite (1400 Ma) complexes (Peterman et al., 1968; Hills and Armstrong, 1974; Premo and Van Schmus, 1989) cover areas on top and south of the Cheyenne Belt. Northward thrusting of an island arc over the northern craton as a consequence of south-dipping subduction is one model for the juxtaposition of the terranes (Johnson et al., 1984; Premo and Van Schmus, 1989). A second model, based on isotopic data of Proterozoic granitoids in the Laramie Range, suggests a predominantly Proterozoic lower crust under the Cheyenne belt, generated by magmatic underplating or underthrusting of Proterozoic crust during terrane accretion (Geist et al., 1989). However, the time difference of about 200 to 400 Ma between the formation of meta-volcanics and the emplacement of the granitic and anorthositic plutons suggests that the accretion was not a single event.

Widely spaced seismic refraction data suggest that the crust thickens from 37-41 km in SE Wyoming to about 48-54 km beneath the Colorado Front Range (Jackson et al., 1963; Jackson and Pakiser, 1965; Prodehl and Pakiser, 1980). COCORP reflection profiles across the Laramie Range exhibit low-amplitude, discontinuous, multi-cyclic arrivals observed over the Denver and Laramie Basins (Allmendinger et al., 1982; Brewer et al., 1982; Johnson and Smithson, 1985, 1986). These events are interpreted as Moho reflections arriving from depths of 48 km north of the Cheyenne Belt. Events in profiles

south of the Cheyenne Belt are identified as Moho reflections from a depth of about 37 to 39 km (Allmendinger et al., 1982; Brewer et al., 1982). Gravity data indicate a gradual increase of crustal depth and/or a more felsic Proterozoic crust that compensates for a difference of about 100 mgal across the suture zone (Johnson et al., 1984).

SEISMIC EXPERIMENT

The seismic experiments were designed to record wide-angle reflections mainly from the lower crust and crust-mantle boundary of the Proterozoic accreted terrane south of the Cheyenne Belt (Fig. 3.1). In two summer field seasons, the University of Wyoming seismic crew acquired data from vibroseis sources and dynamite shots with offsets of up to 130 km. Three densely spaced receiver spreads were deployed. A 48-channel profile (96 channels in parts of the profile) (SY87) with 100 m group spacing was located in the Laramie Range, two spreads (BR87 and BR89), 86 and 192 channels with 100 m group spacing, were deployed in the northernmost Colorado Front Range. Vibroseis sources, consisting of 4 trucks with 9-21 linear sweeps of 10-42 Hz per vibrator point (VP), were located on 54 locations (50 m spacing) in the Laramie Range and on 64 locations (50 m spacing) in the Front Range to be recorded from profiles BR87 and SY87, respectively. Eight dynamite shots detonated from the eastern Laramie Range (WL)

and the southern Laramie Basin (TL) and were recorded by profile BR89. Transverse component geophones replaced the vertical component geophones on profile BR89 for some shots to record shear waves.

PROCESSING

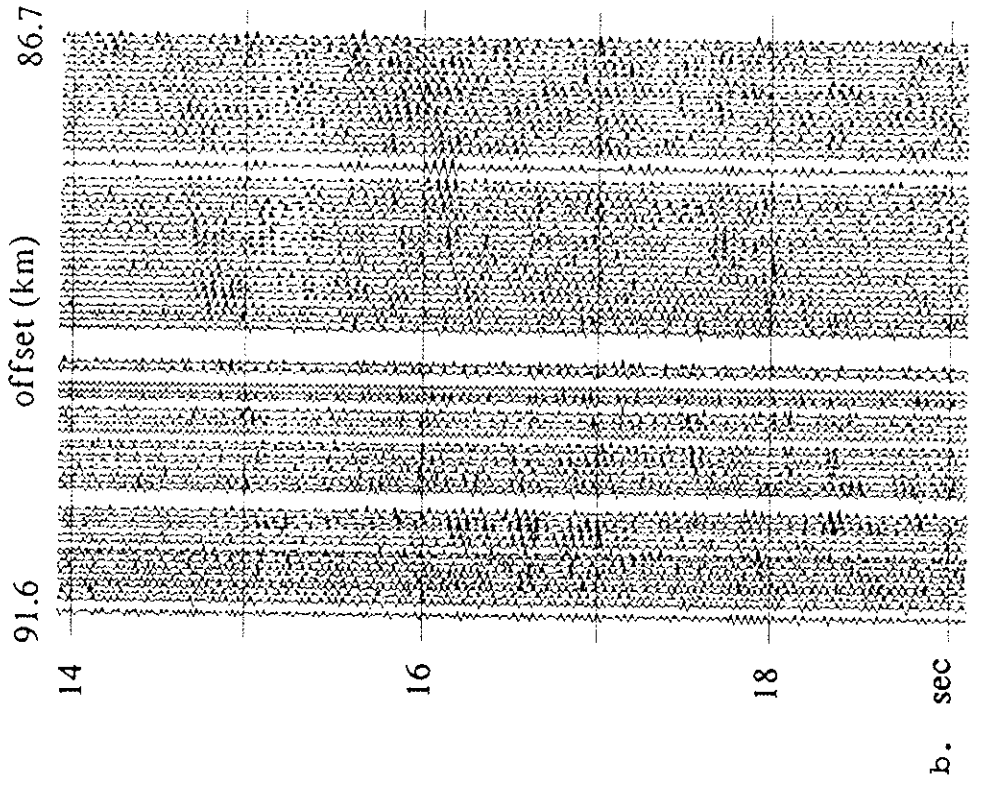
All vibroseis recordings were corrected for elevation statics, edited, vertically stacked, and band-pass filtered within the sweep frequency. The data quality of the recordings changes among the individual VP gathers, probably due to changes in ground coupling when receiver and sources were moved along their profiles. We slant stacked the data from 27 VPs of profile SY87 and 36 VPs of profile BR87 to obtain an immediate estimate of apparent velocities. A coherency filter applied to individual slant stacks by calculating the semblance (Stoffa et al., 1981) aided in the identification of pre- and post-critical phases of high-amplitude coherent signals. The coherency-filtered slant stacks for each receiver profile were summed into a single tau-p gather.

Some vibroseis records contain distinct high-amplitude arrivals, i.e. at 14.5 - 18.5 s at 90 km offset [Fig. 3.2 a,b]. These phases are identified as first arrivals (Pg), a series of mid-crustal refractions and reflections, and multi-cyclic pre-critical lower crustal reflections from the ray-parameter and intercept-time [Fig. 3.3 a,b]. The peak signal

Figure 3.2. Vibroseis records from receiver profiles SY87 (a) and BR87 (b); sources are on reversed profiles. Records are stacks 19 sweeps with a frequency of 10-42 HZ. Bands of seismic arrivals are observed in both recordings.

receiver profile BR87

VP 143



receiver profile SY87

VP 22

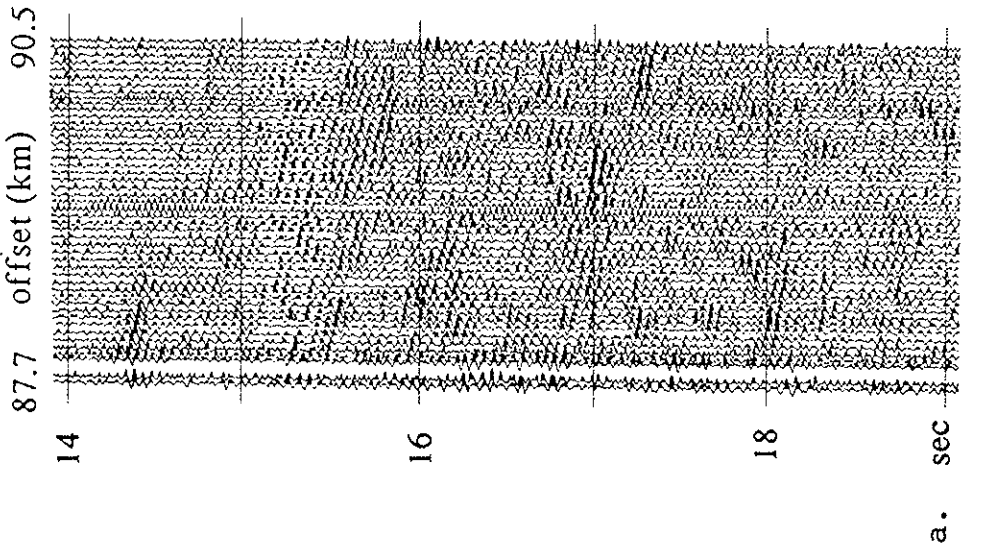
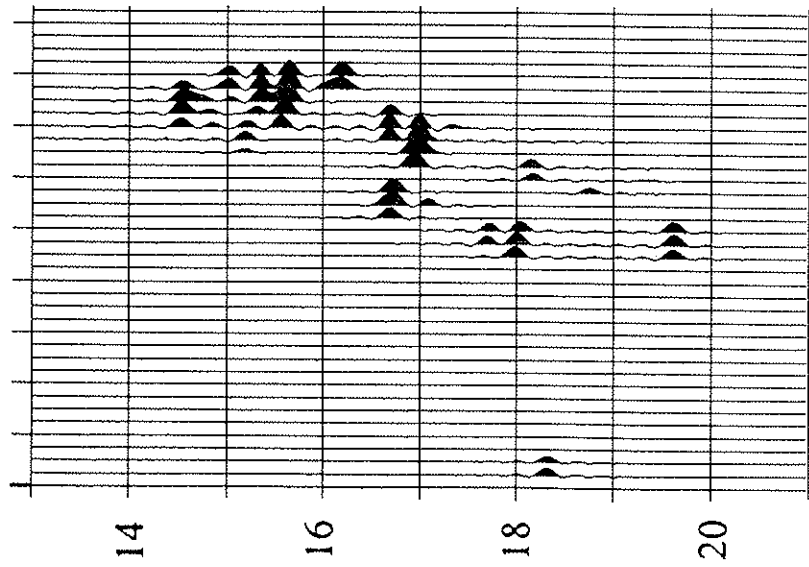


Figure 3.3. Coherency-filtered slant stacks (t-p) of vibroseis records from VP 22 of profile SY87 (a) and VP 143 of profile BR87 (b). T-p arrivals are scattered. High-amplitude events were picked for extremal inversion scheme to estimate depth bounds of reflectors.

VP 22

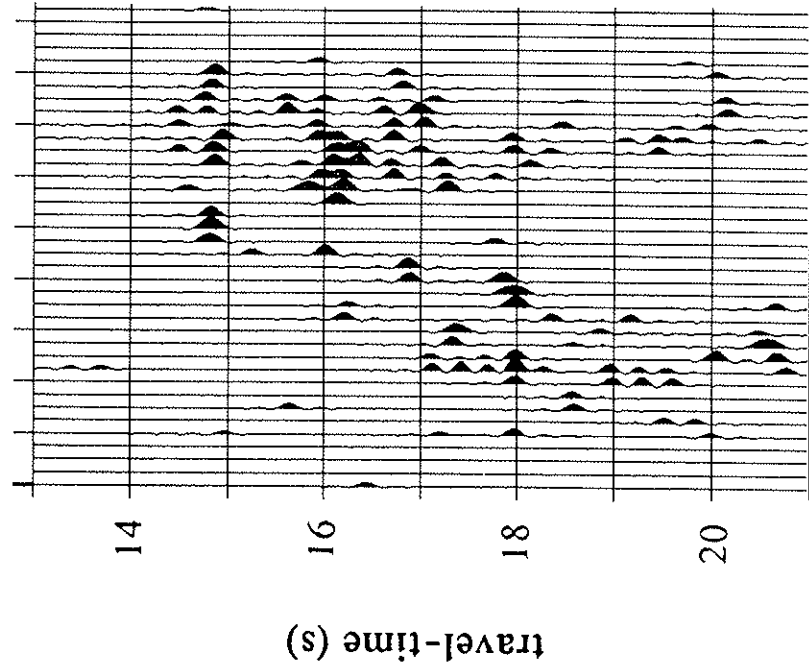
p (s/km)
0.04 0.08 0.12 0.16



a.

VP 143

p (s/km)
0.04 0.08 0.12 0.16



b.

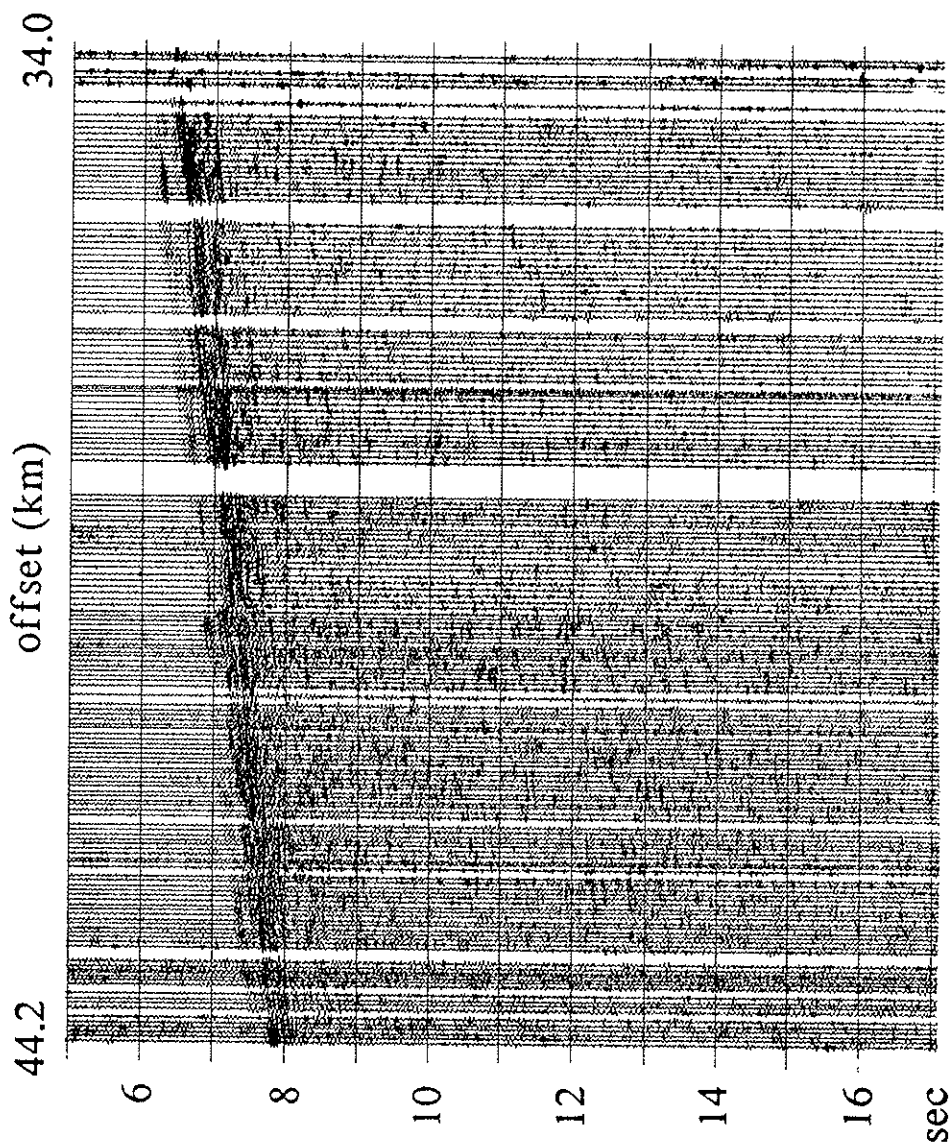
frequency lies at about 20 Hz. The tau-p transformation enhances weak-amplitude phases in other record sections.

The seismic sections from the dynamite shots contain high-amplitude low and high frequency noise which was eliminated by a 10-30 Hz band-pass filter. Peak signal frequencies lie around 20 Hz. Shot gathers were also slant stacked to enhance phase correlation. The summed tau-p gather of the two largest shots from WL (max. 126 km offset) and TS (max. 50 km offset) shows two branches of arrivals: a branch of high-amplitude upper crustal arrivals and a branch of scattered mid- and lower crustal P-wave phases [Fig. 3.6 c].

The dynamite shot gathers contain stronger coherent arrivals than the vibroseis data [Fig. 3.4 a,b]. First breaks and mid- and lower crustal phases arrive within a band of high-amplitude signals on gather WL. A high-amplitude Moho reflection is not visible. A critical arrival from the Moho may be hidden within the multi-cyclic band of lower crustal arrivals, but transformation into the tau-p domain does not indicate evidence for a distinct Moho reflection either [Fig. 3.6 a-c]. The transverse components of shot gather WL show a broad band of arrivals between 35 and 42 seconds [Fig. 3.4 c] with highest amplitudes at ray-parameter 0.27 s/km [Fig. 3.5]. Their travel-time and ray-parameter identify them as lower crustal S-wave reflections from the same depths as the corresponding lower crustal P-wave reflections.

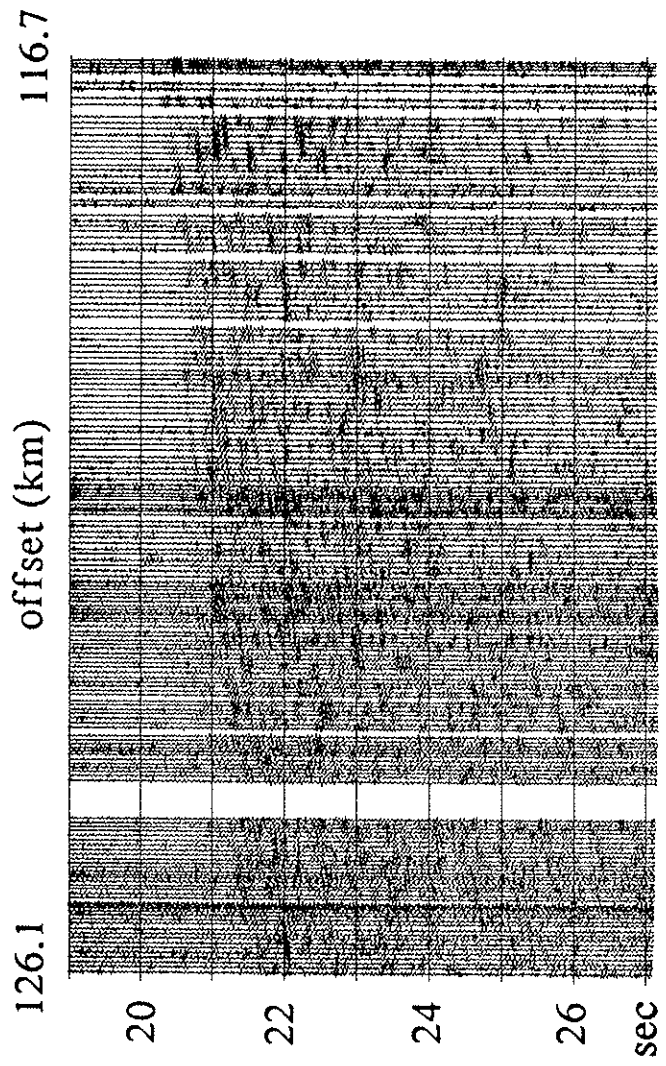
Figure 3.4. Dynamite shot records (BR89), vertical component, sources location TS (a), WL (b), horizontal component, source location WL (c). The shorter offset recording TS contains high-amplitude direct and uppermost crustal P-wave arrivals, but no mid- and lower crustal events and no Moho arrival. The large-offset recording WL shows multi-cyclic mid- and lower crustal arrivals. Although the WL recording approaches critical distance, it does not contain a distinct Moho reflector. A five second long band of low-amplitude arrivals beginning at about 35 s was recorded on the transverse component from shot WL.

receiver profile BR89
dynamite record TS



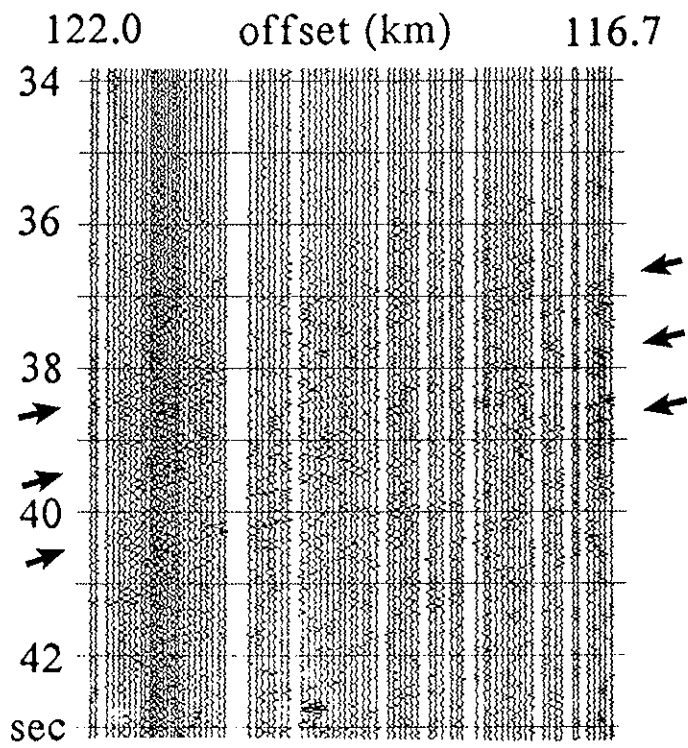
a.

receiver profile BR89
dynamite record WL



b.

receiver profile BR89
dynamite record WL
transverse

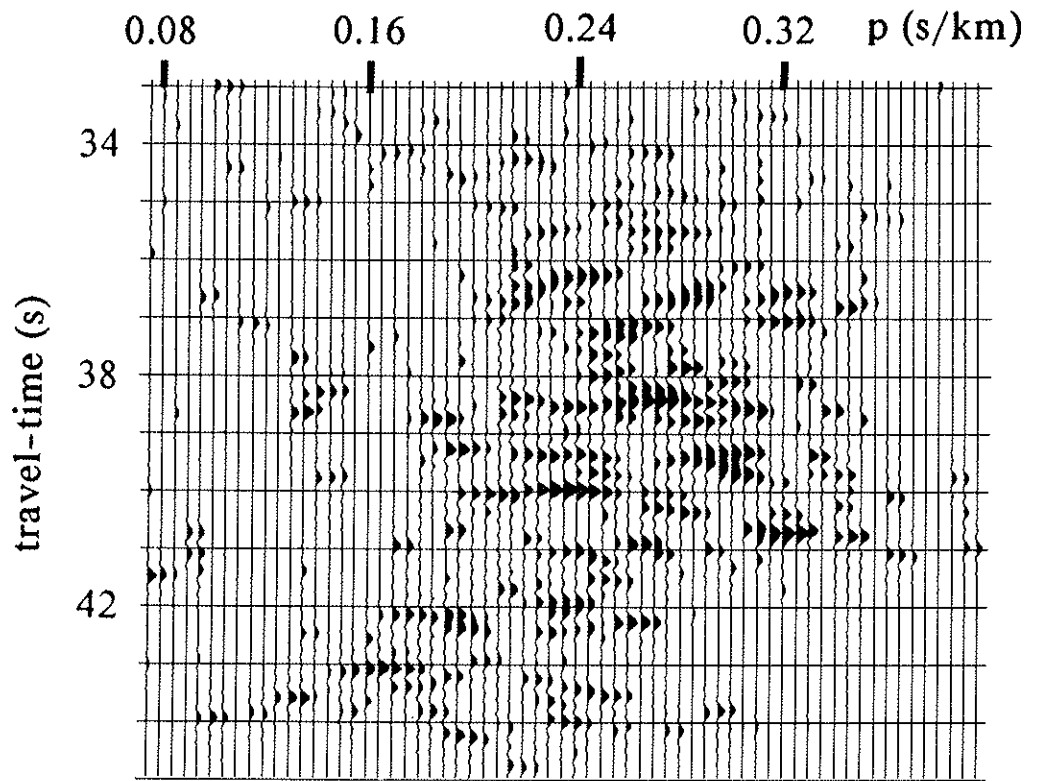


c.

Figure 3.5. Coherency-filtered slant stack (t-p) of transverse component of dynamite record BR89 (source location WL). The lower crustal S-wave event is extremely scattered.

dynamite record WL

transverse



INVERSE AND FORWARD MODELING

Arrivals from individual and summed tau-p gathers [Fig. 3.6 a-c] were modeled for minimum and maximum depth bounds using an extremal inversion method (Bessonova et al., 1974; Hawman and Phinney, 1991). The model was parameterized by implementing a stack of layers with constant slownesses. Slowness values decrease with depth. Minimum and maximum depth bounds were calculated for each layer; slownesses are displayed as layer velocities. Because of the narrow horizontal aperture of the shot gathers (between 4 and 9 km), the slant stacks consist of accumulations of data points rather than elliptic curves. In the first attempt to invert the data, only few highest amplitude data points were picked with uncertainties in tau of 0.1 to 0.15 s. After successfully modeling of these initial picks, more picks with uncertainties between 0.1 and 0.2 s were chosen. The smallest width of depth bounds could be reached for the dynamite profile BR89 and the vibroseis recordings of profile SY87 [Fig. 3.7]. The summed slant stack of profile BR87 [Fig. 3.6 b] contains a few distinct, but scattered, high-amplitude arrivals, producing wide depth bounds [Fig. 3.7]. An interesting result from the one-dimensional inversion model is the observation of bands of different reflectivity within the sections rather than distinct reflections. The crust appears to consist of an upper and lower crust that is more reflective than the middle crust.

Figure 3.6. Summed slant stacks of vibroseis records SY87 (a) and BR87 (b), and dynamite records BR89 from source locations TS and WL (c). High-amplitude events were picked for extremal inversion. Because of better defined arrivals from profile SY87 and the upper 3 seconds (τ) of profile BR89, the assigned uncertainties were only between 0.1 and 0.15 s, resulting in narrower depth bounds in Figure 3.7.

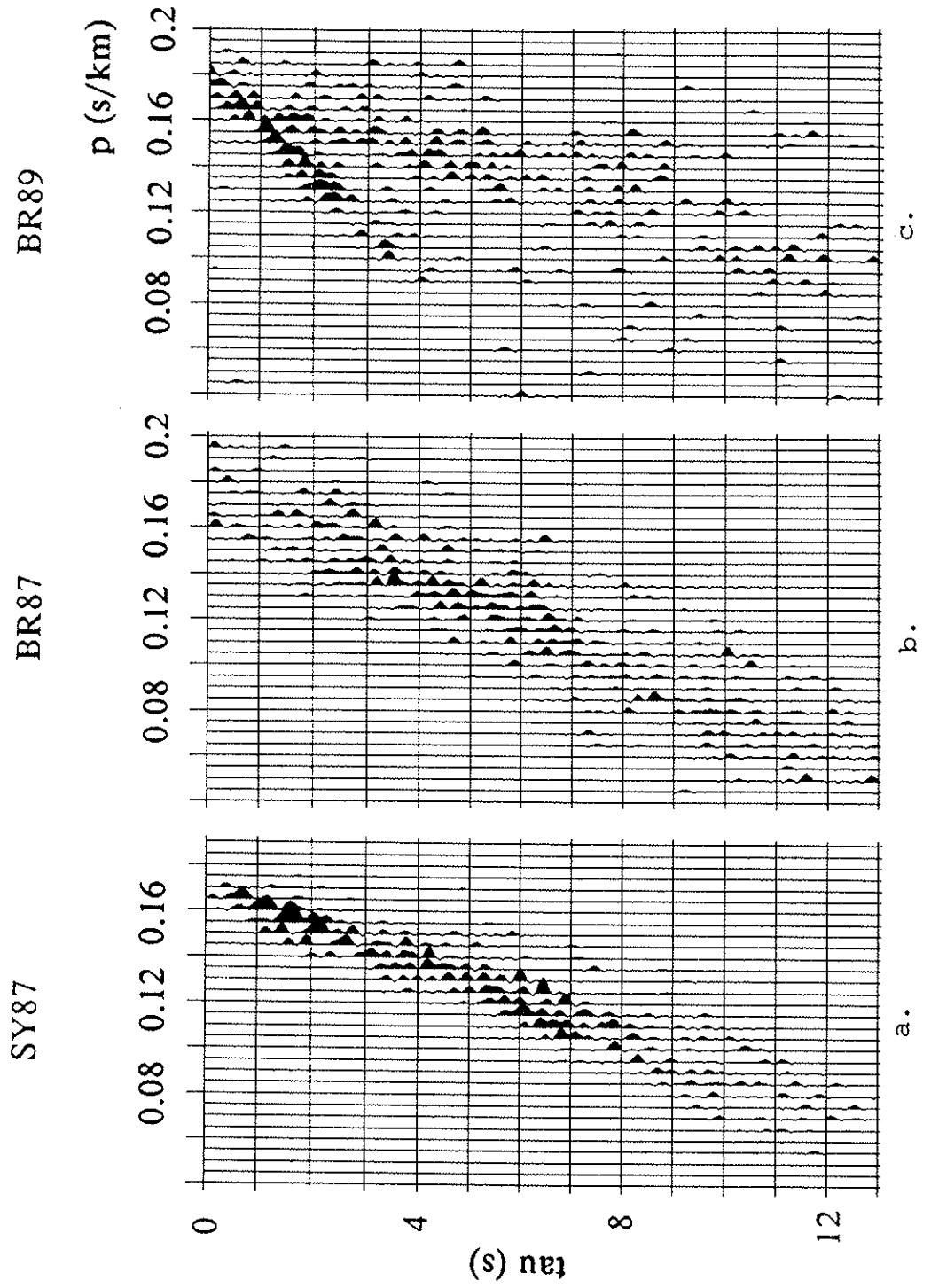
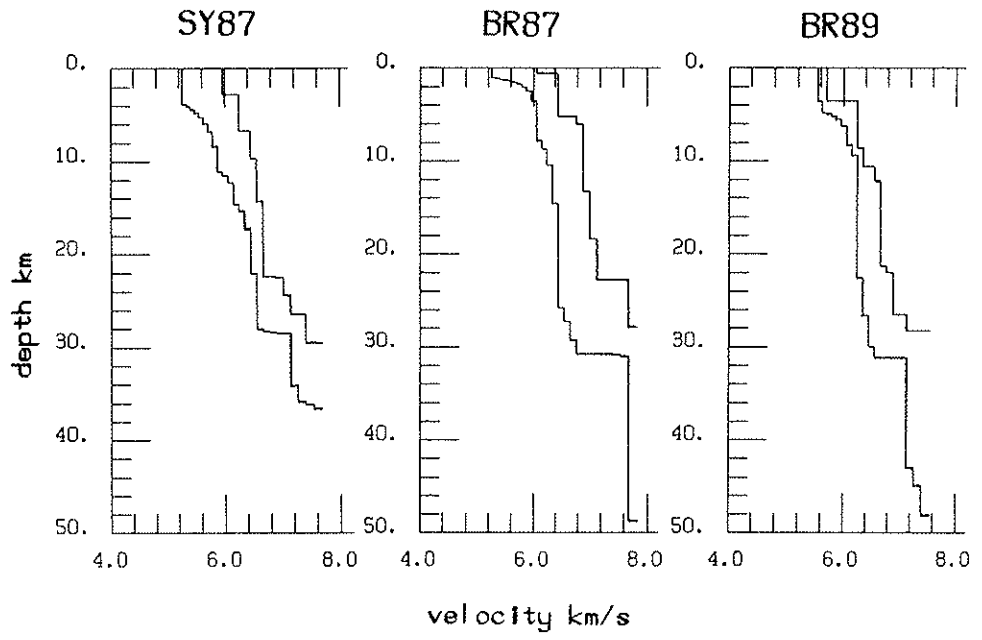


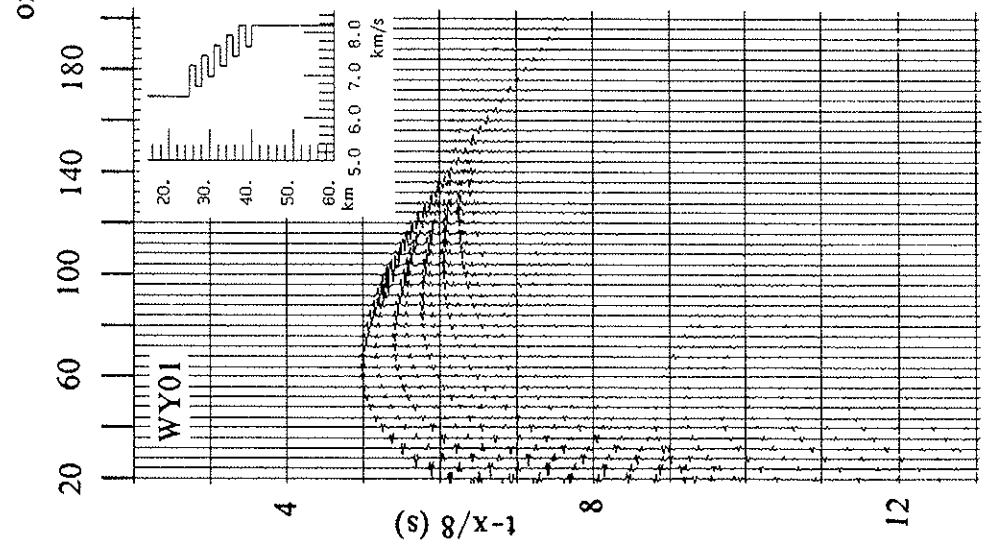
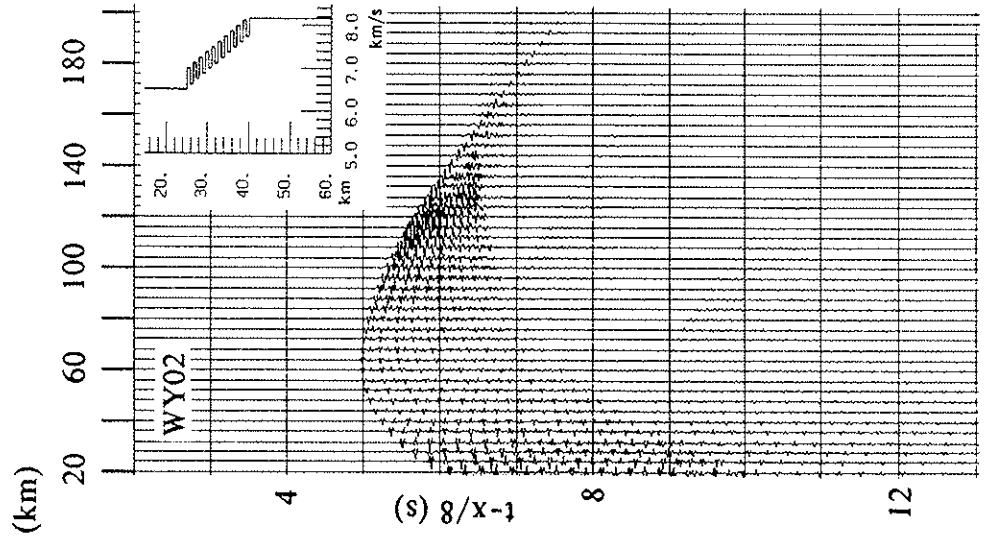
Figure 3.7. Results from 1-D extremal inversion, curves represent upper and lower depth bounds. Note the narrower depth bounds of model SY87 and the upper part of BR89, because of smaller uncertainties of tau-p picks. Depth bounds curves contain upper crustal discontinuities down to about 11 km, and a series of lower crustal discontinuities between 22 and 35 km depth. A distinct Moho is not observed, therefore the uncertainties for crustal depth are large. There is evidence for high velocities of above 7 km/s for the lowermost 8 to 10 km.

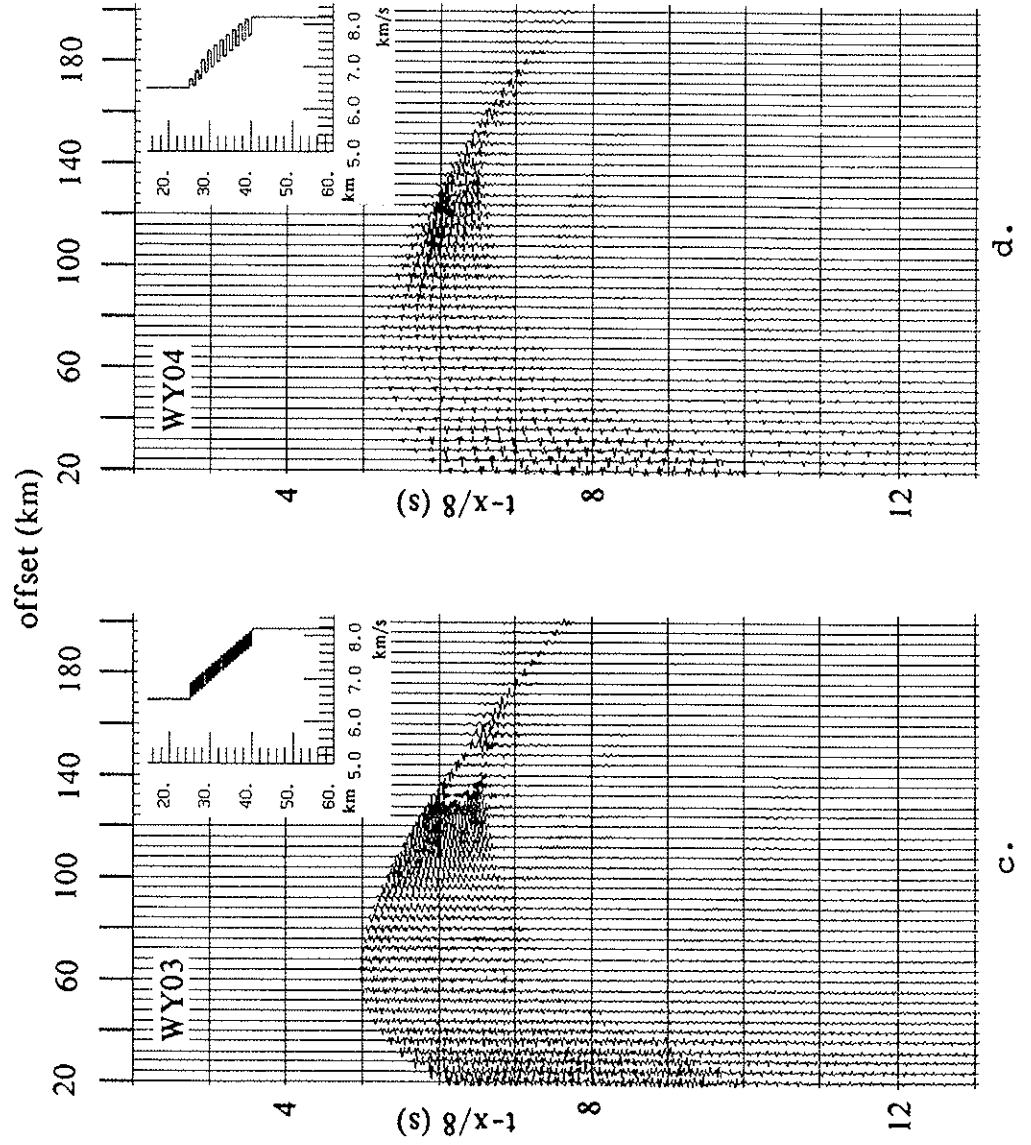


The lower crust especially seems to consist of layered sequences. A distinct Moho reflection is not observed, even at the critical distance data of shot WL. The lowermost reflections are best modeled by discontinuities at depths of 25 to 40 km.

Lower crustal models chosen for the reflectivity method (Fuchs and Mueller, 1971) include a transitional zone from 25 to 40 km depth consisting of layers of alternating low and high velocities [Fig. 3.8 a-c]. We chose this type of model to demonstrate a highly reflective lower crust where a large amount of seismic energy is reflected above the Moho. This type of model also represents observations of exposed lower crust of Phanerozoic and Proterozoic arcs consisting of differentiated layered plutonic complexes ranging from ultramafic to felsic in composition (Hamilton, 1981, 1988; Bard, 1983). The constant thickness of the individual layers within the transitional zone of our models varies between 0.3 km (about one wave-length) and 1.5 km. Velocities range from 6.5 km on top of the zone to upper mantle velocity of 8.2 km/s at the base. The velocity difference between layers lies between 0.4 and 0.5 km/s corresponding to observed velocity contrasts of between noritic-anorthositic-charnockitic and garnet- and pyroxene-granulitic to eclogitic rocks at lower crustal depths and pressure (Birch, 1961; Manghnani et al., 1974; Christensen and Fountain, 1975; Jackson and Arculus, 1984; Fountain et al., 1990). The synthetic seismograms show

Figure 3.8. Synthetic seismograms with corresponding velocity-depth models by using the reflectivity method (a-d). Lower crustal layering with individual layer thicknesses of 0.3 to 1.5 km approximates intermediate/felsic interlayering as observed in exposed cross-sections.





similar features of all four models, such as a 0.8 to 1.3 second broad band of high-amplitude arrivals at critical angle (offset 120-130 km). Model WY04 [Fig. 3.8 d], however, illustrates the best match with the observed data, because it contains a short (0.8 s), strong amplitude band of arrivals, as observed in parts of the large offset (max. 130 km) dynamite recording, and in the pre-critical (85 to 100 km) vibroseis recordings. The broad band of scattered arrivals of the observed data might be due to small-scale random lateral heterogeneities in the lower crust creating a scattering effect in wide-angle data (Gibson and Levander, 1988). Calculated maximum amplitudes at 30 to 40 km offset are about 16 db smaller than the maximum amplitudes at critical distance, and they are distributed over a very broad band of 4 seconds. Such a broad band of low-amplitude phases might not be identified within the noise level of dynamite record TS.

DISCUSSION

Inversion and forward modeling results show that the Proterozoic lower crust in SE Wyoming consists of a zone of high reflectivity. A sequence of alternating low and high velocity layers with velocities ranging from 6.5 to 7.5 km/s might exist between 25 and 37 km depth. If the Proterozoic crust is considered to be the relic of an accreted island arc as the meta-volcanic surface rocks suggest, then a possible

bulk upper and mid-crustal composition would consist of metavolcanic rocks and felsic plutons. Exposures of island-arc middle crust, i.e. in northern Pakistan, are dominated by migmatites and tonalitic batholiths with increasing grade of metamorphism from amphibolite to granulite facies with depth (Bard, 1983; Hamilton, 1988). The lower, highly reflective, crust may contain rocks of more mafic to ultramafic composition interlayered with charnockitic and anorthositic complexes. The metamorphic grade of these layered sequences increases with depth from low pressure to high pressure granulite and eclogite facies (Hamilton, 1988). Examples of such interlayered lower crustal island arc sequences are exposed in northern Pakistan (i.e. Coward et al., 1982; Bard, 1983) and New Zealand (i.e. Mattinson et al., 1986). Our reflectivity models approximate a sequence of interlayered ultramafic and felsic rocks in which the velocities lie within the range of observed values for anorthosites, charnockites, garnet-granulites, and eclogites (Manghnani et al., 1974; Christensen and Fountain, 1975; Jackson and Arculus, 1984; Fountain et al., 1990). Increasing metamorphic grade with depth causes an increase in rock velocities close to those of upper mantle velocities. Hamilton (1981, 1988) argues that the Moho in magmatic arcs is either a zone of intercalated mafic and ultramafic rocks rather than a sharp boundary, or a phase transition from granulite to eclogite facies. Both models would explain the lack of distinct Moho reflections. Also, an

interlayered lower third of the crust with strong impedance contrasts reflects most of the seismic energy before it reaches the crust-mantle boundary. The lack of distinct Moho reflections seems to be a common observation for other Proterozoic accreted arc complexes. Reflection data from the Precambrian midcontinent of the Great Lakes region (Cannon et al., 1991) show features similar to our wide-angle data. In the Great Lakes region, a highly reflective lower crustal zone and a lack of a distinct Moho reflection is observed beneath an Early Proterozoic island arc terrane accreted between two Archean blocks.

The lack of Moho reflections does not permit to verify the crustal model of SW Wyoming derived from gravity and low-resolution refraction data (Prodehl and Pakiser, 1980; Johnson et al., 1984) in which the crust deepens from the Archean craton to the Proterozoic accreted crust. Although the inversion and forward modeling results might be biased to a small degree by that dip effect, our data provide an estimate of crustal composition and formation of an Early Proterozoic island arc complex whose compositional character has been preserved through time.

CONCLUSIONS

Seismic wide-angle data of the Proterozoic crust south of the boundary of the Archean Wyoming Province in SE Wyoming

indicate a moderately reflective upper and lower crust surrounding a less reflective middle crust. Inverse and forward models derived from various large offset (85 - 130 km) vibroseis and dynamite recordings show that the reflective lower crust may consist of a zone of alternating high and low velocities. The lower crustal layer velocities range from 6.5 to 7.5 km/s. The average lower crustal velocity of 6.9 km/s suggests a predominantly mafic composition with interlayered felsic components generating high impedance contrasts. Our model represents observations from exposed lower crust of magmatic arc complexes that show interlayered sequences of gabbroic to ultramafic rocks with more felsic anorthositic and charnockitic rocks. A distinct Moho reflection is not observed, even at the critical distance. A gradational boundary with predominantly olivine-free norites and gabbros above and ultramafic rocks below, or a transitional phase change from high-pressure granulite to eclogite facies (Hamilton, 1981) might be explanations for the lack of Moho reflections. The loss of a Moho arrival in going from Archean into Proterozoic crust is observed in other boundaries as well (Cannon et al., 1991), indicating a major difference of both types of crust. Our observations are consistent with the interpretation that the Proterozoic terrane south of the Cheyenne Belt is an accreted magmatic arc that predominantly consists of complexes of highly fractionated island arc products causing seismic reflections from the lower crust but

not the Moho.

REFERENCES

- Allmendinger, R. W., J. A. Brewer, L. D. Brown, S. Kaufman, J. E. Oliver, and R. S. Houston, 1982, COCORP profiling across the Rocky Mountain Front in southern Wyoming, Part 2: Precambrian basement structure and its influence on Laramide deformation, Geol. Soc. Am. Bull., v. 93, pp. 1253-1263.
- Austin, J. A., P. L. Stoffa, J. D. Phillips, J. Oh, D. S. Sawyer, G. M. Purdy, E. Reiter, and J. Makris, 1990, Crustal structure of the Southeast Georgia embayment-Carolina trough: Preliminary results of a composite seismic image of a continental suture(?) and a volcanic passive margin, Geology, v. 18, pp. 1023-1027.
- Baadsgaard, H., A. P. Nutman, D. Bridgwater, V. R. McGregor, and J. H. Allaart, 1984, The zircon chronology of the Akilia association and Isua crustal belt, West Greenland, Earth Planet. Sci. Lett., v. 68, pp. 221-228.
- Bard, J. P., 1983, Metamorphism of an obducted island arc: example of the Kohistan sequence (Pakistan) in the Himalayan collided range, Earth Planet. Sci. Lett., v. 65, pp. 133-144.
- Barton, P. J., T. R. E. Owen, and R. S. White, 1990, The deep structure of the east Oman continental margin: preliminary results and interpretation, Tectonophysics, v. 173, pp. 319-331.
- Bessonova, E. N., V. M. Fishman, V. Z. Ryaboyi, and G. A. Sitnikova, 1974, The tau method for inversion of travel times - I. Deep seismic sounding data, Geoph. J. R. astr. Soc., v. 36, pp. 377-398.
- Birch, F., 1960, The velocity of compressional waves in rocks to 10 kilobars, 1., J. Geoph. Res., v. 65, pp. 1083-1102.
- Birch, F., 1961, The velocity of compressional waves in rocks to 10 kilobars, 2., J. Geoph. Res., v. 66, pp. 2199-2224.
- Bonatti, E., and M. Seyler, 1987, Crustal underplating and evolution in the Red Sea rift: Uplifted gabbro/gneiss crustal complexes on Zabargad and Brothers Islands, J.

- Geoph. Res., v. 92, pp. 12803-12821.
- Boyd, N., and S. B. Smithson, 1990, Seismic reflection studies of the Archean: The gneiss terrane of southern Minnesota, EOS Transactions (abstract), v. 71, p. 1436.
- Boyd, N., K. Gohl, W. Clement, and S. B. Smithson, 1991, Seismic reflection studies of the Archean: The gneiss terrane of southern Minnesota, presented at Geophysical Solutions to Geologic Problems of Continental Interiors: A Minnesota Workshop, Minnesota Geol. Survey, Minneapolis.
- Braile, L. W., and C. S. Chang, 1986, The continental Mohorovicic discontinuity: Results from near-vertical and wide-angle seismic reflection studies, in Reflection Seismology: A Global Perspective, edited by M. Barazangi and L. Brown, AGU Geodynamics Series Vol. 13, pp. 257-272.
- Brewer, J. A., R. W. Allmendinger, L. D. Brown, J. E. Oliver, and S. Kaufman, 1982, COCORP profiling across the Rocky Mountain Front in southern Wyoming, Part 1: Laramie structure, Geol. Soc. Am. Bull., v. 93, pp. 1242-1252.
- Bridgwater, D., V. R. McGregor, and J. S. Myers, 1974, A horizontal tectonic regime in the Archaean of Greenland and its implications for early crustal thickening, Precambrian Res., v. 1, pp. 179-197.
- Bridgwater, D., L. Keto, V. R. McGregor, and J. S. Myers, 1976, Archean gneiss complex of Greenland, in Geology of Greenland, edited by A. Escher and W. S. Watt, Groenlands Geol. Undersog., pp. 18-74, Copenhagen.
- Brocher, T. M., and M. J. Moses, 1990, Wide-angle seismic recordings obtained during the TACT multichannel reflection profiling in the northern Gulf of Alaska, U.S. Geol. Survey Open-File Rep., Rep. 90-663, 40 pp.
- Brown, M., C. R. L. Friend, V. R. McGregor, and W. T. Perkins, 1981, The late Archaean Qorqut granite complex of southern West Greenland, J. Geophys. Res., v. 86, pp. 10617-10632.
- Burke, M. M., and D. M. Fountain, 1990, Seismic properties of rocks from an exposure of extended continental crust - new laboratory measurements from the Ivrea Zone, Tectonophysics, v. 182, pp. 119-146.
- Cannon, W. F., M. W. Lee, W. J. Hinze, K. J. Schulz, and A. G. Green, 1991, Deep crustal structure of the Precambrian

- basement beneath northern Lake Michigan, midcontinent North America, Geology, v. 19, pp. 207-210, 1991.
- Cervený, V., 1979, Accuracy of ray theoretical seismograms, J. Geophys., v. 46, 135-149.
- Cervený, V., I. Molotkov, and I. Psencik, 1977, Ray Method in Seismology, University Karlova, Prague.
- Chandler, V. W., and D. L. Southwick, 1990, Aeromagnetic Minnesota, EOS Transactions, v. 71, p. 329.
- Chian, D., and K. Loudon, The structure of Archaean/Ketilidian crust along the continental shelf of southwest Greenland from a seismic refraction profile, submitted to Can. J. Earth Sci.
- Christensen, N. I., and D. M. Fountain, 1975, Constitution of the lower continental crust based on experimental studies of seismic velocities in granulite, Geol. Soc. Am. Bull., v. 86, pp. 227-236.
- Clarke, D. B., 1970, Tertiary basalts of Baffin Bay: Possible primary magma from the mantle, Contrib. Mineral. Petrol., v. 25, p. 203.
- Clarke, D. B., and A. K. Pederson, 1976, Tertiary volcanic province of west Greenland, in Geology of Greenland, edited by A. Escher and W. S. Watt, The Geol. Survey of Greenland, Copenhagen, pp. 365-385.
- Clarke, D. B., and B. G. J. Upton, 1971, Tertiary basalts of Baffin Island: Field relations and tectonic setting, Can. J. Earth Sci., v. 8, pp. 248-258.
- Clayton, R. W., and G. A. McMechan, 1981, Inversion of refraction data by wave field continuation, Geophysics, v. 46, pp. 860-868.
- Condie, K. C., 1982, Plate-tectonics model for Proterozoic continental accretion in the southwestern United States, Geology, v. 10, pp. 37-42.
- Coward, M. P., M. Q. Jan, D. Rex, J. Tarney, M. Thirlwall, and B. F. Windley, 1982, Geo-tectonic framework of the Himalaya of N Pakistan, J. Geol. Soc. Lond., v. 139, pp. 299-308.
- Davydova, N. I., I. P. Kosminskaya, N. K. Kapustian, and G. G. Michota, 1972, Models of the earth's crust and M-boundary, Z. Geophysik, v. 38, pp. 369-393.

- Denham, L. R., 1974, Offshore geology of northern West Greenland (69 to 75 N), Rep. Geol. Surv. Greenland 63, 24 pp.
- Diebold, J. B., and P. L. Stoffa, 1981, The travel-time equation, tau-p mapping, and inversion of common midpoint data, Geophysics, v. 46, pp. 238-254.
- Dorman, L. M., 1979, A linear relationship between earth models and seismic body wave data, Geoph. Res. Lett., v. 6, pp. 132-134.
- Duebendorfer, E. M., and R. S. Houston, 1986, Kinematic history of the Cheyenne belt, Medicine Bow Mountains, southeastern Wyoming, Geology, v. 14, pp. 171-174.
- Duebendorfer, E. M., and R. S. Houston, 1987, Proterozoic accretionary tectonics at the southern margin of the Archean Wyoming craton, Geol. Soc. Am. Bull., v. 98, pp. 554-568.
- Fountain, D. M., 1976, The Ivrea-Verbano and Strona-Ceneri Zones, northern Italy: A cross-section of the continental crust - New evidence from seismic velocities, Tectonophysics, v. 33, pp. 145-165.
- Fountain, D. M., 1989, Growth and modification of lower continental crust in extended terrains: The role of extension and magmatic underplating, in Properties and Processes of Earth's Lower Crust, edited by R. F. Mereu, S. Mueller, and D. M. Fountain, AGU Geophysical Monograph 51, IUGG Volume 6.
- Fountain, D. M., C. A. Hurich, and S. B. Smithson, 1984, Seismic reflectivity of mylonite zones in the crust, Geology, v. 12, pp. 195-198.
- Fountain, D. M., M. H. Salisbury, and J. Percival, 1990, Seismic structure of the continental crust based on rock velocity measurements from the Kapuskasing uplift, J. Geoph. Res., v. 95, pp. 1167-1186.
- Friend, C. R. L., and A. P. Nutman, 1991, Refolded nappes formed during late Archaean terrane assembly, Godthaabsfjord, southern West Greenland, J. Geol. Soc. Lond., v. 148, pp. 507-519.
- Fuchs, K., and G. Mueller, 1971, Computation of synthetic seismograms with the reflectivity method and comparison with observations, Geoph. J. R. astr. Soc., v. 23, pp. 417-433.

- Furlong, K. P., and D. M. Fountain, 1986, Continental crustal underplating: thermal considerations and seismic-petrologic consequences, J. Geoph. Res., v. 91, pp. 8285-8294.
- Garmany, J., 1979, On the inversion of travel times, Geoph. Res. Lett., v. 6, pp. 277-279.
- Geological Survey of Canada, 1988a, Gravity anomaly map of the continental margin of Eastern Canada; Geol. Surv. of Canada, Map 1708A, scale 1:500,000.
- Geological Survey of Canada, 1988b, Magnetic anomaly map of the continental margin of Eastern Canada; Geol. Surv. of Canada, Map 1709A, scale 1:500,000.
- Geological Survey of Greenland, 1982, Geological map of Greenland, sheet 2, Frederikshaab Isblink - Soendre Stroemfjord, Geol. Surv. of Greenland, scale 1:500,000.
- Geist, D. J., C. D. Frost, A. Kolker, and B. R. Frost, 1989, A geochemical study of magmatism across a major terrane boundary: Sr and Nd isotopes in Proterozoic granitoids of the southern Laramie Range, Wyoming, J. Geology, v. 97, pp. 331-342.
- Gibbs, A. K., B. Payne, T. Setzer, L. D. Brown, J. E. Oliver, and S. Kaufman, 1984, Seismic-reflection study of the Precambrian crust of central Minnesota, Geol. Soc. Am. Bull., v. 95, pp. 280-294.
- Gibson, B. S., and A. R. Levander, 1988, Lower crustal reflectivity patterns in wide-angle seismic recordings, Geoph. Res. Lett., v. 15, pp. 617-620.
- Gohl, K., S. B. Smithson, and Y. Kristoffersen, The structure of the Archean crust in SW Greenland from seismic wide-angle data: A preliminary analysis, in press.
- Goldich, S. S., and C. E. Hedge, 1974, 3,800 myr granite gneiss in southwestern Minnesota, Nature, v. 252, pp. 467-468.
- Greenhalgh, S. A., 1981, Seismic investigations of crustal structure in east-central Minnesota, Phys. Earth Planet. Int., v. 25, pp. 372-389.
- Griffin, W. L., and S. Y. O'Reilly, 1987, Is the continental Moho the crust-mantle boundary, Geology, v. 15, pp. 241-244.
- Hale, L. D., and G. A. Thompson, 1982, The seismic reflection

- character of the continental Mohorovicic discontinuity, J. Geoph. Res., v. 87, pp. 4625-4635.
- Hamilton, W. B., 1981, Crustal evolution by arc magmatism, Phil. Trans. R. Soc. Lond. A, v. 301, pp. 279-291.
- Hamilton, W. B., 1988, Plate tectonics and island arcs, Geol. Soc. Am. Bull., v. 100, pp. 1503-1527.
- Hawman, R. B., R. H. Colburn, D. A. Walker, and S. B. Smithson, 1990, Processing and inversion of refraction and wide-angle reflection data from the 1986 Nevada PASSCAL Experiment, J. Geoph. Res., v. 95, pp. 4657-4691.
- Hawman, R. B., and R. A. Phinney, 1991, Analysis of sparse wide-angle reflection data in the tau-p domain, Bull. Seis. Soc. Am., v. 81, pp. 202-221.
- Herzberg, C. J., W. S. Fyfe, and M. J. Carr, 1983, Density constraints on the formation of the continental Moho and crust, Contrib. Mineral. Petrol., v. 84, pp. 1-5.
- Hills, F. A., and R. L. Armstrong, 1974, Geochronology of Precambrian rocks in the Laramie Range and implications for the tectonic framework of Precambrian southern Wyoming, Precambrian Res., v. 1, pp. 213-225.
- Hinz, K., H.-U. Schlueter, A. C. Grant, S. P. Srivastava, D. Umpleby, and J. Woodside, 1979, Geophysical transects of the Labrador Sea: Labrador to southwest Greenland, Tectonophysics, v. 59, pp. 151-183.
- Houston, R. S., E. M. Duebendorfer, K. E. Karlstrom, and W. R. Premo, 1989, A review of the geology and structure of the Cheyenne belt and Proterozoic rocks of southern Wyoming, in Proterozoic Geology of the Southern Rocky Mountains, edited by J. A. Grambling and B. J. Tewksbury, Geol. Soc. Am. Special Paper 235, pp. 1-12.
- Hurich, C. A., S. B. Smithson, D. M. Fountain, and M. C. Humphreys, 1985, Seismic evidence of mylonite reflectivity and deep structure in the Kettle Dome metamorphic core complex, Washington, Geology, v. 13, pp. 577-580.
- Hyndman, R. D., 1973, Evolution of the Labrador Sea; Can. J. Earth Sci., v. 10, pp. 637-664.
- Hyndman, R. D., 1975, Marginal basins of the Labrador Sea and the Davis Strait hot spot, Can. J. Earth Sci., v. 12, pp. 1041-1045.

- Jackson, I., and R. J. Arculus, 1984, Laboratory wave velocity measurements on lower crustal xenoliths from Calcutteroo, South Australia, Tectonophysics, v. 101, pp. 185-197.
- Jackson, W. H., and L. C. Pakiser, 1965, Seismic study of crustal structure in the southern Rocky Mountains, U.S. Geol. Surv. Prof. Paper 525-D, pp. 85-92.
- Jackson, W. H., S. W. Steward, and L. C. Pakiser, 1963, Crustal structure in eastern Colorado from seismic-refraction measurements, J. Geoph. Res., v. 68, pp. 5767-5776.
- Johnson, R. A., K. E. Karlstrom, S. B. Smithson, and R. S. Houston, 1984, Gravity profiles across the Cheyenne Belt, a Precambrian crustal suture in southeastern Wyoming, J. Geodynamics, v. 1, pp. 445-472.
- Johnson, R. A., and S. B. Smithson, 1986, Interpretive processing of crustal seismic reflection data: examples from Laramie Range COCORP data, in Reflection Seismology: A Global Perspective, edited by M. Barazangi and L. Brown, AGU Geodynamics Series, v. 13, pp. 197-208.
- Johnson, R. A., and S. B. Smithson, 1985, Thrust faulting in the Laramie Mountains, Wyoming, from reanalysis of COCORP data, Geology, v. 13, pp. 534-537.
- Johnson, G. L., S. P. Srivastava, J. Campsie, and M. Rasmussen, 1982, Volcanic rocks in the Labrador Sea and environs and their relationship to the evolution of the Labrador Sea, in Current Research, Part B, Geol. Surv. of Canada, Paper 82-1B, pp. 7-20.
- Karlstrom, K. E., and R. S. Houston, 1984, The Cheyenne belt; Analysis of a Proterozoic suture in southern Wyoming, Precambrian Res., v. 25, pp. 415-446.
- Karlstrom, K. E., A. J. Flurkey, and R. S. Houston, 1983, Stratigraphy and depositional setting of Proterozoic metasedimentary rocks in southeastern Wyoming; Record of an Early Proterozoic Atlantic-type cratonic margin, Geol. Soc. Am. Bull., v. 94, pp. 1257-1294.
- Keen, M. S., and G. L. Williams (eds.), 1990, Geology of the Continental Margin of Eastern Canada, Geol. Soc. Am., The Geology of North America, v. I-1.
- Keen, C. E., and B. de Voogt, 1988, The continent-ocean boundary at the rifted margin off eastern Canada: New results from deep seismic reflection studies, Tectonics, v. 7, pp. 107-124.

- Kennett, B. L. M., and J. A. Orcutt, 1976, A comparison of travel time inversions for marine refraction profiles, J. Geoph. Res., v. 81, pp. 4061-4070.
- Kern, H., and A. Richter, 1981, Temperature derivatives of compressional and shear wave velocities in crustal and mantle rocks at 6 kbar confining pressure, J. Geophys., v. 49, pp. 47-56.
- LASE Study Group, 1986, Deep structure of the US East Coast passive margin from large aperture seismic experiments (LASE), Marine and Petrol. Geol., v. 3, pp. 234-242.
- Laughton, A. S., 1971, South Labrador Sea and the evolution of the North Atlantic, Nature, v. 232, pp. 612-617.
- Laughton, A. S., 1972, The southern Labrador Sea - A key to the Mesozoic and early Tertiary evolution of the North Atlantic, in: Initial reports of the Deep Sea Drilling Project, v. 12, Washington, D.C., U.S. Govt. Printing Office, pp. 1155-1179.
- Le Pichon, X., R. D. Hyndman, and G. Pautot, 1971, Geophysical study of the opening of the Labrador Sea, J. Geoph. Res., v. 76, pp. 4724-4743.
- Lister, G. S., M. A. Etheridge, and P. A. Symonds, 1986, Detachment faulting and the evolution of passive continental margins, Geology, v. 14, pp. 246-250.
- Manderscheid, G., 1980, The geology of the offshore sedimentary basin of West Greenland, in Facts and Principles of World Petroleum Occurrence, edited by A. D. Miall, Can. Soc. Petrol. Geol. Mem. 6, pp. 951-974.
- Manghnani, M. H., R. Ramanantoandro, and S. P. Clark, Jr., 1974, Compressional and shear wave velocities in granulite facies rocks and eclogites to 10 kbar, J. Geoph. Res., v. 70, pp. 5427-5446.
- Mattinson, J. M., D. L. Kimbrough, and J. Y. Bradshaw, 1986, Western Fiordland orthogneiss - Early Cretaceous arc magmatism and granulite facies metamorphism, New Zealand, Contrib. Mineral. Petrol., v. 92, pp. 383-392.
- McCarthy, J., and G. A. Thompson, 1988, Seismic imaging of extended crust with emphasis on the western United States, Bull. Bull. Geol. Soc. Am., v. 100, pp. 1361-1374.
- McGregor, V. R., 1973, The early Precambrian gneisses of the Godthaab district, West Greenland, Philos. Trans. R. Soc.

London, Ser. A, v. 273, pp. 343-358.

- McGregor, V. R., 1979, Archaean gray gneisses and the origin of the continental crust : Evidence from the Godthaab region, West Greenland, in Trondhjemites, Dacites and Related Rocks, edited by F. Barker, pp. 169-205, Elsevier, Amsterdam.
- McGregor, V. R., D. Bridgwater, and A. P. Nutman, 1983, The Qarusuk dykes: post-Nuk, pre-Qorqut granitoid magmatism in the Godthaab region, southern West Greenland, Rep. Geol. Surv. Greenland, v. 112, pp. 101-112.
- McGregor, V. R., and B. Mason, 1977, Petrogenesis and geochemistry of metabasaltic and metasedimentary enclaves in the Amitsoq gneisses, West Greenland, Am. Mineral., v. 62, pp. 887-904.
- McGregor, V. R., A. P. Nutman, and C. R. L. Friend, 1986, The Archean geology of the Godthaabfjord region, southern West Greenland, Tech. Rep. 86-04, Lunar and Planet. Inst., Houston, pp. 113-169.
- McKenzie, D., 1978, Some remarks on the development of sedimentary basins, Earth Planet. Sci. Lett., v. 40, pp. 25-32.
- McMechan, G. A., and R. Ottoloni, 1980, Direct observation of a p-tau curve in a slant stacked wave field, Bull. Seismol. Soc. Am., v. 70, pp. 775-789.
- Meissner, R., 1986, The Continental Crust, A Geophysical Approach, Academic Press, Inc., Toronto, 426 pp.
- Meissner, R., 1973, The 'Moho' as a transition zone, Geoph. Surveys, v. 1, pp. 195-216.
- Morey, G. B., 1972, The middle Precambrian - Minnesota River Valley, in Geology of Minnesota: A Centennial Volume, edited by P. K. Sims, and G. B. Morey, Minnesota Geol. Survey, pp. 260-262.
- Morey, G. B., and P. K. Sims, 1976, Boundary between two Precambrian W terranes in Minnesota and its geologic significance, Geol. Soc. Am. Bull., v. 87, pp. 141-152.
- Nutman, A. P., D. Bridgwater, E. Dimroth, R. O. C. Gill, and M. Rosing, 1983, Field work on the early (3700 Ma) Archaean rocks of the Isua supracrustal belt and adjacent gneisses, Groenl. Geol. Unders., Rapp., v. 112, PP. 5-22.
- Nutman, A. P., D. Bridgwater, and B. J. Fryer, 1984, The

iron-rich suite from the Amitsoq gneisses of southern West Greenland: Early Archaean plutonic rocks of mixed crustal and mantle origin, Contrib. Mineral. Petrol., v. 87, pp. 24-34.

- Nutman, A. P., C. R. L. Friend, H. Baadsgaard, and V. R. McGregor, 1989, Evolution and assembly of Archean gneiss terranes in the Godthaabfjord region, southern West Greenland: structural, metamorphic, and isotopic evidence, Tectonics, v. 8, pp. 573-589.
- Peterman, Z. E., C. E. Hedge, and W. A. Braddock, 1968, Age of Precambrian events in the northeastern Front Range, Colorado, J. Geoph. Res., v. 73, pp. 2277-2296.
- Phinney, R. A., K. Roy Chowdhury, and L. N. Frazer, 1981, Transformation and analysis of record sections, J. Geoph. Res., v. 86, pp. 359-377.
- Premo, W. R., and W. R. Van Schmus, 1989, Zircon geochronology of Precambrian rocks in southeastern Wyoming and northern Colorado, in Proterozoic Geology of the Southern Rocky Mountains, edited by J. A. Grambling and B. J. Tewksbury, Geol. Soc. Am. Special Paper 235, pp. 13-32.
- Prodehl, C., and L. C. Pakiser, 1980, Crustal structure of the southern Rocky Mountains from seismic measurements, Geol. Soc. Am. Bull., v. 91, pp. 147-155.
- Reid, I. D., and C. E. Keen, 1990(a), Deep crustal structure beneath a rifted basin: results from seismic refraction measurements across the Jeanne d'Arc Basin, offshore eastern Canada, Can. J. Earth Sci., v. 27, pp. 1462-1471.
- Reid, I. D., and C. E. Keen, 1990(b), High seismic velocities associated with reflections from within the lower oceanic crust near the continental margin of eastern Canada, Earth and Planet. Sci. Lett., v. 99, pp. 118-126.
- Robertson, S., 1986, Evolution of the late Archaean lower continental crust in southern West Greenland, in The Nature of the Lower Continental Crust, edited by J. B. Dawson, D. A. Carswell, J. Hall, and K. H. Wedepohl, Geol. Soc. Special Publ. No. 24, pp. 251-260.
- Sims, P. K., K. D. Card, G. B. Morey, and Z. E. Peterman, 1980, The Great Lakes tectonic zone - A major crustal structure in central North Minnesota, Geol. Soc. Am. Bull., v. 91, pp. 690-698.
- Smithson, S. B., 1989, Contrasting types of lower crust, in

Properties and Processes of Earth's Lower Crust, edited by R. F. Mereu, S. Mueller, and D. M. Fountain, AGU Geophysical Monograph 51, IUGG Volume 6, pp. 53-63.

Smithson, S. B., and R. A. Johnson, 1989, Crustal structure of the western U.S. based on reflection seismology, in Geophysical Framework of the United States, edited by L. Pakiser and W. D. Mooney, Geol. Soc. Am. Mem. 172, pp. 577-612.

Smithson, S. B., R. A. Johnson, and C. A. Hurich, 1986, Crustal reflections and crustal structure, in Reflection Seismology: The Continental Crust, edited by M. Barazangi and L. Brown, AGU Geodynamics Series, v. 14, pp. 67-73.

Soper, N. J., P. R. Dawes, and A. K. Higgins, 1982, Cretaceous-Tertiary magnetic and tectonic events in North Greenland and the history of adjacent ocean basins, Nares Strait and the drift of Greenland: A conflict in plate tectonics, Geoscience, v. 8, pp. 205-220.

Srivastava, S. P., 1983, Davis Strait: Structures, origin and evolution, in Structure and Development of the Greenland-Scotland Ridge, edited by M. H. P. Bott, S. Saxov, M. Talwani, and J. Thiede, Plenum, New York, pp. 159-189.

Srivastava, S. P., 1978, Evolution of the Labrador Sea and its bearing on the early evolution of the North Atlantic, Geophys. Jour. R. Astr. Soc., v. 52, pp. 313-357.

Srivastava, S. P., R. K. H. Falconer, B. MacLean, 1980, Labrador Sea, Davis Strait, Baffin Bay: Geology and geophysics - A review, Can. Soc. Petr. Geol. Mem. 7, pp. 333-398.

Srivastava, S. P., and C. R. Tapscott, 1986, Plate kinematics of the North Atlantic, Chapter 23 in The Western North Atlantic Region, edited by P. R. Vogt and B. E. Tucholke, The Geology of North America, v. M, pp. 379-404.

Stergiopoulos, A. B., 1984, Geophysical crustal studies off the southwest Greenland margin, M.S. thesis, Dalhousie University, 250 pp.

Stoffa, P. L., P. Buhl, J. B. Diebold, and F. Wenzel, 1981, Direct mapping of seismic data to the domain of intercept time and ray parameter: A plane wave decomposition, Geophysics, v. 46, pp. 255-267.

Taylor, F. C., 1972, The Nain Province, in Variations in

- Tectonic Styles in Canada, edited by R. A. Price and R. J. W. Douglas, Geol. Ass. of Canada, Special Paper 11, pp. 435-452.
- Thorning, L., 1984, Aeromagnetic maps of parts of southern and central West Greenland, Groenlands Geol. Undersol., Rapp. 122, with map, 36 pp.
- Thorning, L., 1986, A decade of geophysical surveying in Greenland, in Developments in Greenland Geology, edited by F. Kalsbeek and W. S. Watt, Groenlands Geol. Undersol., Rapp. 128, pp. 12-133.
- Trehu, A. M., A. Ballard, L. M. Dorman, J. F. Gettrust, K. D. Klitgord, and A. Schreiner, 1989, Structure of the lower crust beneath the Carolina Trough, U.S. Atlantic continental margin, J. Geoph. Res., v. 94, pp. 10585-10600.
- van der Linden, W. J. M., 1975, Crustal attenuation and sea floor spreading in the Labrador Sea, Earth and Planet. Sci. Lett., v. 27, pp. 409-423.
- Walsh, J. B., 1965, The effect of cracks on the compressibility of rocks, J. Geoph. Res., v. 70, pp. 381-390.
- Weigel, W., G. Wissmann, and P. Goldflam, 1982, Deep seismic structure (Mauritania and Central Morocco), in Geology of the Northwest African Continental Margin, edited by U. vanRad, K. Hinz, M. Sarntheim, and E. Seibold, Springer Verlag, pp. 132-159.
- Wernicke, B., 1985, Uniform-sense normal simple shear of the continental lithosphere, Can. J. Earth Sci., v. 4, pp. 105-115.
- White, R., and D. McKenzie, 1989, Magmatism at rift zones: The generation of volcanic continental margins and flood basalts, J. Geoph. Res., v. 94, pp. 7685-7729.
- Woodside, J. M., and J. Verhoef, 1989, Geological and tectonic framework of eastern Canada as interpreted from potential field imagery, Geol. Survey of Canada, Paper 88-26.
- Zelt, C. A., and R. B. Smith, Traveltime inversion for 2-D velocity structure, submitted to Geoph. J. Int.